TWO-DIMENSIONAL ANALYSIS OF WATER-FILLED GEOMEMBRANE TUBES USED AS TEMPORARY FLOOD-FIGHTING DEVICES

By

Tung Chun Huong

Thesis submitted to the Faculty of
Virginia Polytechnic Institute and State University
in partial fulfillment of the requirements for the degree of

MASTER OF SCIENCE
IN
CIVIL ENGINEERING

Approved by:

Raymond H. Plaut, Co-chairman	George M. Filz, Co-chairman

Marte S. Gutierrez

February 2001
Blacksburg, Virginia

Keywords: Flood control, flood-fighting devices, geomembrane tube, geotextile, numerical modeling, soil-structure interaction

TWO-DIMENSIONAL ANALYSIS OF WATER-FILLED GEOMEMBRANE TUBES AS TEMPORARY FLOOD-FIGHTING DEVICES

Tung C. Huong
Raymond H. Plaut, Co-chairman
George M. Filz, Co-chairman
Civil and Environmental Engineering

(ABSTRACT)

A water-filled geomembrane tube is considered for the purpose of temporary flood protection. With proper design, this tube can be a cheap and efficient breakwater, temporary levee, or cofferdam. This thesis considers a single tube resting on clay and sand foundations.

A finite difference program, FLAC, is used in the numerical analyses. The tube is assumed to be infinitely long, and it is modeled two-dimensionally. Beam elements are used to model the tube. The tube is inflated with water. The hydrostatic pressure in the tube is converted to point loads and applied at the beam nodes in the direction perpendicular to the chord connecting two adjacent nodes.

Two of FLAC's built-in soil models are used: elastic and Mohr-Coulomb. The Mohr-Coulomb model is used in all the cases except the preliminary analyses, in which the elastic soil model is used. The Mohr-Coulomb soil model is able to model the soil's nonlinear stress-strain and path-dependent deformation behavior.

A tube without external water is placed on clay with various shear strengths to study how the clay consistency affects the height and the stresses in the tube. A tube with external water on one side is placed on medium dense sand. A wooden block is placed on the side opposite the floodwater. Three types of block geometry and two sizes are studied. The floodwater level is increased until the system fails. Three failure modes, rolling, sliding, and piping, are studied.

The effect of pore pressure on these failure modes is examined. The influence of a filter placed under part of the tube and block is also investigated.

The tube's tensile forces, shear forces, moments, and settlements are included. Soil stresses and pore pressures at the soil-tube interfaces are computed. The cross-section of the tube at various external water levels, and the pore pressures in the soil, are calculated. These results are compared with experimental results that were obtained by graduate students in geotechnical engineering at Virginia Tech.

Acknowledgements

Most of all, I would like to express my sincere appreciation to my advisors, Dr. Raymond Plaut, and Dr. George Filz, for their advice, assistance, consideration, and patience in this research and thesis. I would like to thank Dr. Marte Gutierrez for his help in debugging the FISH function codes and for being a member of my graduate committee.

I want to acknowledge financial support from the National Science Foundation under Grant No. CMS-9807335. Also, I appreciate Dr. Peter Cundall and Dr. Roger Hart from Itasca Consulting Group, Inc., for their help in learning FLAC.

Last but not least, I would like to thank my wife for her understanding, and also Dr. Jose Weissmann from the University of Texas at San Antonio for his endless encouragement.

Table of Contents

Chapter 1: Introduction and Literature Review

1.1 Introduction……. 1

1.2 Literature review …… 1

1.2.1. Geosynthetics……2

1.2.2. Application of geomembrane tubes …….. 2

1.2.3. Benefits from using the tubes ……..…….. 4

1.2.4. Previous analyses ……..……5

1.3 Scope ……..……7

Chapter 2: Single Tube Resting on Various Soft Clays ……...8

2.1. General ……...…….……... 8

2.2. Foundation soils ……..…..……... 8

2.2.1. Soil properties ……..……..9

2.2.2. Soil mesh ……...10

2.3. Tube ……..……...11

2.4. Tube material properties ……..……13

2.5. Tube-soil interface properties ……..……13

2.6. Internal water pressure ……..…….. 14

2.7. Results ……..……... 18

2.7.1. Effects of soil's shear strength on the height, settlement, and width of the tube ……19

2.7.2. Tube load and soil resistance……..……... 27

2.7.3. Tension forces in the tube ……29

2.7.4. Vertical soil stresses ……..31

3.7.5. Settlement of the soil ……33

2.8. Limitations ……..34

Chapter 3: Stability of a Single Tube Without Pore Pressure Effect ……35

3.1. Introduction …… 35

3.2. Soil ……..35

3.3. Tube ……..……..36

3.4. Interface properties ……..…… 36

3.5. Block shapes ……...37

3.6. External water ……38

3.7 Results …… 38

3.7.1. Floodwater levels and tube heights associated with block height and block shapes …….. 39

3.7.2. Tube shapes …….. 40

3.7.3. Stability of block ……...46

3.7.4. Tube height ……... 48

3.8. Further studies …… 48

3.8.1. Tube shape and contact length ……..49

3.8.2. Stresses at the interfaces…….……... 50

3.8.3. Soil stresses at the bottom of the tube and at the bottom of the wooden block ……52

3.8.4. Tension forces in the tube ……56

3.8.5. Shear forces and moments in the tube …….. 58

3.8.6. Volume of the tube at various floodwater levels …….. 59

3.8.7. Tube's height and width ……61

3.8.8. Stress in wooden block frame …….……..61

3.9. Comments …….……..63

Chapter 4: Stability of a Single Tube with the Effect of Pore Pressure. ……64

4.1. Introduction …….…... 64

4.2. Soil ……..64

4.3. Tube ……69

4.4. Block …….. 70

4.5. Filter ……... 70

4.6. Loading of the floodwater …….. 70
4.7. Results ……..... 71
4.7.1. 0.06m block height case …….……...71
4.7.2. 0.12m block height case …….……...75
4.8. Proof that pore pressure in the soil has no effect
on the rolling failure mode ……. 78
4.9. Discussion …….. 80

Chapter 5: Comparison Between Numerical Results and Experimental Results ……. 81
5.1. Introduction …… 81
5.2. Comparison between the experimental results and
the results obtained in Chapter 3 and Chapter 4 …….……81
5.3. New calculations …… 83
5.4. The relationship between rolling failure and internal water pressure…….…… 84
5.5. Filter ……... 84
5.6. Inflow and outflow ……. 85
5.7. Tube with no external water …….……..86
5.8. Modulus of elasticity….. …… 87
5.9. Piping……. …….……88
5.9.1. Piping for the 6cm block height case……88
5.9.2. Piping for the 12cm block height case……... 89
5.10. Rolling …… 90
5.10.1. 6cm block height case ……... 90
5.10.2. 12cm block height case ……90
5.11. Pore pressure……... 92
5.12. Groundwater flow rates ……... 94
5.13. Tube deformations …….……94
5.13.1. 6cm block height case ……... 94
5.13.2. 12cm block height case ……97
5.14. Tube height and width …… 99
5.14.1. 6cm block height case ……... 99

5.14.2. 12cm block height case ……..…… 101
5.15. Tube shape ……..……103
5.15.1. 6cm block height case ……... 103
5.15.2. 12cm block height case ……..…… 106
5.16. Tube's circumference and cross-sectional area …….. 108
5.16.1. 6cm block height case ……... 108
5.16.2 12cm block height case ……109
5.17. Soil settlement……...…….. 110

Chapter 6: Conclusions and Recommendations ……...113
6.1. Conclusions…… 113
6.2. Recommendations for further research …….. 114

References ……..116

Appendix A: Sample FLAC Programs……..119

Appendix B: Program Validation Tests……129
B1 Soil stresses caused by surface load without pore water pressure effect…… 129
B1.1 Soil stresses computed by FLAC……... 129
B1.2 Soil stresses computed by using spread load method…… 132
B1.3 Soil stresses computed based on the Boussinesq equation…… 133
B1.4 Comments…….. 134
B2 Normal and shear stresses at the interface caused by surface loads
with and without pore water pressure effect…….…….. 135
B2.1 Soil stresses without surface load…….. 135
B2.2 Pore pressure at interface……... 136
B2.3 Normal stresses at the interface with pore pressure effect……138
B2.4 Sliding resistance at the interface…….. 139
B2.4.1 Sliding resistance without pore pressure effect…….. 140
B2.4.2 Sliding resistance with pore pressure effect……140

B2.4.3 Comparison between sliding resistances
with and without pore pressure effect……141

Vita ……143

List of Figures

Figure 2.1. Soil mesh 10
Figure 2.2. Inflated tube with its nodal numbers 11
Figure 2.3. Tube with 18 beam elements 12
Figure 2.4. Water head vs. tube height above the ground level 13
Figure 2.5. Illustration of internal tube loads 15
Figure 2.6. Tensile force vs. position for two sets of equations 17
Figure 2.7. Tube shapes for equations 2.5 & 2.6, and equations 2.7 & 2.8 18
Figure 2.8. Tube on clay of 90psf shear strength 20
Figure 2.9. Tube on clay of 60psf shear strength 20
Figure 2.10. Tube on clay of 30psf shear strength 21
Figure 2.11. Tube on clay of 15psf shear strength 22
Figure 2.12. Tube on clay of 15psf shear strength that shows settlement and uplifting regions 22
Figure 2.13. Tube on clay of 5psf shear strength 23
Figure 2.14. Tube on clay of 2psf shear strength 24
Figure 2.15. Tube width, tube height, and tube settlement versus shear strength of the clay 25
Figure 2.16. Total load, shear resistance, and buoyancy resistance versus shear strength 26
Figure 2.17. Cross-section of a typical tube 28
Figure 2.18. Maximum tube tension force versus shear strength of the clay 30
Figure 2.19. Tension force versus nodal number (position) 30
Figure 2.20. Soil stress contours for S_u = 90psf case 32
Figure 2.21. Soil stress contours for S_u = 2psf case 32
Figure 2.22. Soil deflection contours for S_u = 90psf 33
Figure 2.23. Soil deflection contours for S_u = 2psf 33
Figure 2.24. Tube on clay of 1psf shear strength, unconverged solution 34

Figure 3.1. Grid layout for the soil mesh ……35
Figure 3.2. Illustration of fixed internal tube pressure ……... 36
Figure 3.3. Shapes of blocks ……...37
Figure 3.4. Critical floodwater level, tube height and tube width versus block height ……...40
Figure 3.5. Block shape 1, block height = 0.06m, flood water level = 0.23m ……41
Figure 3.6. Block shape 1, block height = 0.06m, floodwater level = 0.24m ……41
Figure 3.7. Block shape 1, block height = 0.09m, floodwater level = 0.28m …… 42
Figure 3.8. Block shape 1, block height = 0.09m, floodwater level = 0.29m …… 42
Figure 3.9. Block shape 1, block height = 0.12m, floodwater level = 0.31m …… 43
Figure 3.10. Block shape 1, block height = 0.12m, floodwater level = 0.32m ……..……43
Figure 3.11. Block shape 2, block height = 0.06m, floodwater level = 0.23m ……..……44
Figure 3.12. Block shape 2, block height = 0.06m, floodwater level = 0.24m ……..……44
Figure 3.13. Block shape 3, block height = 0.12m, floodwater level = 0.31m ……..……45
Figure 3.14. Block shape 3, block height = 0.12m, floodwater level = 0.32m ……..……45
Figure 3.15. Soil stress under the block, block shape 1, block height = 6cm …….. 46
Figure 3.16. Soil stress under the block, block shape 2, block height = 6cm ……...46
Figure 3.17. Soil stress under the block, block shape 1, block height = 12cm ……..……47
Figure 3.18. Soil stress under the block, block shape 3, block height = 12cm ……..……47
Figure 3.19. Tube shapes at different floodwater levels ……...49
Figure 3.20. Contact length versus floodwater level ……..... 50
Figure 3.21. Vertical stresses at the interface between tube and soil ……... 50
Figure 3.22. Stresses at the interface between block and soil at different floodwater levels ……51
Figure 3.23. Schematics of a wooden block frame ……...52
Figure 3.24. Vertical soil stress contours for zero floodwater level ……..…… 53
Figure 3.25. Vertical soil stress contours for floodwater level equals to 0.1m …… 53
Figure 3.26. Vertical soil stress contours for floodwater level equals to 0.2m …… 54
Figure 3.27. Vertical soil stress contours for floodwater level equals to 0.3m …… 54

Figure 3.28. Vertical soil stress contours for floodwater level equals to 0.31m …….. 55
Figure 3.29. Full view of vertical soil stress contours at 0.3m floodwater level ……..…… 55
Figure 3.30. Vertical soil stresses corresponding to floodwater levels……. 56
Figure 3.31. Tensile force versus nodal number (position) …….. 58
Figure 3.32. Shear force versus nodal number ……..…… 59
Figure 3.33. Moment versus nodal number …….. 59
Figure 3.34. Volume of water in the tube versus external floodwater level ……60
Figure 3.35. Percent difference in tube volume versus floodwater level ……..…… 60
Figure 3.36. Tube's height and tube's width versus floodwater level …….. 61
Figure 3.37. Axial force in the wooden block frame at different floodwater level …….. 62
Figure 3.38. Bending moments in the wooden frame at various floodwater level ……... 62
Figure 3.39. Shear forces in the block frame at various floodwater levels …….. 63

Figure 4.1. Soil grid mesh …….. 65
Figure 4.2. Problem of using high K_w ……..……67
Figure 4.3. Results for using $K_w = 10^5$ Pa……... 68
Figure 4.4. Block height = 0.12m, floodwater level = 0.2m, $K_w = 10^2$ Pa …….…… 68
Figure 4.5. Placements of tube, filter, and block, and loading of floodwater ……70
Figure 4.6. Block height = 6cm, floodwater level = 0.23m ……72
Figure 4.7. Block height = 6cm, floodwater level = 0.24m ……72
Figure 4.8. Rollover view, block height = 6cm, floodwater level = 0.24m ……73
Figure 4.9. Magnified view of Figure 4.6 ……...74
Figure 4.10. Block height = 0.12m, floodwater level = 0.1m ……...76
Figure 4.11. Block height =12cm, Floodwater level =0.25m ……... 77
Figure 4.12. Block height = 12cm, Floodwater level = 0.3m ……... 78
Figure 4.13. Comparison of the total stresses at the soil-tube interfaces ……..78
Figure 4.14. Components of interface stresses ……..…… 80

Figure 5.1. Internal pressure head for numerical model and experimental model…….. 82
Figure 5.2. An example of the convergence of groundwater flow …… 86
Figure 5.3. Tube shape without external water, internal pressure = 0.465m ……..87

Figure 5.4. Block height = 6cm, floodwater = 0.22m, internal pressure = 0.397m …… 89
Figure 5.5. Block height = 6cm, floodwater = 0.229m, internal pressure = 0.397m …….. 90
Figure 5.6. Block height = 0.12m, floodwater level = 0.265m, internal pressure = 0.349m ……... 91
Figure 5.7. Block height = 0.12m, floodwater level = 0.273m, internal pressure = 0.349m ……... 91
Figure 5.8. Pore pressure for the 6cm block height case …… 93
Figure 5.9. Pore pressure for the 0.12m block height case ……. 93
Figure 5.10. Total groundwater flow rate versus floodwater level…… 94
Figure 5.11. Deformation of tube ……..…… 95
Figure 5.12. Horizontal deformation of the tube …….. 96
Figure 5.13. The movement of a point on the tube, 6cm block height case…….……. 97
Figure 5.14. Horizontal deformation of the tube for the 12cm block height case…….…… 98
Figure 5.15. The movement of a point on the tube, 12cm block height case…… 98
Figure 5.16. Tube height vs. floodwater level for the 6cm block height case…….……... 99
Figure 5.17. Tube width vs. floodwater level for the 6cm block height case…… 100
Figure 5.18. Tube height over tube width ratio vs. floodwater level for the 6cm block height case……... 100
Figure 5.19. Tube height versus floodwater level for the 12cm block height case……... 102
Figure 5.20. Tube width versus floodwater level for the 12cm block height case…… 103
Figure 5.21. Tube height over tube width ratio versus floodwater level for the 12cm block height case……. 103
Figure 5.22a. Tube shape at 0.107m floodwater level, block height = 6cm……104
Figure 5.22b. Tube shape at 0.159m floodwater level, block height = 6cm……104
Figure 5.22c. Tube shape at 0.206m floodwater level, block height = 6cm……105
Figure 5.22d. Tube shape at 0.229m floodwater level, block height = 6cm……105
Figure 5.23a. Tube shape at 0.158m floodwater level, block height = 12cm……..106
Figure 5.23b. Tube shape at 0.227m floodwater level, block height = 12cm……..107
Figure 5.23c. Tube shape at 0.273m floodwater level, block height = 12cm……..107
Figure 5.24. Percent difference in area versus floodwater level for the 6cm block height case……... 108

Figure 5.25. Percent difference in tube area for the 12cm block height case……..……... 109
Figure 5.26. Settlements of the foundation soil surface. …….. 111

Figure B.1. Soil mesh for testing the subsurface stress due to the surface load……...129
Figure B.2. Spread load method……... 132
Figure B.3. Stress diagram used by Boussinesq equation…… 133
Figure B.4. Change of vertical soil stress versus depth……135
Figure B.5. Pore pressure distribution……..137
Figure B.6. Surface pore pressure versus distance from left edge……... 138
Figure B.7. Horizontal reaction versus applied horizontal load……...142

List of Tables

Table 2.1: Soil properties for very soft clay ……. 9

Table 2.2: Soil properties, tube height, tube settlement, and tube width ……..18

Table 3.1: Computer results ……..39

Table 4.1: Soil self-stresses computed by FLAC and by hand ……..…… 69

Table 5.1: Numerical and experimental critical floodwater levels ……...81

Table 5.2: Comparison of critical floodwater levels …… 83

Table 5.3: Tube's circumference and cross-sectional area associated with different values of modulus of elasticity……... 88

Table 5.4: Tube height, width, and height over width ratio ……..…… 99

Table 5.5: Tube height and width for the tube with constant internal pressure……... 101

Table 5.6: Tube height and width for the tube with variable internal pressure …… 101

Table 5.7: Tube's circumference and cross-sectional area at various floodwater levels ……..…… 108

Table 5.8: Tube's circumference and area with constant internal pressure ……..……..…… 109

Table 5.9: Tube's circumference and area with variable tube pressure…… 110

Table B.1: FLAC calculated vertical and horizontal soil self stresses……... 130

Table B.2: The initial and total stresses……. 130

Table B.3: FLAC's normal reaction at the interface…….. 132

Table B.4: Soil stresses computed by spread load method…… 133

Table B.5: Soil stresses computed using Boussinesq equation…….. 134

Table B.6: Self-stress of the soil without surface load……... 136

Table B.7: FLAC's normal reaction at interface…… 139

Table B.8: Horizontal reaction at the interface corresponds to the applied horizontal load……. 140

Table B.9: Horizontal resistance at the interface with pore pressure effect……... 141

Chapter 1

Introduction and Literature Review

1.1 Introduction

There are many natural disasters in the world. One of these disasters is flooding. It has taken many lives and much property. According to Plaut et al. (1998), floods in the United States have killed more than 175 people and damaged about $25 billion of property in the past five years. Therefore, safer and more effective methods of flood fighting are urgently needed.

Ancient people built earth levees to fight floods. Modern people built concrete dams, concrete levees, and sometimes earth dams also. These are expensive and permanent. For places where floods do not occur very often, building these expensive and massive structures may not be justified. As time passes by, these dams or levees may lose their intended purpose as deposits build up. Thus, people find other less expensive and convenient alternatives. One of these alternatives is sandbagging.

Sandbagging is common in North America because it is cheap and can be built at the emergency location (Landis, 2000). But, it is labor-intensive and time-consuming. During the emergency, labor and time are usually in shortage.

In addition, after the floods are over, the sandbags create environmental problems. Disposal of sandbags requires time and labor again. Fortunately, in the late 1980s, an alternative to sandbags emerged (Landis, 2000). This temporary dam is made up of a geosythetic tube and water itself. The following literature review discusses works that have been done previously.

1.2 Literature Review

The structures that are modeled in this thesis use a geomembrane as the main material. This geomembrane is formed into a tube. This tube is filled with water to fight against external water.

Since a geomembrane is one type of geosynthetic, the next section discusses geosynthetics and some of their applications.

1.2.1 Geosynthetics

A geosynthetic is made up of high-strength fabric woven with synthetic fibers. It can be either water permeable or impermeable. A water-permeable geosynthetic tube can be filled with concrete slurry, sand, and dredged material, and can become a permanent structure. Because of its high strength and porous characteristic, permeable geosynthetic sheets can be used as filters. One common use of it is to drain water away from a retaining wall to reduce the horizontal earth pressure on the wall.

A water-impermeable geosynthetic is not absolutely impermeable; its permeability ranges from $5x10^{-9}$ to $5x10^{-13}$cm/sec. Oftentimes, people call this relatively impermeable geosynthetic a geomembrane because of its high flexibility characteristic. The primary function of a geomembrane is to act as a liquid or gas barrier (Koerner, 1994, p. 426).

A tube made from a geomembrane is called a geomembrane tube. The synthetic fibers of this tube can be coated with polyvinyl chloride or acrylic to prevent fiber degradation by ultraviolet rays (Gutman, 1979). Since the major structure considered in this thesis is a geomembrane tube, the following section reviews some of the applications of this tube.

1.2.2 Applications of geomembrane tubes

Besides fighting floods, geomembrane tubes are also used in storing wastes, retaining back-filled soil, protecting shorelines, restoring soundness of scoured bridge pier footings, protecting surrounding areas by isolating a contaminated site, diverting water during the installation of underwater structures, and keeping transportation routes open by placing the tube along the sides of roadways.

A geosynthetic tube manufacturer, Aqua-Barrier, has claimed that they successfully protected the parking lot of a casino boat in Mississippi from rising floodwaters. They also claimed that contractors have used their tube to dewater the work areas for the boat ramp installation in Warroad, Minnesota, for the retaining wall repair in Eagle Lake, Texas, for the sea wall repair in Elkhart, Indiana, and for the pipeline installation and removal of old pipeline in the Roanoke River, Virginia.

Judy Munz, a property manager for the Woodside condominiums, Northeastern Sacramento, California, used 1700-ft-long and 1-ft to 3-ft-high geomembrane water dams to protect a 56-acre property. Also, the Army Corps of Engineers has successfully used the geotextile water dams many times to protect the levees of Sutter Bypass, California, from overflow (Landis, 2000).

During the 1998 El Nino weather event, Chuck Roof, a manager for the Skylark Shores Motel Resort in northern California's Lake County, used about 1000 feet of geotextile dams to guard the property from flooding. Since it was the only dry property in the area, Red Cross and the National Guard used the resort as their headquarters for flood relief efforts.

In Sao Paulo, Brazil, a continuous retaining dike made of geotextiles was constructed for retaining backfill. A city, "New Cubatao", was built on the fill with roughly 32,500 inhabitants (Bogossian et al., 1982). Geosynthetic tubes are also used as offshore breakwaters. Sarti and Larsen (1983) successfully placed Longard tubes offshore at depths between 3 and 4 ft. They tested the possibility of underwater filling, that is, filling the tube with sand under the water.

According to Gutman (1979), a 150-ft-long groin was constructed at Lynn Beach in Massachusetts for temporary shoreline protection. This groin was constructed of sand-filled nylon bags. These sandbags can be built for only $40 to $60 per cubic yard. The removal of the sandbags is also easy since it only requires removing the nylon bags and leaving the sand on the beach. The negative side is that a sandbag groin is very vulnerable to vandalism.

Geosynthetic tubes can be used as flexible concrete forms. They were used to successfully restore the bearing capacity of the scoured bridge pier footings for a bridge that crosses the Susquehanna River (Koerner and Koerner, 1996).

Perrier (1986) showed the use of soil-filled synthetic pillows for erosion and pollution control along a beach and a riverbank. His experimental site is situated on the bay of "Le Pas-de Calais" coast to prevent hydrocarbon pollution, and to preserve the beauty of a popular tourist area.

1.2.3 Benefits from using the tubes

Geomembrane tubes become important in engineering because they have been proven to be a cost-effective alternative in the construction of breakwaters, groins, and temporary levees. According to a geosynthetic tube manufacturer, Aqua-Barrier, using the Aqua-Barriers is more cost and time efficient than the conventional sandbagging in fighting flooding. For example, to install a 3-foot-high, 100-foot-long Aqua-Barrier tube costs only $3,127 and 20 minutes of installation time. For a similar water barrier, traditional sandbagging would cost $10,200 and take 238 minutes. After the crisis is past, the water-filled tube can be drained, rolled up, and stored for its next use. On the other hand, sandbags have no salvage value after the flood is over, and they create a large amount of solid waste. These wastes are expensive to dispose of.

"During the flood situation, time is everything." This is the experience of Skip Simkins, who looks after the Clear Lake levee system in Lake County, California. He has experience with both sandbagging and a geomembrane water wall. He mentioned in Landis (2000) that an 18-in.-high, 100-ft-long water wall can be laid in less than 4 man-hours. In contrast, the same level and length of a sandbag flood protection wall would require 42 man-hours. In addition to the benefit from the speed of construction, a geomembrane water wall satisfies the EPA guidelines, complies with the Clean Water Act, and is easy to transport and to disassemble after use.

Another example provided by Landis (2000) is the low cost in using a geomembrane water barrier. Deb Burey is a manager for the White Pines Resort in Sicamous, British Columbia. He used 2000 feet of geomembrane water dams to keep the 800 feet of beachfront property and 24 duplex units dry from the flooding caused by the spring, 1999, snow melt on the nearby

mountains. Burey reported that by using the geomembrane water barriers, the total flooding related expenses were reduced to at least 50% less than the 1997 sandbagging costs. In addition to cost savings, he also stressed that a geomembrane breakwater is more robust than sandbags in resisting the wave forces created by the storms and the moving boats.

1.2.4 Previous analyses

Sprague and Koutsourais (1992) discussed the design of concrete bags for revetments. Their idea is that by stacking the concrete-filled bags in a pyramid shape, one can create an efficient breakwater. These stacked bags are stable against the force of the waves. In addition, the authors also discussed the placement of a filter mat under the groin to prevent scour.

Biggar and Masala (1998) compared different alternatives for temporary flood control, and computed cost and specification comparison tables for different geosynthetic tube manufacturers. They also looked into the friction problem between foundations and tubes, and the seepage problem within the foundation. They reported that the stability calculations provided by the manufacturers of water-filled geomembrane tubes might not be correct. Because of the high flexibility of the tube and the horizontal water pressure, the tube becomes very irregular, and is difficult to be analyzed by the normal static analysis.

The Clement system is the most recommended flood-fighting system by Biggar and Masala. This system works by stacking the tubes in a pyramid shape with an impermeable blanket on the water-impounding side. The stacked tubes are tightened together to prevent relative movement between each other.

Kazimierowicz (1994) studied the shape and the cross-sectional height of a tube as a function of internal pressure. He used the governing system of differential equations to find the solution for the tube's cross-section. The tension force in the tube and the tube-soil contact length were tabulated for several values of the tube height. But he neglected the friction between tube and soil, and the external water load was not applied.

Hsieh and Plaut (1990), Wu and Plaut (1996), Mysore et al. (1997, 1998), and Plaut et al. (1998) performed 2D and 3D numerical studies on anchored inflatable dams. Computer simulations were carried out to determine the dam's dynamic response and stability. These properties are affected by the geometry and material of the structure, the support conditions, the internal dam pressure, and the external water pressure or flow.

Two-dimensional analyses on geosynthetic tubes that hold water on one side, and rest on a rigid or deformable Winkler foundation, were carried out by Plaut and Suherman (1998) and Watson et al. (1999). The tube was modeled as an inextensible and weightless membrane. Closed-form solutions for the cross-sectional shape and the circumferential tension were obtained.

Silvester (1986) presented the results of a numerical analysis in the form of a nondimensional chart and table for a particular circumference of a tube. It was stated that the numerical shape of the tube had been verified experimentally. Leshchinsky et al. (1996) studied the effect of pumping pressure on the stresses of a tube.

Plaut and Klusman (1998) used Mathematica to perform two-dimensional analyses of a single tube, two stacked tubes, and a 2-1 stacked formation. The configuration of 2-1 formation is that one tube is placed on the top of the other two tubes and forms a pyramid cross section with a wide base at the bottom. The friction between tubes, and between tube and foundation, was neglected. The bending stiffness and the extensibility of the tube were also neglected in the analyses. External water on one side of the single tube and the 2-1 formation was modeled, with stationary rigid blocks placed to prevent the tubes from sliding. The tubes' shapes, heights, and circumferential tension, and the ground deflections, were obtained.

Seay and Plaut (1998) used the finite element program ABAQUS to model the geotextile tubes three-dimensionally. The tube shapes, tube-ground contact region, tube stresses, and tube heights were studied with varying internal tube pressure. They found that the stresses in the tube and the height of the tube increase when the internal tube pressure increases, and the tube-ground contact region is smaller at higher tube pressure.

1.3 Scope

A computer program, Fast Lagrangian Analysis of Continua (FLAC), version 3.4, is used to carry out all the numerical analysis in this thesis. AUTOCAD is utilized to plot the FLAC's output. Microsoft Excel is utilized in manual calculations and in creating charts.

The foundation soil models, the tube's formulation, and the internal tube pressure formulation are discussed in Chapter 2. It also covers a single tube resting on soft clay with various shear strengths to study the response of the soil grid. The relationship of the shear strength magnitude with the soil settlement, tube stresses, and general tube behavior is observed.

Chapter 3 includes the preliminary analyses and the determination of the block's sizes and shapes for the field experiments and further analyses. Experiments were conducted recently at Virginia Tech in conjunction with the analysis presented in this thesis. This chapter studies the stability of a single tube without the effect of pore pressure underneath the tube. The floodwater acts on one side of the tube.

Chapter 4 includes a study of the effect of pore pressure on the tube from Chapter 3. It uses a more realistic foundation soil model – the Mohr-Coulomb soil model. Two block height cases are considered - the 6 cm block height case and the 12 cm block height case.

Chapter 5 compares the results obtained from chapter 3 and chapter 4 with the results obtained from the experiments. After the comparison, more numerical analyses are carried out to try to find out what causes the differences between the numerical results and experimental results.

Chapter 6 summarizes the work done in the previous six chapters, presents the conclusions of the studies, and makes recommendations for further research. The major program files that are used to do the analyses in this thesis are included in Appendix A. Some brief FLAC program verification procedures and results are reported in Appendix B.

Chapter 2

Single Tube Resting on Various Soft Clays

2.1 General

A computer program, Fast Lagrangian Analysis of Continua (FLAC), is used to model a water-filled membrane tube resting on very soft clay. FLAC is a finite difference and command-driven commercial software developed by ITASCA Consultants (Itasca Consulting Group, 1998).

In addition to the standard FLAC codes, a powerful programming language FLACish (FISH) is also used extensively. FISH is embedded in FLAC, and it gives the users the flexibility to write their own codes for their specific needs that are hard or impossible to be performed by using FLAC codes alone.

2.2 Foundation soils

FLAC has 10 built-in constitutive soil models. Three of them are used at this time – the null models, the Mohr-Coulomb soil model, and the elastic soil model. A null model is used for representing the materials or soils that are removed from the model. For the Mohr-Coulomb soil model, users are required to input the basic soil parameters such as bulk modulus, shear modulus, internal friction angle, apparent cohesion, tension, and dilation angle. In addition, FLAC also allows users to modify the built-in soil models to fit their needs.

The elastic soil model represents homogeneous, isotropic, and linear stress-strain soil behavior. It is less complicated and can be executed faster. However, it is used for testing the written FISH codes only because it does not represent the natural soil behavior very well. It cannot model the nonlinear stress-strain behavior and path-dependent deformation of the soil. Therefore, the Mohr-Coulomb soil model is used, which follows the Mohr-Coulomb failure criterion. For the saturated clay soil modeled in these analyses, the undrained, or $\phi = 0$, assumption is used. In this case, the Mohr-Coulomb failure criterion reduces to the Tresca criterion.

2.2.1 Soil properties

The soil used in the model is very soft clay with different shear strengths. It is also assumed to be fully saturated and in an undrained condition. The soil parameters are listed in Table 2.1.

Table 2.1: Soil properties for very soft clay

S_u (Pa)	4309 (90 psf)	3591 (75 psf)	2873 (60 psf)	2155 (45 psf)	1436 (30 psf)	1053 (22psf)	718 (15 psf)	240 (5 psf)	96 (2psf)
E_u (Pa)	1.72×10^6	1.44×10^6	1.15×10^6	8.62×10^5	5.75×10^5	4.21×10^5	2.87×10^5	9.6×10^4	3.8×10^4
B_u (Pa)	2.9×10^8	2.4×10^8	1.9×10^8	1.4×10^8	9.6×10^7	7.0×10^7	4.8×10^7	1.6×10^7	6.4×10^6
S_h (Pa)	5.7×10^5	4.8×10^5	3.8×10^5	2.9×10^5	1.9×10^5	1.4×10^5	9.6×10^4	3.2×10^4	1.3×10^4

Soil density: $\rho = 1441$ kg/m^3

Poisson's ratio: $\upsilon = 0.499$

Undrained shear strength of clay: S_u

Young's modulus of clay: $E_u = KS_u$

K is the clay modulus factor

Bulk modulus: $B_u = \dfrac{E_u}{3(1-2\upsilon)}$ (2.1)

Shear modulus: $S_h = \dfrac{E_u}{2(1+\upsilon)}$ (2.2)

It is assumed that the soil is highly plastic clay with the following index values:

Plasticity Index: PI = 42%

Liquid Limit: LL = 60%

Overconsolidation Ratio: OCR = 1

Based on the above-mentioned index values and the chart developed by Duncan and Buchignani (1987), K is approximately equal to 400. Therefore, $E_u = KS_u = 400S_u$.

2.2.2 Soil mesh

In FLAC, soil stresses are represented by the stresses in the center of grid zones (stresses are constant in an element). Soil movement is represented by the displacement of the grid. As the grid zones become finer, the soil stress distribution will be more accurate. Strain localization is also dependent on the size of the grid elements. For example, if the number of grid zones is insufficient in the plastic region, strain localization or shear bands may not be detected. There is no limit to how fine the grid mesh can be. But, the finer the grid mesh is, the longer the computer time that is needed to solve the problem.

The foundation soil mass for the above mentioned water-filled tube problem is represented by a finer grid mesh of 0.025m x 0.025m square grid zones embedded in the center of a coarse grid mesh of 0.05m x 0.05m square grid zones, as shown in Figure 2.1.

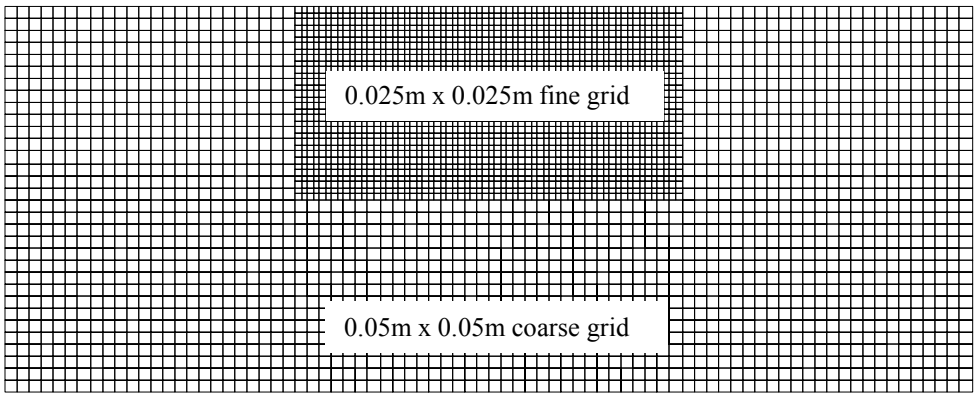

Figure 2.1: Soil mesh

An empty tube is placed on top of the fine grid mesh and then filled with water. This fine grid mesh takes care of the maximum stressed area of the soil mass. Most probably some part of this highly stressed soil will become plastic. The coarse grid mesh represents the less stressed soil. With the combination of fine and coarse grid meshes, tremendous stepping time is saved and the program is still able to obtain a good solution.

The overall soil mesh created is 4m long by 1.6m high and its grid zones are assigned the previously mentioned soil properties. The top of the soil mass is a free surface, which is allowed to settle or swell. The sides of the grid mass are allowed to move freely in the vertical direction

so as to simulate vertical displacement only, and it is assumed that there is no horizontal displacement at both sides. The base of the grid is fixed to simulate an underlying stiff soil condition. Each grid zone can be distorted so as to simulate the displacement of the soil that is subjected to load. Since the assigned Poisson's ratio of the soil is almost equal to 0.5, the grid zones can be distorted to different shapes but their size will remain essentially the same. Before the placement of any load, the initial stresses in the soil mass are determined based on the soil's own self-weight.

2.3 Tube

The tube is assumed to be indefinitely long, so it can reasonably be modeled two-dimensionally with a unit longitudinal length (1 m). The tube is modeled as many beam segments that are connected sequentially and form a closed loop. An inflated tube with its nodal numbers is shown in Figure 2.2. The example used here has 102 beam elements, $n_{beam} = 102$. If it were a full circle, its diameter, d, would be 1m. Therefore, each beam element length, l, is $\pi d/n_{beam}$. However, after the tube is filled with water, l will be longer than its original length since the tube material behavior follows Hooke's stress-strain law.

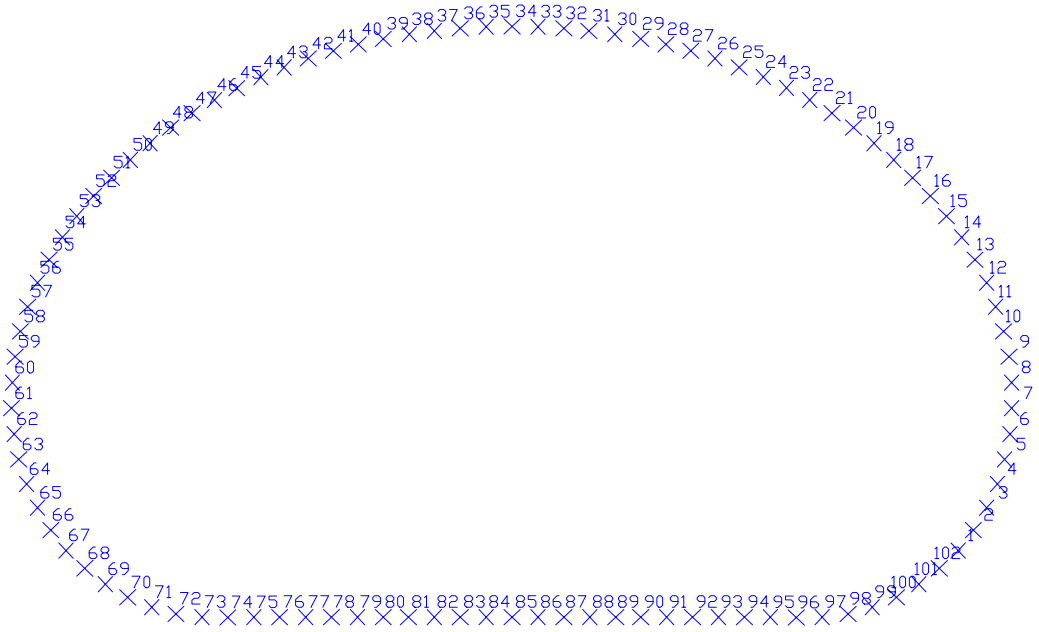

Figure 2.2: Inflated tube with its nodal numbers

The number of beam elements chosen in this example is arbitrary. However, it would be more realistic and accurate to use more beam elements. This is because in FLAC no load can be applied on the beam and only point loads can be applied at the nodes. The point load that is applied on the node is calculated based on the assumption that constant pressure is acting on its tributary area, although the hydrostatic pressure acting on the wall of the tube is not constant with respect to height. For more information about applying internal tube loads, please refer to the Internal Water Pressure section.

As the number of beam elements increases, or in other words, when the number of nodes increases, the error introduced in applying the hydrostatic water load on the nodes will be reduced. The distance between two nodes would be shortened and less area would be used in computing the load. Thus, the calculated point load magnitudes will be decreased and the point loads will be spaced more closely. Consequently, the tube will be curved nicely instead of bent sharply at the nodes. For example, the tube with 18 beam elements in Figure 2.3 is sharply bent at the nodes, whereas the tube with 102 beam elements shown later in Figure 2.7 is curved nicely throughout the tube. This is also due to the limitation of the finite difference method, which does not interpolate the stresses and deflections for a beam between two nodes. In other words, it only calculates the stresses and deflections at the nodes. However, if the number of beam elements goes to infinity, exact hydrostatic pressure will be applied on the tube.

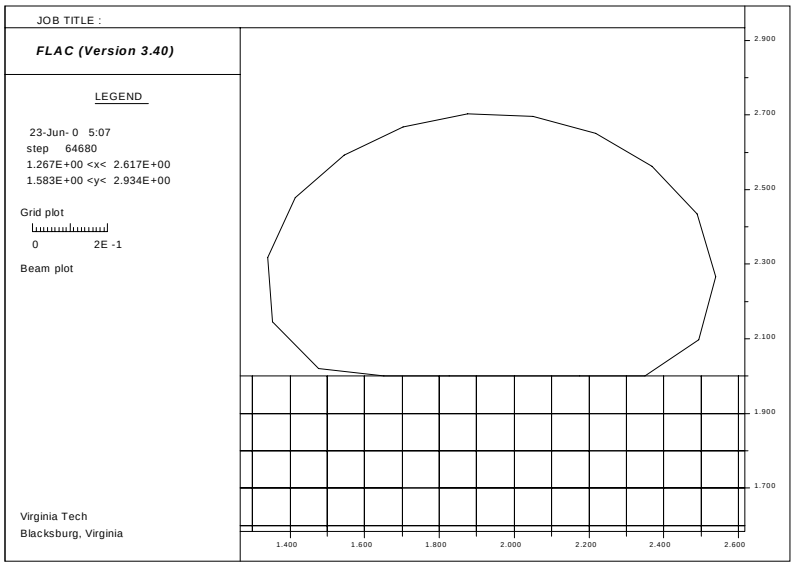

Figure 2.3: Tube with 18 beam elements.

2.4 Tube material properties

According to Van Santvoort (1995), a geomembrane of polyethylene is water-impermeable, elastic, and durable. This material works well in revetments of reservoirs and containing the liquid pollutants. Therefore, high-density polyethylene is chosen to be the suitable tube material. This material has a unit weight of 950 kg/m^3 and its modulus of elasticity ranges between 0.6 and 6 MPa (Van Santvoort, 1995). It is reasonable to choose 1 MPa to be the modulus of elasticity for the tube that is modeled here.

The effect of the tube thickness on the tube height above the stiff elastic ground is determined by varying the tube thickness from 2mm to 4mm. The results are shown in Figure 2.4. The 2mm, 3mm, and 4mm thick tubes lead to approximately the same tube heights corresponding to various internal water heads. This indicates that the behavior of the highly flexible tube is not highly sensitive to its thickness. A 3mm tube is chosen arbitrarily for this model.

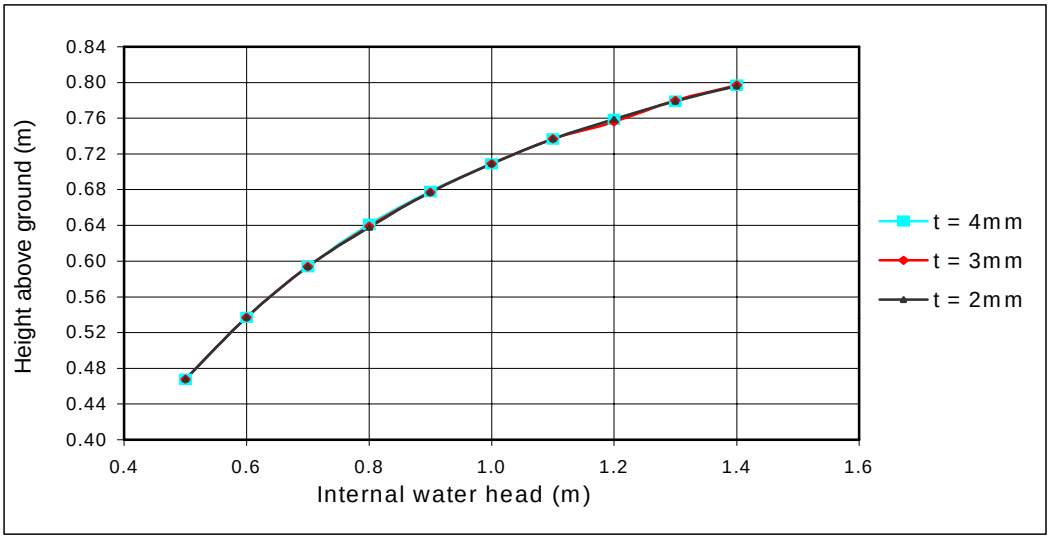

Figure 2.4: Water head vs. tube height above the ground level

2.5 Tube-soil interface properties

The interface is created to simulate the interaction between tube and soil. FLAC provides three types of interface. They are glued interface, Coulomb shear-strength interface, and tension bond. The Coulomb shear-strength interface is used in this model as it is governed by the Coulomb shear failure criterion. When the friction resistance and adhesion resistance are exceeded, the

tube will slide. The glued interface and tension bond interface are not suitable to be used in this model because there is no tension bond between the tube and the soil, and the tube should be allowed to separate from the soil freely.

For the Coulomb shear-strength interface, FLAC requires users to assign normal stiffness, shear stiffness, dilation angle, friction angle, and adhesion for the interface. The interface properties used in this model are:

Normal stiffness, $K_n = 1 \times 10^{9}\ ^{Pa}/_{m}$

Shear stiffness, $K_s = 5 \times 10^{8}\ ^{Pa}/_{m}$

Dilation angle = 0

Friction angle, $\delta = 0$

Adhesion, $a = \frac{1}{2}S_u$

Normal stiffness is required so that the soil mesh can hold the tube on its surface, otherwise the tube will penetrate into the soil mesh. It is good to set this stiffness as low as possible to speed up the convergence of the solution, but high enough to prevent significant penetration of the tube into the soil mesh. $K_n = 1 \times 10^{9}\ ^{Pa}/_{m}$ is selected arbitrarily and K_s is assumed to be half of K_n. Since the foundation soil is in an undrained condition, it is reasonable to assume that the tube-soil interface has an adhesion of half of the clay shear strength, and has no friction.

2.6 Internal water pressure

The tube is initially set flat on the ground. Then it is gradually filled up with a specified water head. A constant 1m water head above the datum is considered for this model, and is referred to the initial ground level. A specific FISH code is written to simulate the realistic filling process that gradually increases the applied nodal loads until they reach the maximum nodal loads, which correspond to the specified water head. This is to prevent sudden loading on the tube and soil.

Hydrostatic water pressure is assumed to act normal to the tangent of the internal tube surface. So the hydrostatic pressure inside the tube is determined by the difference in elevation between the datum and the point of interest as shown in the formula below:

$$P_{hy} = P_{datum} - (EL_{interest} - EL_{datum})\,\gamma_{water} \qquad (2.3)$$

where P_{hy} = hydrostatic pressure at point of interest

P_{datum} = hydrostatic pressure at datum

$EL_{interest}$ = elevation at point of interest

EL_{datum} = elevation at datum

γ_{water} = unit weight of water

For 2-D analysis, a unit width (1m) perpendicular to the cross section is assumed and the hydrostatic pressure is converted to force per linear meter. Since the distributed loads on the tube cannot be modeled by FLAC, the distributed loads are converted to point loads. These point loads are applied to the beam nodes. To illustrate this, two beam elements are extracted from the tube as shown in Figure 2.5.

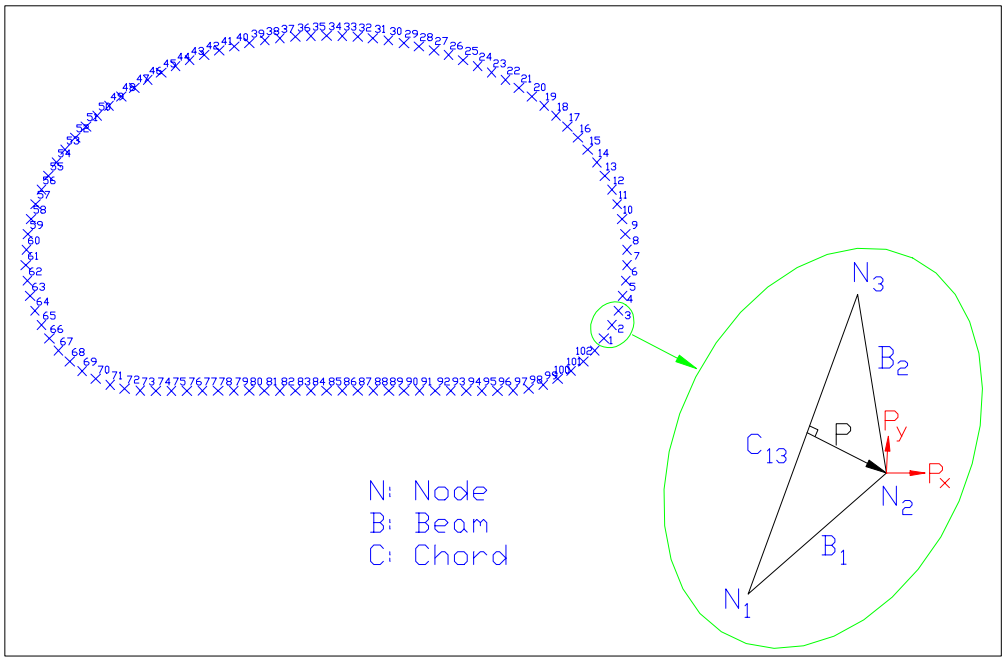

Figure 2.5: Illustration of internal tube loads

In order to simplify the computation of load, two assumptions are made. First, the equal length beam elements are assumed to be straight, and second, the distributed load is assumed to be constant acting from the mid-point of beam 1 (B_1) to the mid-point of beam 2 (B_2). Therefore,

the point load (P) at node 2 (N_2) is equal to the hydrostatic pressure (P_{hy}) at node 2 times 1m (1m strip) and times half of the lengths B2 and B1:

$$P = P_{hy} \times 1m \times l \tag{2.4}$$

where l is half of the length B_1 plus half of the length B_2

The load P is applied at node 2 in the direction perpendicular to the chord (C_{13}) connecting node 1 to node 3. Therefore, the vertical (P_y) and horizontal (P_x) force components are:

$$P_y = \frac{-P(x_3 - x_1)}{\text{length of } C_{13}} \tag{2.5}$$

$$P_x = \frac{P(y_3 - y_1)}{\text{length of } C_{13}} \tag{2.6}$$

A FISH code is written to apply these formulas to every node of the tube and is executed automatically by FLAC. As the nodal coordinates change, the nodal loads change, and the length and slope of the chord also change. FLAC automatically updates the new nodal load components caused by these changes.

In each FLAC calculation step, the position of each structural node (the connection between two beam elements) is retrieved from FLAC's internal data file. The formulas for calculating P_y and P_x use these new retrieved coordinates to compute new nodal loads. Then, these load components replace the old nodal loads in FLAC's data file. This procedure is repeated over and over until the system is in equilibrium.

The system is considered in equilibrium when the maximum unbalanced nodal forces at each grid point and at each structural node are small compared to the applied forces. The user has to choose this criterion, and it is usually considered sufficient when the ratio of the unbalanced force over the average applied force (equilibrium ratio) reaches 1%. Depending on the required degree of precision, one might use a higher or a lower equilibrium ratio to judge system equilibrium.

A more rational approximation would be:

$$P_y = \frac{-P(x_3 - x_1)}{2} \tag{2.7}$$

$$P_x = \frac{P(y_3 - y_1)}{2} \tag{2.8}$$

The equations 2.5 and 2.6 give slightly higher pressure on the tube than the equations 2.7 and 2.8 do. But, if the beams are collinear (angle between beams is 180°), these two sets of equations give the same pressure on the tube. Anyway, their $\frac{P_y}{P_x}$ ratios are the same, and the pressure difference is small and negligible. For example, Figure 2.6 shows that the tension forces in the tube obtained by these two sets of equations are apparently the same. The maximum difference in tensile forces is less than 0.2%. As shown in Figure 2.7, the tube shapes obtained by these two sets of equations also match each other. These indicate that the results obtained by equations 2.5 and 2.6 are almost the same as the results obtained by equation 2.7 and 2.8. Therefore, the nodal loads for all the future tubes will be calculated by equations 2.5 and 2.6, as they are considered more conservative. The foundation soil and tube properties used for testing these two sets of formulas are the same as those mentioned in Chapter 4, except the circumference is 1.486m.

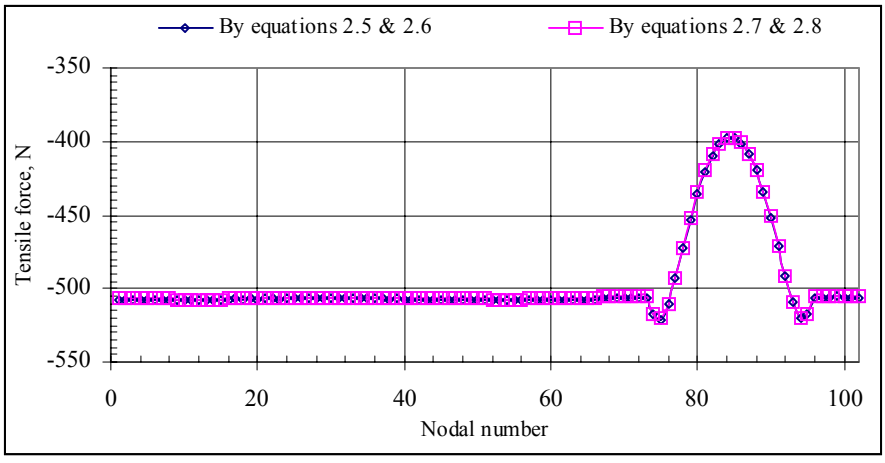

Figure 2.6: Tensile forces vs. position for two sets of equations

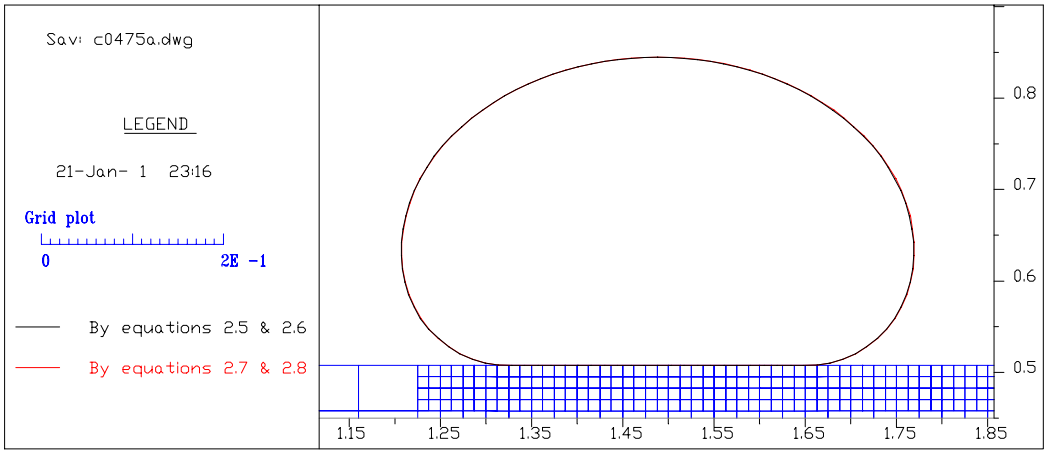

Figure 2.7: Tube shapes for equations 2.5 & 2.6, and equations 2.7 & 2.8

2.7 Results

Eight different shear strengths of clay are considered and each of them leads to a different height, settlement and width of the tube, as given in Table 2.2. The settlement, the height, and the width of the tube are controlled by three variables. They are the soil density, the soil shear strength, and the water head. The soil density in this model is fixed at 1441kg/m^3 and the water head is fixed at 1m above the initial ground level. The only variable then is the soil's shear strength. A detailed discussion of the results is presented in the following sections.

Table 2.2: Soil properties, tube height, tube settlement, and tube width

S_u (Pa)	a (Pa)	E_u (Pa)	B_u (Pa)	S_h (Pa)	*Tube height (m)	**Settlement m	Width (m)
4309 (90psf)	2155	1.72 x 10^6	2.9 x 10^8	5.7 x 10^5	0.71	0.00272	1.196
3591 (75psf)	1796	1.44 x 10^6	2.4 x 10^8	4.8 x 10^5	0.71	0.00322	1.196
2873 (60psf)	1436	1.15 x 10^6	1.9 x 10^8	3.8 x 10^5	0.709	0.00424	1.196
2155 (45psf)	1078	8.62 x 10^5	1.4 x 10^8	2.9 x 10^5	0.707	0.00771	1.196
1436 (30psf)	718	5.75 x 10^5	9.6 x 10^7	1.9 x 10^5	0.697	0.0646	1.187
1053 (22psf)	527	4.21 x 10^5	7.0 x 10^7	1.4 x 10^5	0.661	0.153	1.170
718 (15 psf)	360	2.87 x 10^5	4.8 x 10^7	9.6 x 10^4	0.617	0.252	1.146
240 (5psf)	120	9.6 x 10^4	1.6 x10^7	3.2 x 10^4	0.525	0.391	1.100
96 (2psf)	48	3.8 x 10^4	6.4 x10^6	1.3 x 10^4	0.504	0.428	1.091

*Maximum tube height above the original ground level.

**Maximum settlement below the original ground level.

2.7.1 Effects of soil's shear strength on the height, settlement, and width of the tube

Consider Figures 2.8 and 2.9, which show the water filled-tube resting on clay with S_u equal to 4309Pa (90psf) and 2873Pa (60psf), respectively. Although the soil shear strength is decreased by 30psf, from 90psf in Figure 2.8 to 60psf in Figure 2.9, visually they are not different except there is a slight grid deformation at the bottom of the tube in Figure 2.9. The numerical results in Table 2.2 show that the tube height above the ground is almost constant, 0.710m for S_u = 90psf and 0.709m for S_u = 60 psf. When looking at the tube settlement, the latter settles more than 50% when compared to the tube settlement of the S_u=90psf case. In both cases, the tube's width remains the same, which is equal to 1.196m.

The situation is getting worse in Figure 2.10. As before, there is a 30psf decrease in S_u from 60psf (2873Pa) in Figure 2.9 to 30psf (1436Pa) in Figure 2.10. But, both the shape and settlement of the tube change considerably. The top part of the tube still looks the same, but the bottom part of the tube becomes concave downward instead of flat. Table 2.2 shows that the height of the tube above the original ground is decreased by 12mm and the settlement of the tube is increased by 60mm when compared to the S_u = 60psf case. It is obvious that the increment of tube settlement is not proportional to the decrement of the soil's shear strength. The width of the tube becomes smaller; it changes from 1.196m in the S_u = 60psf case to 1.187m in the S_u = 30psf case.

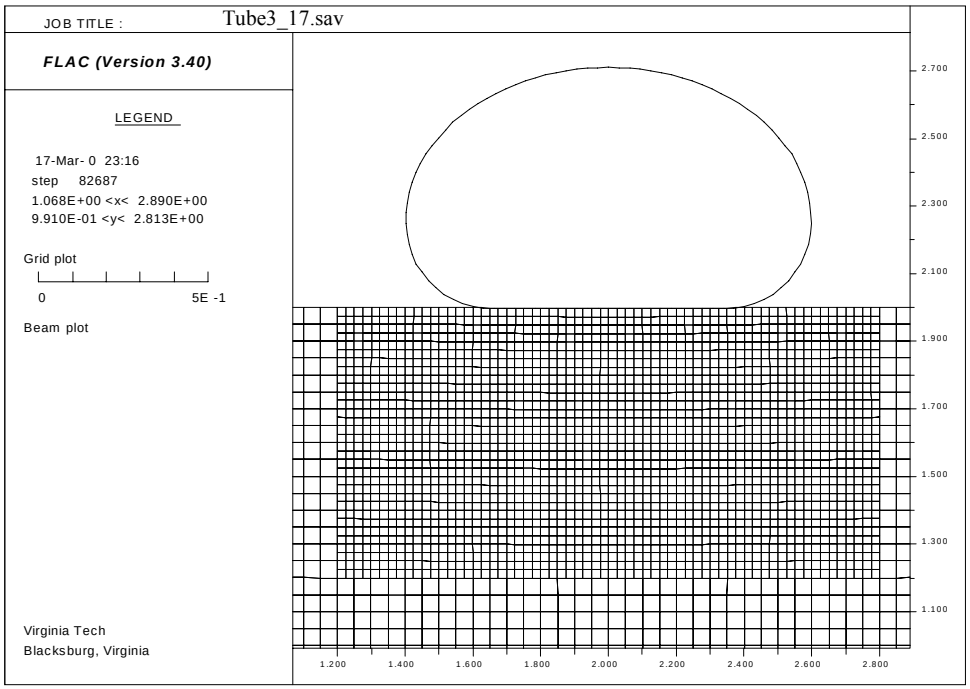

Figure 2.8: Tube on clay of 90psf shear strength

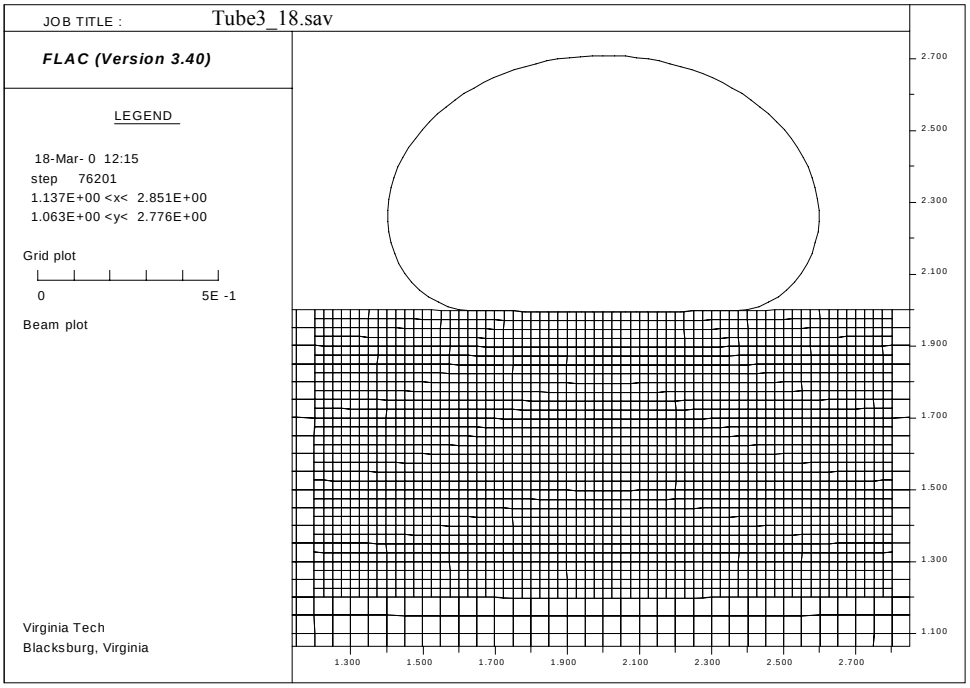

Figure 2.9: Tube on clay of 60psf shear strength

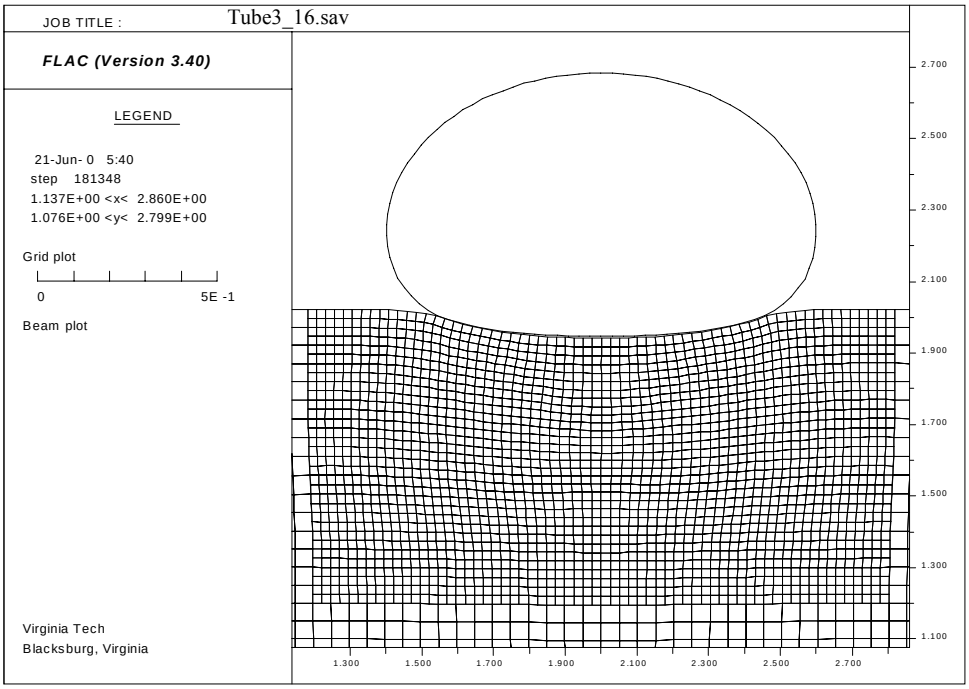

Figure 2.10: Tube on clay of 30psf shear strength

The tube becomes egg-shaped in Figure 2.11. The grids around the tube bottom are severely distorted. The original ground elevation is 2m, but now it raises up to approximately 2.08m at the sides of the tube. This is because in the undrained condition, when the tube settles, the soil underneath the tube is displaced to the side and thus the soil bulges upward. For example, Figure 2.12 shows that the soil underneath the tube settles downward but the soil beside the tube raises upward. Although the soil shear strength only decreases by 15psf from 30psf (1436Pa) in Figure 2.10 to 15psf (718Pa) in Figure 2.11, it has a tremendous effect on the tube's settlement, shape, and height. Table 2.2 shows that the height of the tube is decreased by 80mm (from 697mm to 617mm) and the settlement is increased by 187mm from the S_u = 30psf case. The width of the tube is decreased by 41mm, from 1.187m in the S_u = 30psf case to 1.146m in the S_u = 15psf case.

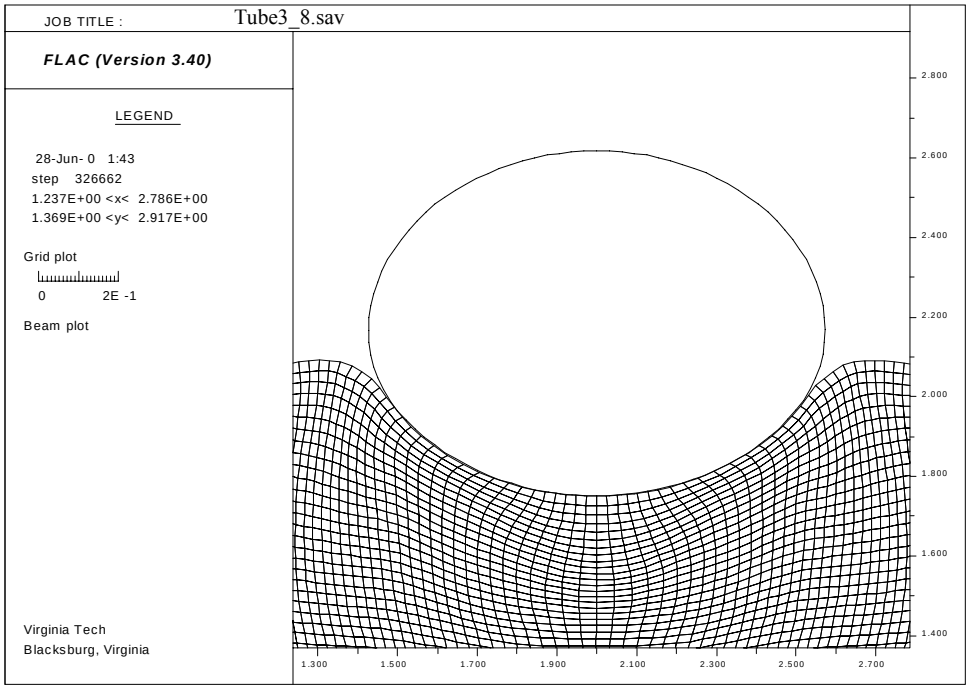

Figure 2.11: Tube on clay of 15psf shear strength

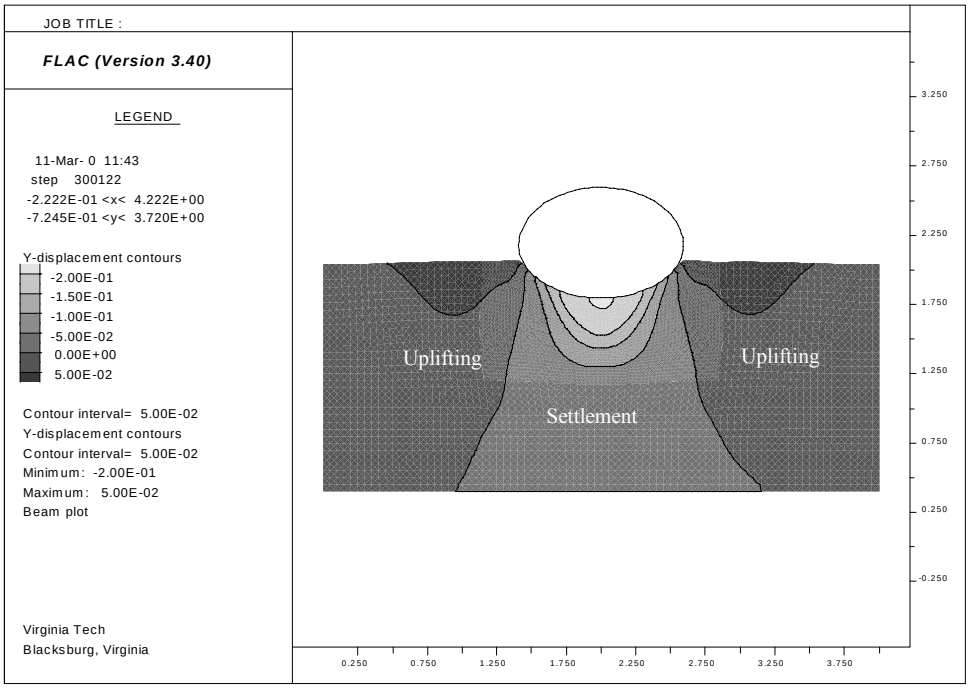

Figure 2.12: Tube on clay of 15psf shear strength that shows settlement and uplifting regions

Figure 2.13 shows a tube resting on clay of 5psf shear strength. This tube sinks 47% of its total volume into the ground. The soil beside the tube bulges up more compared to the previous case, which has a soil shear strength of 15psf. The top of the tube is 0.525m above the original ground surface, while the bottom of the tube is 0.391m below the original ground surface. The width of the tube is reduced to 1.1m.

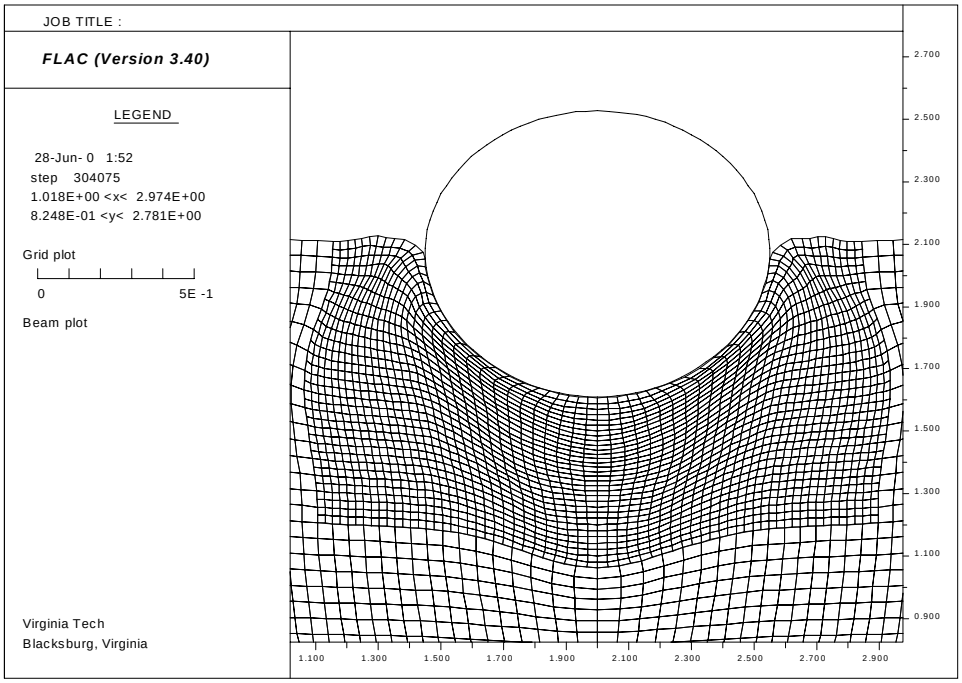

Figure 2.13: Tube on clay of 5psf shear strength

When the soil shear strength reduces to 2psf, the tube sinks even more and reaches 56% of its total volume into the ground, as shown in Figure 2.14. This is the last case for which the solution converged. The tube has almost the same shape but is in a different position when compared to the previous case. The tube height decreases to 0.504m, while the tube settles 0.391m below the initial ground level. The tube width is 1.091m, which is almost the same compared to the S_u = 5psf case.

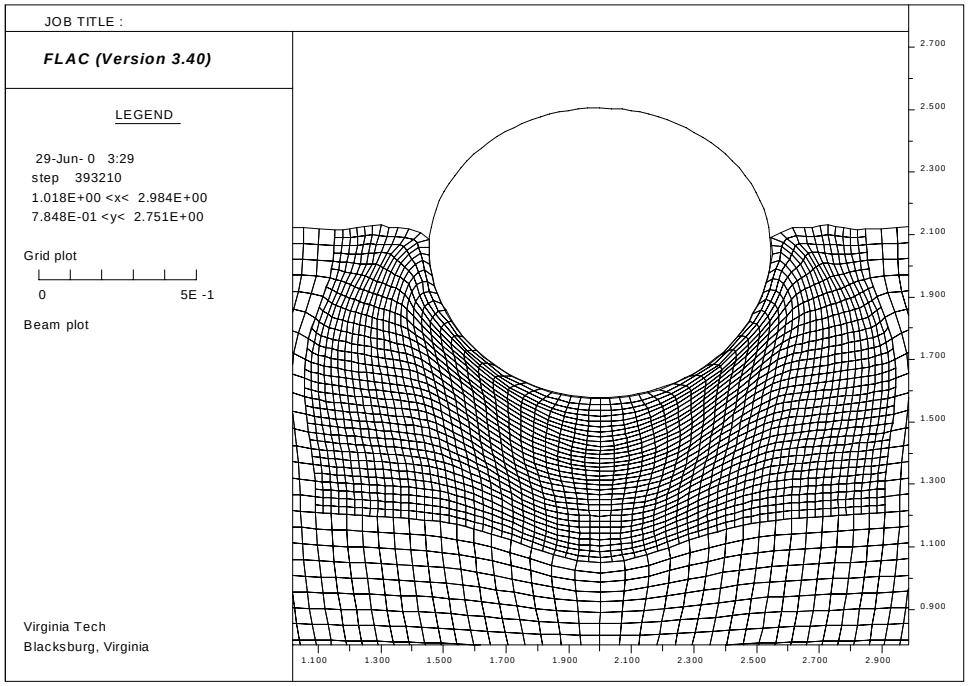

Figure 2.14: Tube on clay of 2psf shear strength

A plot of the tube width, height, and settlement versus shear strength is shown in Figure 2.15. For graphical definitions of tube width, tube height, and tube settlement, please refer to Figure 2.17. The curves for the tube width and the tube height above the original ground level versus shear strength in Figure 2.15 are almost horizontal when the shear strength of the clay is stronger than 36psf (1750Pa). The slope becomes steeper as the tube height decreases when the shear strength approaches 0 from 36psf.

The curve characteristic for the tube width versus shear strength is similar to the curve characteristic for the tube height versus shear strength. The only difference is that in the soft clay region its slope is smaller than the slope for the curve of the tube height versus shear strength.

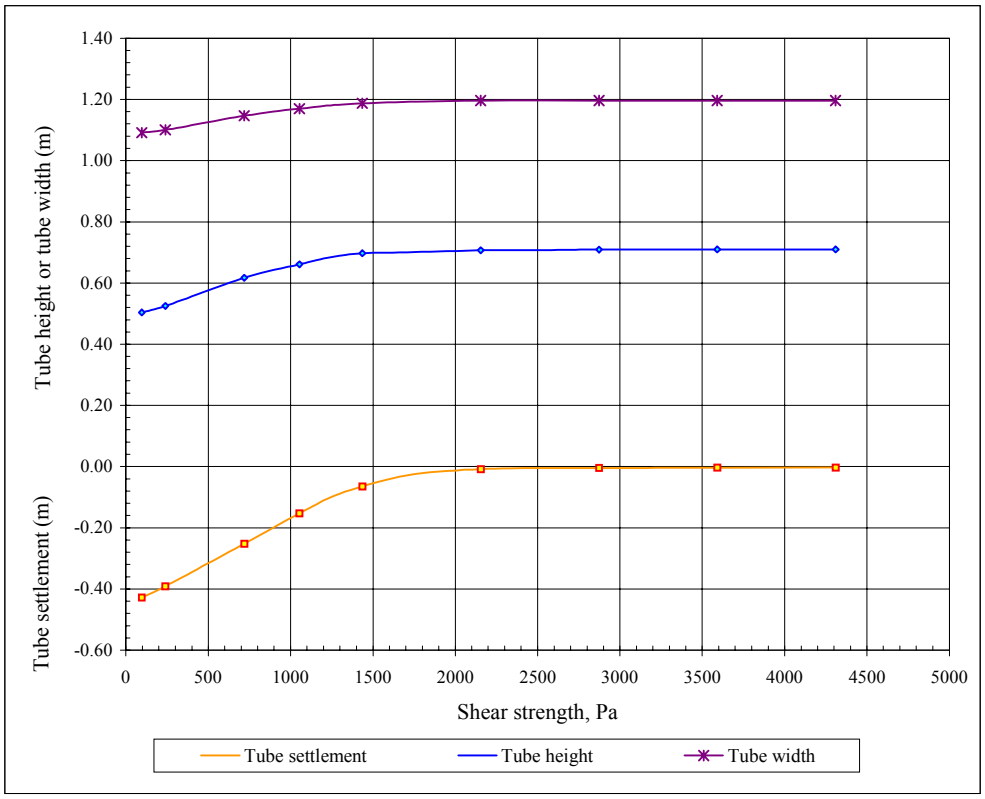

Figure 2.15: Tube width, tube height, and tube settlement versus shear strength of the clay

The curve for the settlement below the original ground level versus shear strength has an approximately horizontal slope when the shear strength of the clay is stronger than 45psf (2150Pa). It increases progressively when the shear strength decreases from 45psf. When the shear strength is below 30psf (1436Pa) the curve becomes almost a straight line, which indicates that the settlement increases with a constant rate. These curve characteristics show that the water-filled tube settles more when the clay shear strength decreases, and one may want to classify the shear strength between 45psf and 30psf as the transition zone. Above the transition zone (i.e., for higher shear strengths), the tube settles very little, but before the transition zone, the tube settles much more.

By looking at both the tube height and tube settlement curves, one may notice that they are parallel to each other when the shear strength is high. When the shear strength decreases, the vertical distance between the two curves increases, and the slope for the tube height versus shear strength increases slower than the slope for the tube settlement versus shear strength. This

indicates that the magnitude of the increase in settlement does not match the magnitude of the decrease in tube height because the tube bottom becomes rounder when the ground become softer.

When the tube settles, the internal hydrostatic pressure at the bottom of the tube increases. This can be visualized by assuming a constant water head supplied by a pump to the tube. For all the cases in this example model, the water head is maintained at 1m above the original ground surface. As the tube is filling up, the ground settles, and the water head at the bottom of the tube will be increased in proportion to the amount of settlement of the tube.

With the combination of the increased internal hydrostatic pressure head and the rounder tube shape, more water will be filled to maintain the constant water pressure at the datum. For instance, the red curve in Figure 2.16 shows that the total water load in the tube increases when the shear strength decreases from 35psf (1676Pa).

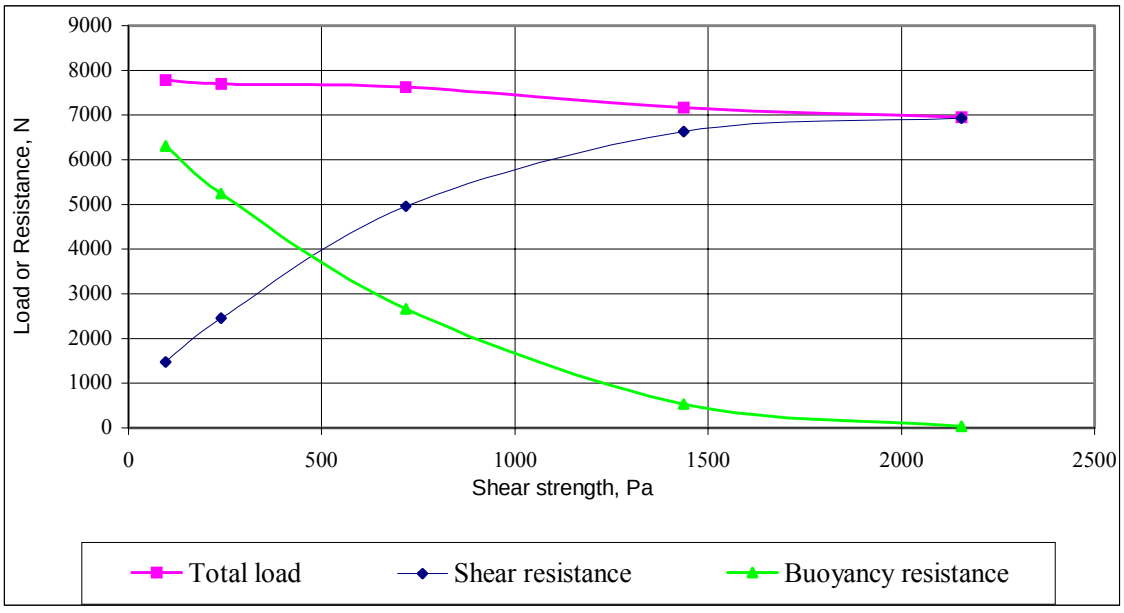

Figure 2.16: Total load, shear resistance, and buoyancy resistance versus shear strength

When the shear strength decreases, as shown by the blue curve in Figure 2.16, the shear resistance to the load also decreases. This causes the tube settlement to increase. As the tube settlement increases, the buoyancy resistance to the load increases as illustrated by the green curve in Figure 2.16.

The soil density has direct impact on the buoyancy resistance. A soil with higher density provides higher buoyancy resistance, and hence reduces the tube settlement. The sum of the shear resistance and buoyancy resistance has to be equal to the total load in order to maintain the system in an equilibrium state.

2.7.2 Tube load and soil resistance

A spreadsheet is utilized to calculate the total water load. Because the tube is not perfectly round or elliptical, there is no specific formula that can be used to calculate the tube volume. Therefore, the tube volume is approximated as follows.

First, FLAC outputs the tube's nodal coordinates and the first and last contact points between the tube and the ground surface. Take the average level of the first and the last contact points as the fixed reference level, which is the horizontal straight line inside the tube shown in Figure 2.17. Next, break the tube into many little trapezoidal shapes corresponding to the nodal positions, as shown in the enlarged portion of Figure 2.17.

To compute the area for each trapezoidal piece, the horizontal distance and the average height above the reference level between two consecutive nodes are first calculated. For example, to calculate the trapezoidal piece bounded by node 11 and node 12, shown in the enlarged portion of Figure 2.17, the following formulas are used:

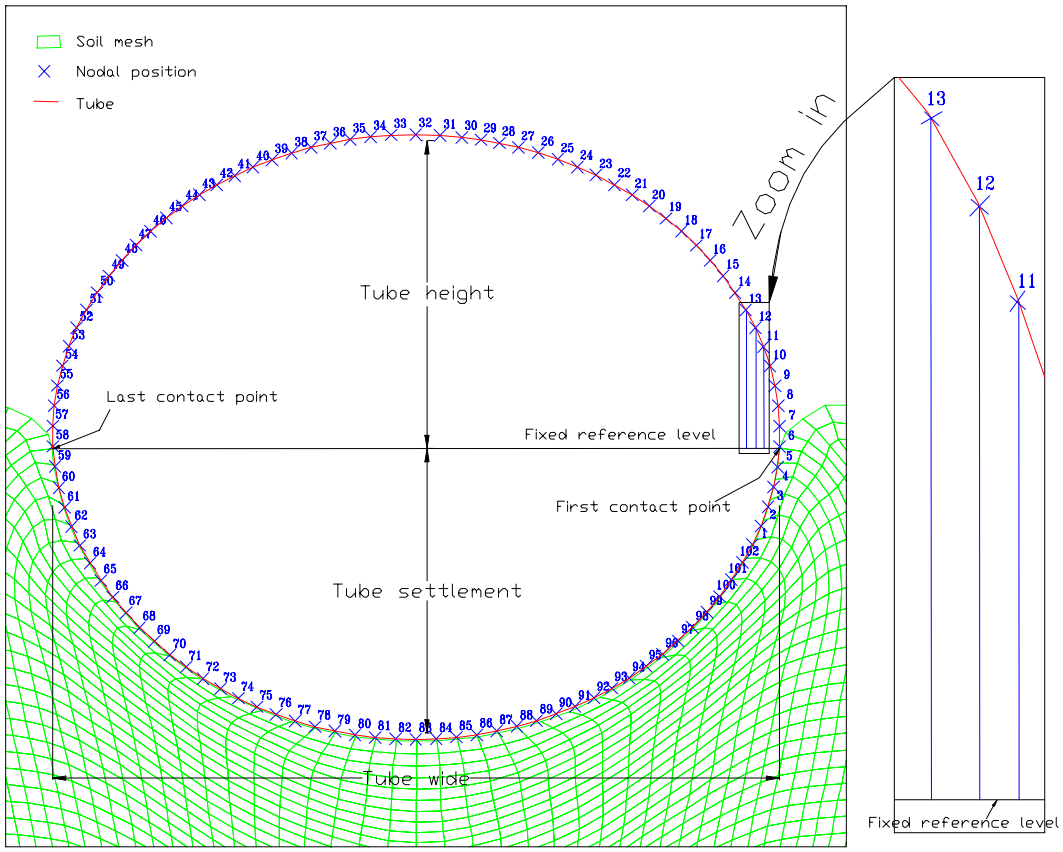

Figure 2.17: Cross-section of a typical tube.

$$D_h = X_{11} - X_{12} \tag{2.9}$$

$$D_v = \frac{(Y_{11} - RL) + (Y_{12} - RL)}{2} \tag{2.10}$$

$$\text{Area} = D_h \times D_v \tag{2.11}$$

where D_h = horizontal distance between node 11 and node 12.

X_{11} = x-coordinate for node 11

X_{12} = x-coordinate for node 12

D_y = Average height above the fixed reference level

Y_{11} = y-coordinate for node 11

Y_{12} = y-coordinate for node 12

RL = fixed reference level

Area = area of the trapezoidal piece bounded by node 11 and node 12 at the top.

Carry out the same procedure for the rest of the pieces except for the trapezoidal pieces below the fixed reference level, in which D_v is the average deflection below the reference level instead of the average height above the reference level. The total area is the summation of all the little trapezoidal areas. Since a unit length perpendicular to the paper is assumed, the total area is also the total volume of the tube and the total load is the product of the total volume and the unit weight of the water.

The total buoyancy resistance is the product of the total integrated areas below the fixed reference level and the unit weight of the soil. In an equilibrium condition, the total load has to be equal to the total reaction; therefore, the total vertical shear resistance is the total load minus the total buoyancy resistance.

2.7.3 Tensile forces in the tube

Special attention may be required for the tensile stresses in the tube wall. These stresses increase as the tube settles. Figure 2.18 illustrates the relationship between the maximum tensile force and the clay shear strength in a one-meter strip of tube. The tensile force increases progressively when the shear strength of the clay decreases toward zero from 60psf (2873Pa). The maximum tensile force in the tube is constant when the shear strength of the clay exceeds 60psf. The maximum tensile force increases as the shear strength decreases because lower shear strengths produce more settlement and higher water pressure in the tube.

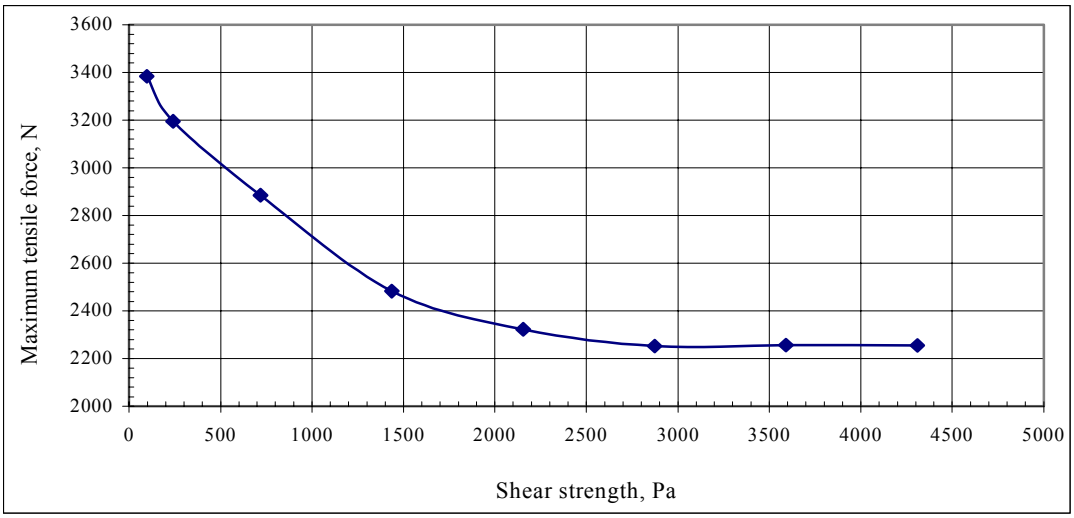

Figure 2.18: Maximum tube tensile force versus shear strength of the clay

Figure 2.19 illustrates the relationship between tensile force and nodal location for the S_u = 90psf case through the S_u = 5psf case. Rough nodal locations are shown in Figure 2.2 of section 2.3, but the exact nodal positions are different. This is because the tube shape and the amount of settlement are different for each case.

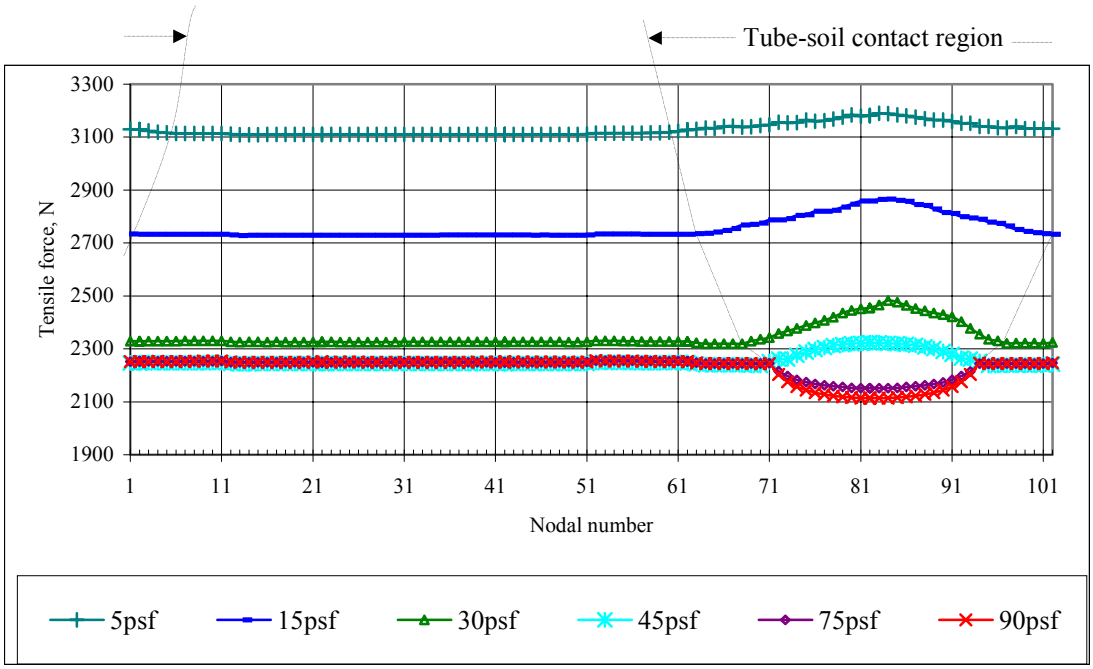

Figure 2.19: Tensile force versus nodal number (position)

Tensile forces in the tube for the S_u = 90psf, the S_u = 75psf, and the S_u = 45psf cases are essentially the same except at the soil-tube contact regions, in which the traction forces provided by the soil come into play. The stronger the soil, the greater traction force will be provided by the soil to reduce the tension force in the tube where it contacts the soil. For example, S_u = 90psf is the strongest soil considered among all the cases. Its curve in the tube-soil contact region decreases the most, followed by the S_u = 75psf case. For these two cases, the lowest tensile force occurs at the center of the bottom of the tube.

When it comes to the S_u = 45psf case, the situation changes. The curve in the tube-soil contact region rises. This is because this soil is softer and it leads to more settlement. Settlement causes higher hydrostatic pressure at the bottom of the tube, and weak soil reduces the traction that it provides to act against the tensile force at the bottom of the tube.

When the soil's shear strength becomes weaker than 45psf, the whole curve shifts upward. This means that the tensile forces in every part of the tube increase, especially at the bottom of the tube. This is because the whole tube sinks downward and its bottom becomes rounder. Figure 2.19 also illustrates that the maximum tube's tensile force shifts from the unrestrained side of the tube to the center-bottom of the tube as the shear strength of the clay decreases from 90psf to 5psf.

It is interesting to note that the tensile force is constant in the part of the tube that is not in contact with the soil. The old version of FLAC 3.40 was used to perform all the calculations except the 5psf and 15psf cases. A revised FLAC 3.40 is used in analyzing these two cases.

2.7.4 Vertical soil stresses

Soil vertical stress contours in Figure 2.20 and Figure 2.21 illustrate that the loading of the tube affects the stresses in the soil to a greater depth for the stronger soil than the softer soil. The soil stresses beneath the tube in Figure 2.20 increase tremendously to some depth. For instance, in Figure 2.20, the soil stresses represented by the yellow contour band, which has soil stress between 10,000 Pa and 15,000 Pa, extend all the way to the surface right beneath the tube. In

addition, the purple and red contour bands are concave upward. It is obvious that the loading of the tube has increased the soil stresses beneath the tube. On the other hand, the contours shown in Figure 2.21 are almost straight lines. It is difficult to see that the loading of the tube has an effect on soil stresses on this soft soil.

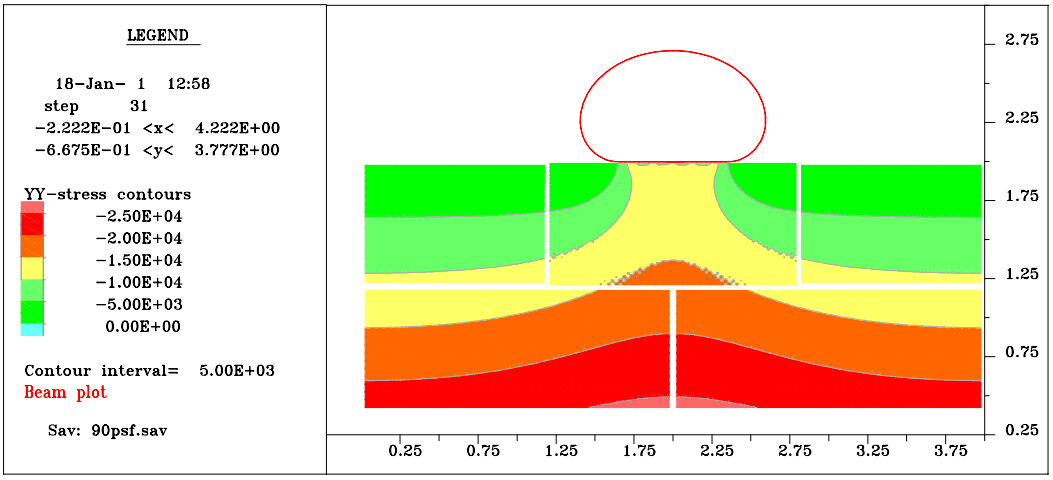

Figure 2.20: Soil stress contours for S_u = 90psf case

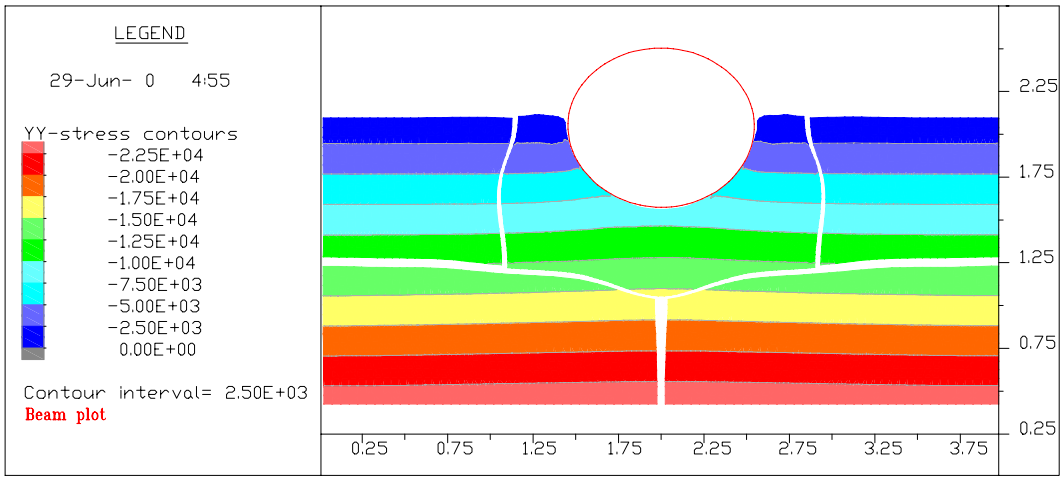

Figure 2.21: Soil stress contours for S_u = 2psf case

2.7.5 Settlement of the soil

Both strong soil and soft soil settle when subject to load. As shown in Figure 2.22 and Figure 2.23, their settlement contours have similar shapes but have different magnitudes. The soft soil settles more than the strong soil.

One might notice that the ground surface in Figure 2.23 is higher than the ground surface shown in Figure 2.22. The original ground level is 2m, but in Figure 2.23, it reaches above 2.1m. This indicates the uplift of the soil or the volume of soil displaced by the tube. If the length of the mesh were longer, the uplift magnitude may be reduced. The height of the tube above the original ground level could be lower and the tube could settle more.

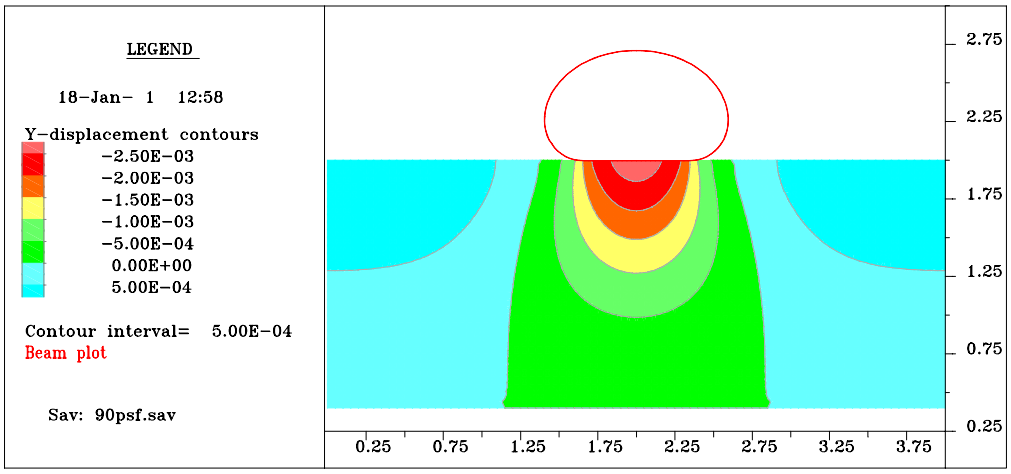

Figure 2.22: Soil deflection contours for S_u = 90psf

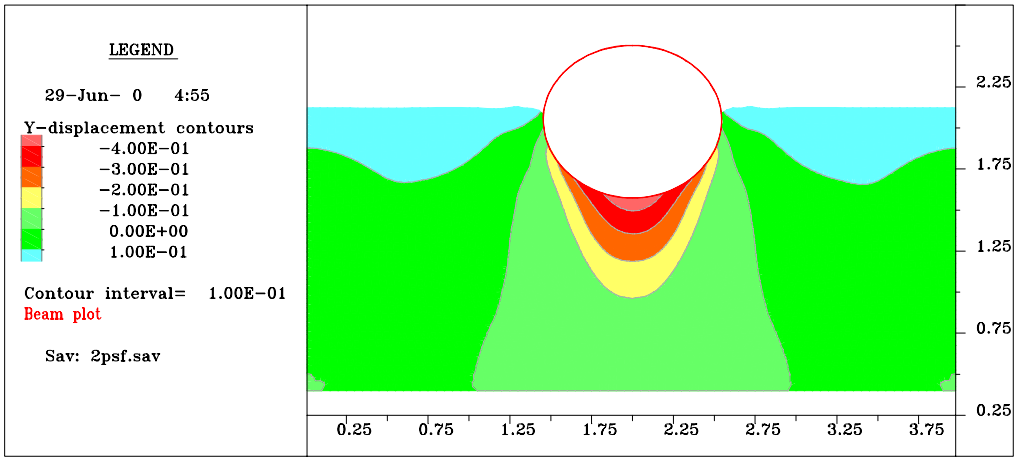

Figure 2.23: Soil deflection contours for S_u = 2psf

2.8 Limitations

Unfortunately, when the shear strength is too low, the solution does not converge. Figure 2.24 shows an unconverged solution for a tube resting on very soft clay of 1psf (48Pa) shear strength. The program is unable to proceed further due to the bad grid geometry at the bottom of the tube. This bad geometry is due to the over-distortion of grid zones.

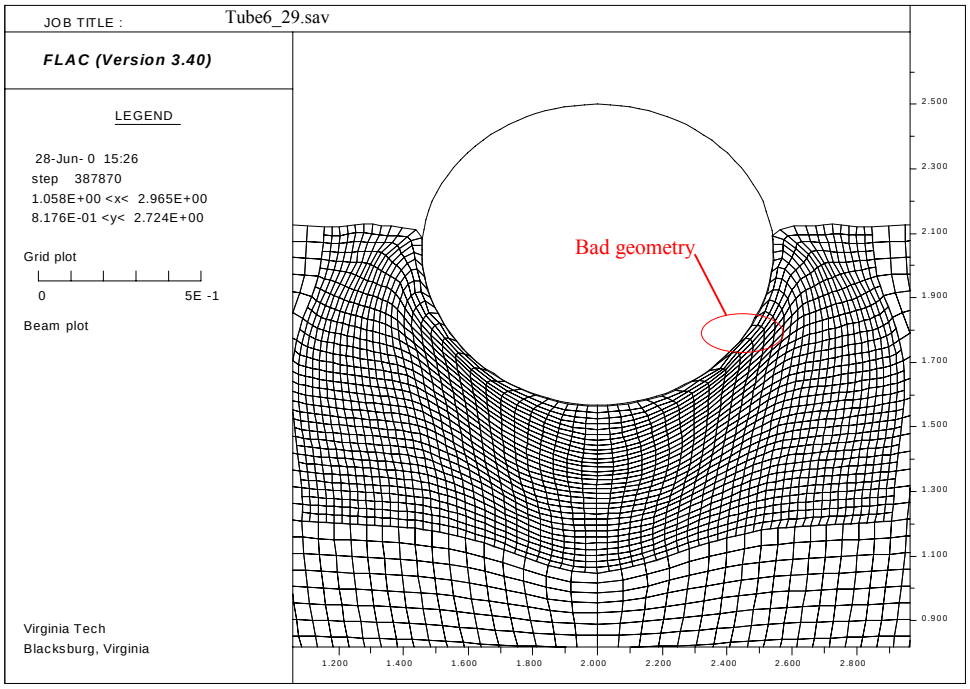

Figure 2.24: Tube on clay of 1psf shear strength, unconverged solution.

Chapter 3

Stability of a Single Tube Without Pore Pressure Effect

3.1 Introduction

The main objective of this chapter is to study the stability of a single tube associated with the critical flood water levels above the ground surface and the heights and shapes of the triangular wooden blocks. The effect of pore pressure on the stability of the tube is neglected. The tube tensile force and the soil stress just before the tube becomes unstable will be investigated.

3.2 Soil

The soil is assumed to be mica schist sand and has an internal friction angle of 36° and dry density of 1600kg/m^3. The pore water pressure effect on the rolling and sliding of the tube is neglected. Since the elastic soil model is the simplest and can be executed faster than any other soil models provided in FLAC, it is used in this preliminary testing.

Figure 3.1 shows the soil mesh for the model. This mesh has a fine and uniform grid at the center. As it extends to the sides and to the bottom of the soil mesh, the grid becomes coarser. This arrangement of fine and coarse grids is used to reduce the number of grid elements in the soil mesh, and thus the solution can be obtained faster.

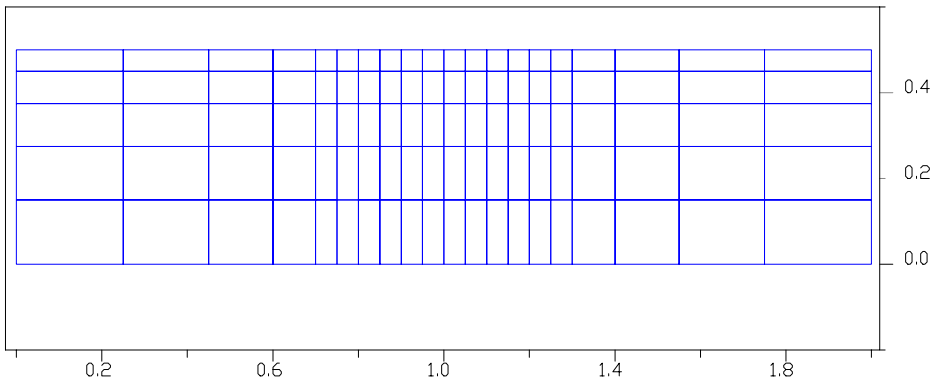

Figure 3.1: Grid layout for the soil mesh.

The flow of groundwater and the effect of pore pressure are not modeled in this chapter. The bulk modulus is assumed to be 50MPa, so that no significant settlement will occur under the tube. The shear modulus is assumed arbitrarily to be 30MPa.

3.3 Tube

The tube formulation and internal pressure formulation are the same as in sections 2.3, and 2.6, respectively. In addition to the discussion in section 2.6, the concept of internal tube pressure is further illustrated in Figure 3.2. The tube circumference in this model is 1.47m, and the tube internal pressure head is fixed at 0.46m above the original ground level. This is also the diameter of the tube if it were perfectly circular and unstrained. Fixed internal pressure head is maintained throughout the test by letting the water supply inlet be opened and connected to the fixed water source. The wall of the tube is 0.508mm thick. It is assumed that the tube is made up of a smooth PVC geomembrane and has a modulus of elasticity of 1GPa.

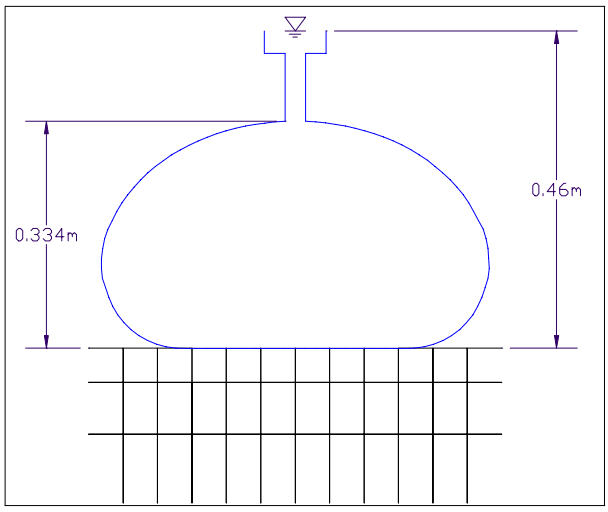

Figure 3.2: Illustration of fixed internal tube pressure

3.4 Interface properties

According to Koerner (1994), the interface friction angle between mica schist sand and smooth PVC geomembrane can be estimated as 0.79 times the internal friction angle of mica schist sand. Potyondi (1961) reported that the friction angle between dense sand and wood can be estimated

as 0.79 times the internal friction angle of sand, provided the wood is sheared parallel to the grain. Based on these two concepts, the interface properties used in this model are as follows:

Soil-tube = 28°

Wood-soil = 28°

It is assumed that the interface between wood and tube is 15° since this interface is most probably wet and slippery.

3.5 Block shapes

A triangular block that is made up of wood and hollow in the center is placed at the right side of the tube to stop the tube from rolling. Three basic triangular block shapes are considered, and they are shown in Figure 3.3.

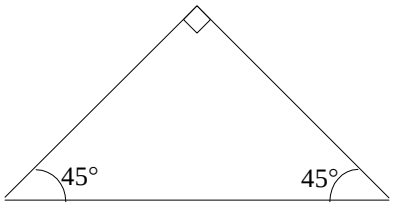

Shape 1: 45° – 90° – 45°

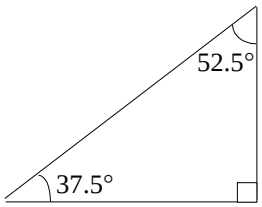

Shape 2: 37.5° – 52.5° – 90°

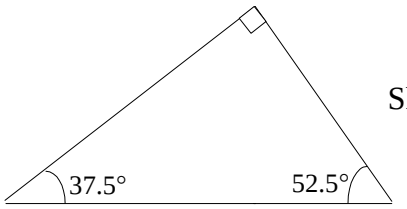

Shape 3: 37.5° – 90° – 52.5°

Figure 3.3: Shapes of blocks

Each of these wooden blocks is modeled by 12 beam elements, which include 8 beam elements for the left edge, 3 beam elements for the base, and 1 beam element for the right edge. Douglas fir's properties are assigned to each of these beams. These properties are as follows:

Modulus of elasticity = 10.8 GPa

Density = 450 kg/m^3

Thickness = 2.5 cm

It is assumed that this wood has unlimited yield strength.

3.6 External water

After a block is placed on the right side of the tube, the external water pressure is applied on the left side of the tube. A FISH function is written to find the highest node in the tube subjected to external water and the first left tube-soil contact node, then to convert the external water pressure to point loads, and apply these point loads on the structural nodes between the highest node and the first left tube-soil contact node. The formulation of these nodal loads is the same as equations 2.4, 2.5, and 2.6, but the load is applied in the opposite direction. The magnitude of the external water head is to be input manually. As was discussed in section 2.6, FLAC will update the new nodal loads based on the level of external water and the coordinates of the nodes automatically at each calculation step. For further information, a sample program file, fwload.dat, is included in Appendix A.

3.7 Results

A water head of 0.46m above the original ground level is assumed for all cases. This water head leads to a 0.334m initial tube height as shown in Figure 3.2. After the floodwater load is applied, the tube shape and height change, depending on the flood water level and the height of the block. The equilibrium ratio that was mentioned in section 2.6 is used to judge the system equilibrium. This ratio is set at 1%, which means when the unbalanced force becomes less than 1% of the average applied force, FLAC will automatically stop the calculations.

3.7.1 Floodwater levels and tube heights associated with block heights and block shapes

Table 3.1 presents the computer results that include the new tube heights corresponding to the floodwater levels above the ground level and the block heights. It also gives the minimum floodwater levels that cause the tube to roll over the blocks of different sizes and shapes.

Table 3.1: Computer results.

Block Geometry	Block height (m)	Flood water level (m)	Tube height (m)	Tube width (m)
Shape 1	0.06	0.23	0.3635	0.5362
		0.24	Rolling over the block	
	0.09	0.27	0.3779	0.5365
		0.28	0.3798	0.5289
		0.29	Rolling over the block	
	0.12	0.31	0.3919	0.5245
		0.32	Rolling over the block	
Shape 2	0.06	0.23	0.3635	0.5361
		0.24	Rolling over the block	
Shape 3	0.12	0.31	0.3935	0.5305
		0.32	Rolling over the block	

The results indicate that the critical water levels are the same for all the considered block shapes that have same block height. For example, both block shapes 1 and 2 with 0.06m block height lead to a 0.23m critical floodwater level. Both block shapes 1 and 3 with 0.12m block height lead to a 0.31m critical floodwater level. The increment in the floodwater level used in the testing is 0.01m. The critical floodwater levels could be different for the different block shapes with the same block height if a finer floodwater level increment were used in the testing.

When the block height is equal to 0.06m, the tube height at the critical floodwater level is the same for shape 1 and shape 2. When the block height is equal to 0.12m, the tube height for shape 1 is only slightly lower than the tube height for shape3. These results indicate that the tube height is not sensitive to the block shape.

The relationship between critical floodwater levels and block heights, and the relationship between critical tube heights, critical tube widths and block heights are shown in Figure 3.4. Both critical water level and new tube height have almost a linear relationship with the block height. But the slope for the critical water level curve is steeper than the slope for the critical tube height curve. This means that the critical water level curve will eventually cross the critical tube height curve, and thus the floodwater will overflow the tube if the wooden block is big enough to resist the tube from rolling over it.

The tube width curve shows that the tube width decreases as the tube height increases. The slope of the tube width curve is gentler than the slope of the tube height curve, indicating that the tube width decreases at a slower rate than the increasing rate of the tube height.

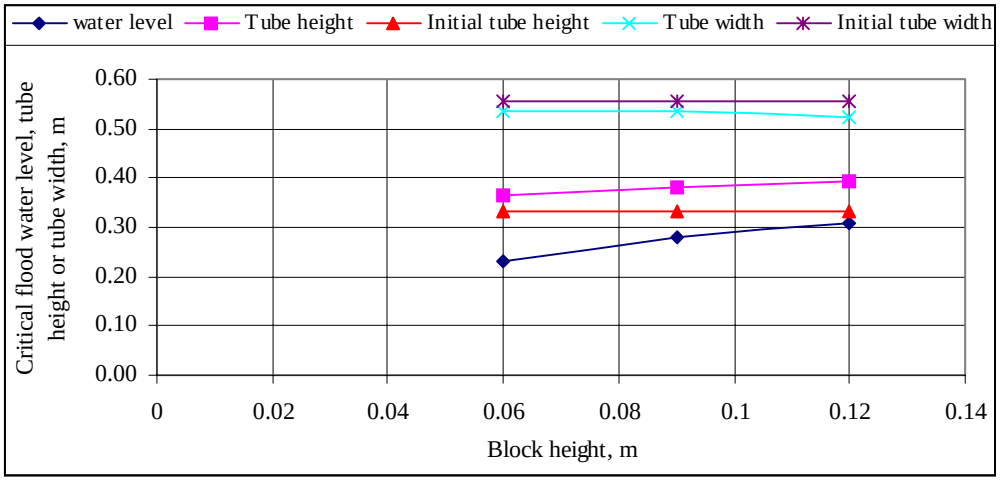

Figure 3.4: Critical floodwater level, tube height and tube width versus block height.

3.7.2 Tube shapes

Tube shapes at the critical flood water level and just before rolling over the block are shown in Figure 3.5 through Figure 3.14. Please note that the solutions at failure are not converged. Figures 3.6, 3.8, 3.10, 3.12, and 3.14 illustrate that the tube fails in rolling, and the tube will continue to roll.

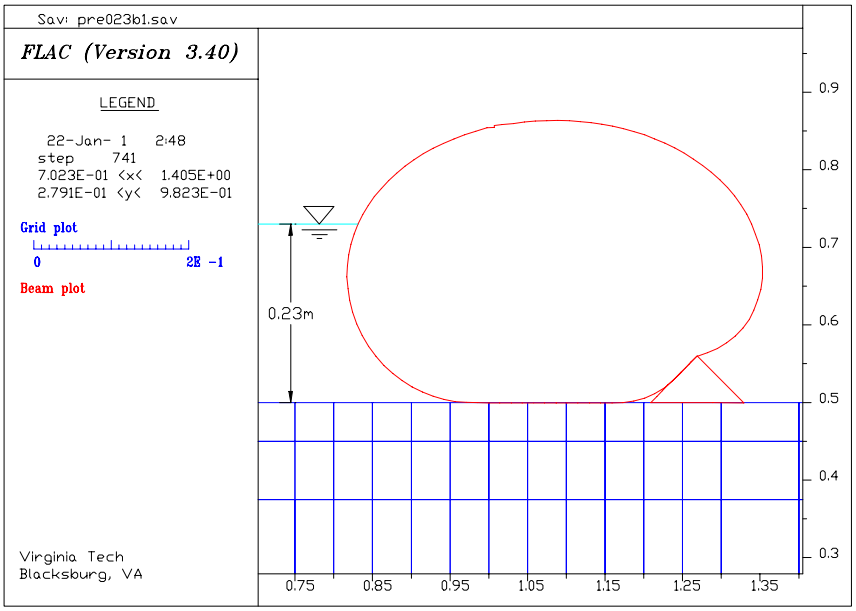

Figure 3.5: Block shape 1, block height = 0.06m, flood water level = 0.23m.

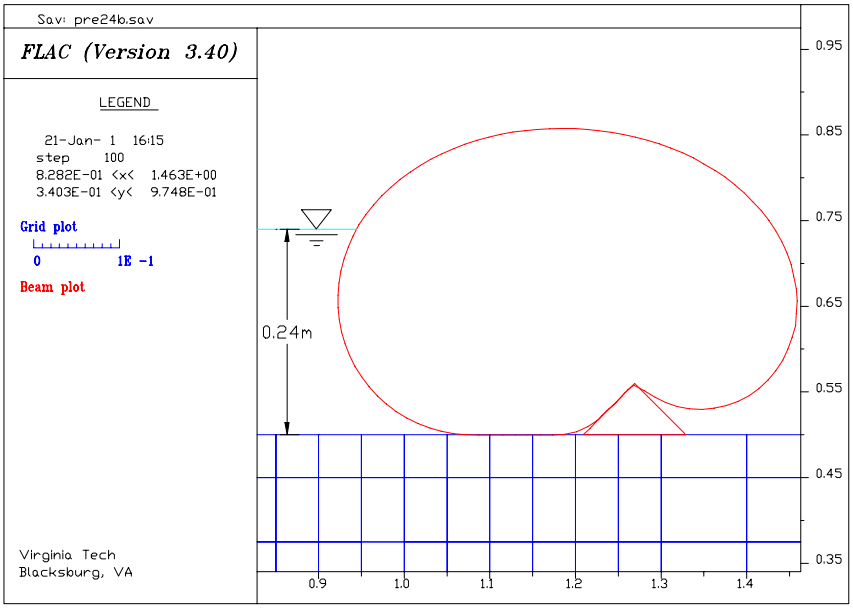

Figure 3.6: Block shape 1, block height = 0.06m, floodwater level = 0.24m.

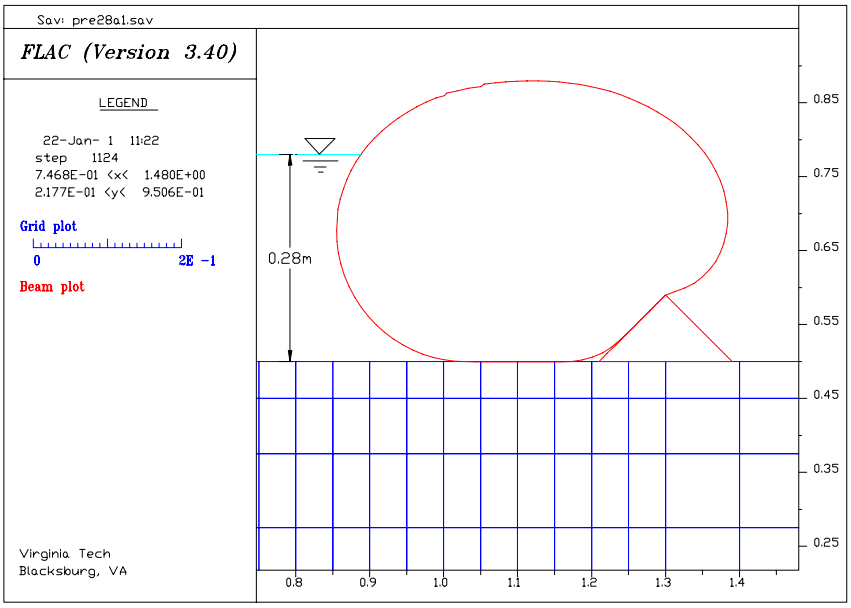

Figure 3.7: Block shape 1, block height = 0.09m, floodwater level = 0.28m.

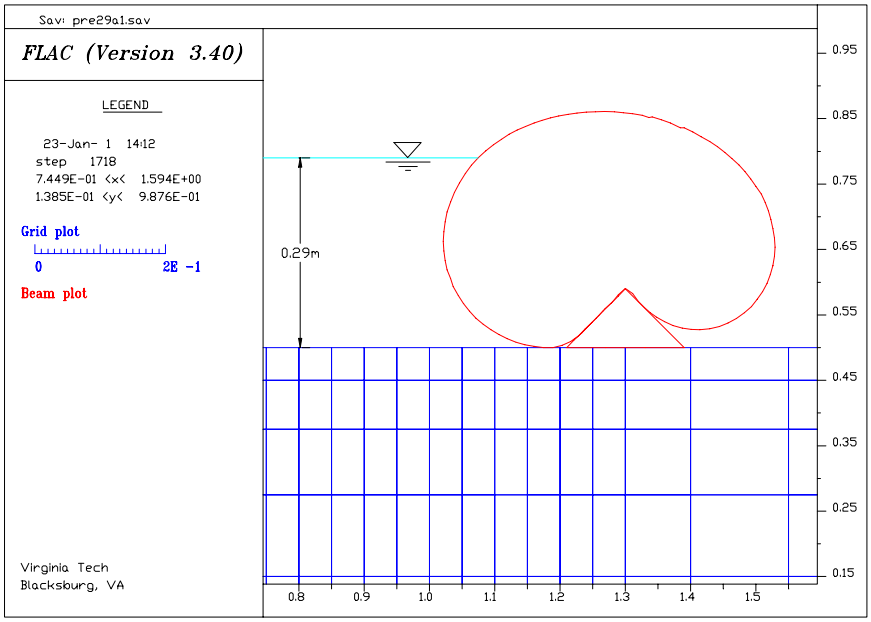

Figure 3.8: Block shape 1, block height = 0.09m, floodwater level = 0.29m.

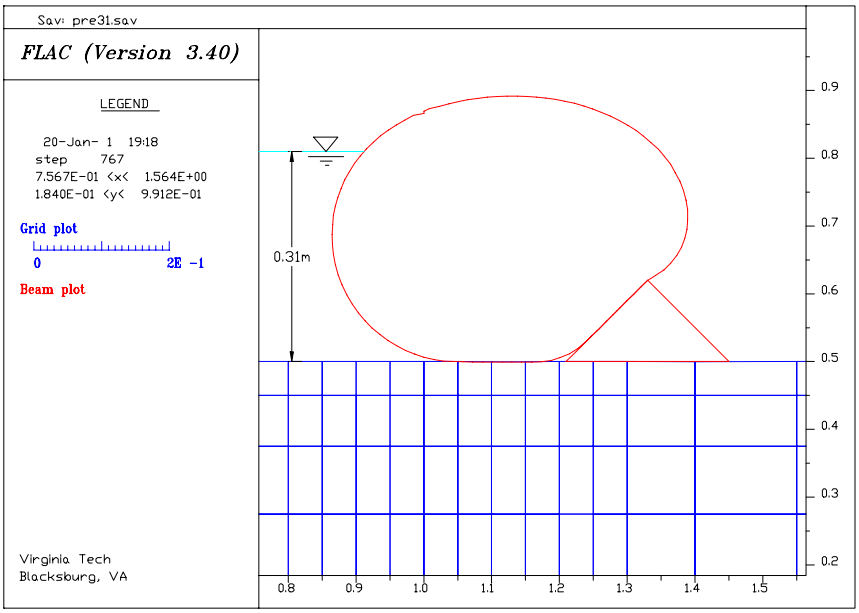

Figure 3.9: Block shape 1, block height = 0.12m, floodwater level = 0.31m.

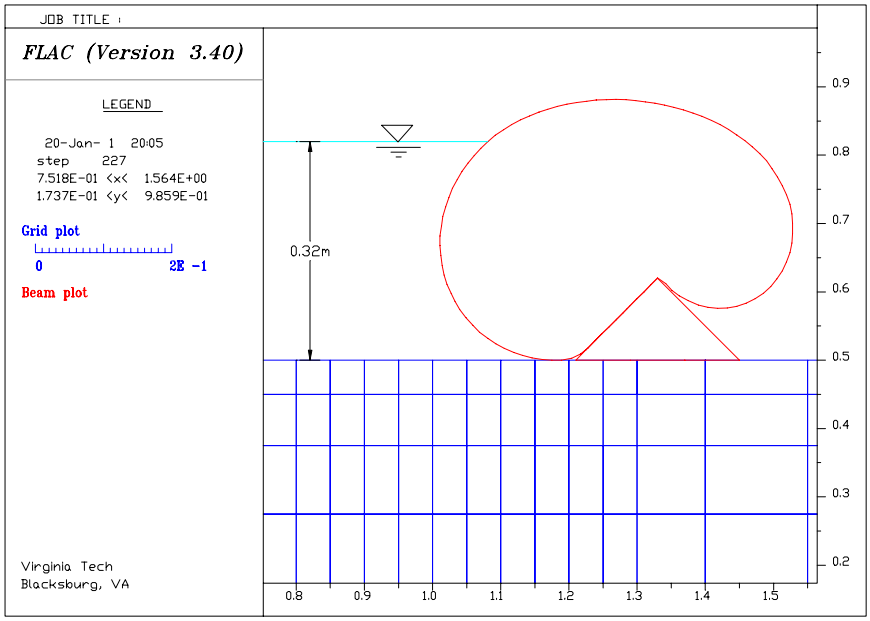

Figure 3.10: Block shape 1, block height = 0.12m, floodwater level = 0.32m

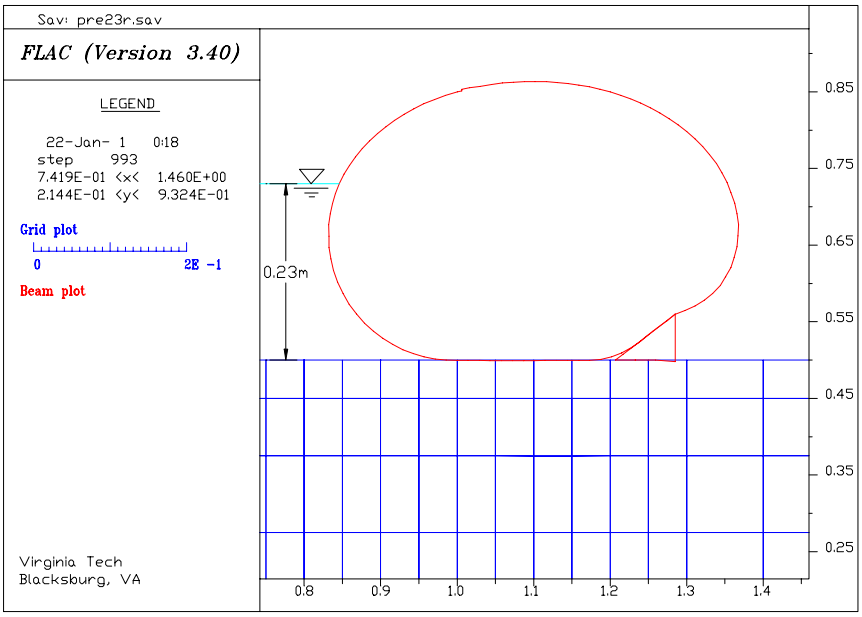

Figure 3.11: Block shape 2, block height = 0.06m, floodwater level = 0.23m

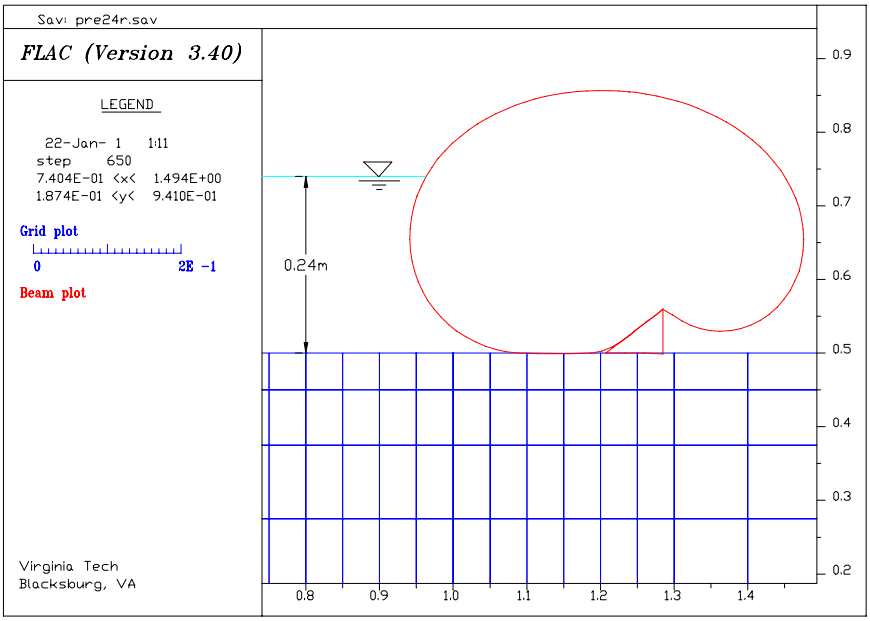

Figure 3.12: Block shape 2, block height = 0.06m, floodwater level = 0.24m.

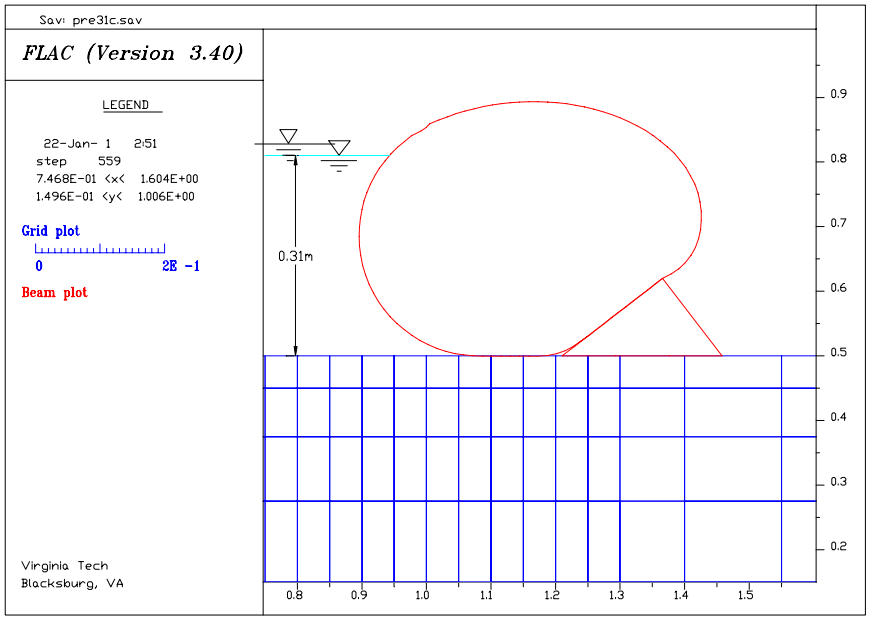

Figure 3.13: Block shape 3, block height = 0.12m, floodwater level = 0.31m.

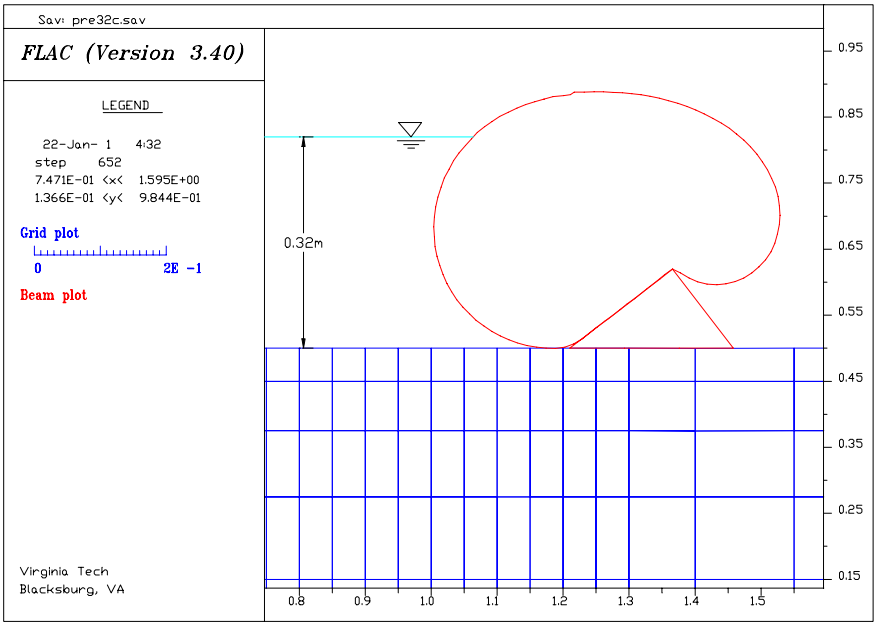

Figure 3.14: Block shape 3, block height = 0.12m, floodwater level = 0.32m.

3.7.3 Stability of block

Figures 3.15 through 3.18 show the soil stresses under the block of different shapes at the critical floodwater levels. When comparing the soil stress contours under the block in Figure 3.15 with the contours under the block in Figure 3.16, the soil stresses under the shape-2-block are higher than the soil stresses under the shape-1-block. Plus, the soil stresses under the shape-2-block are concentrated at the right edge of the block, while the soil stresses under the shape-1-block are spread over a larger area. These mean that the block of shape 2 may tip if the ground is soft.

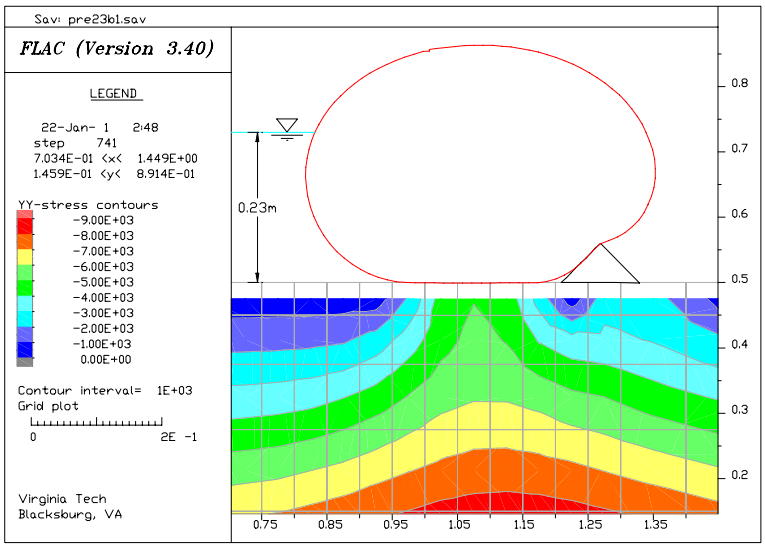

Figure 3.15: Soil stress under the block, block shape 1, block height = 6cm.

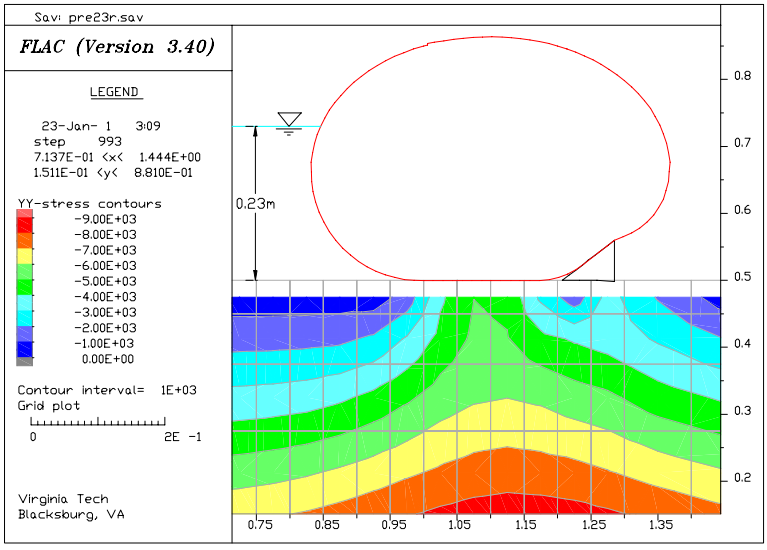

Figure 3.16: Soil stress under the block, block shape 2, block height = 6cm.

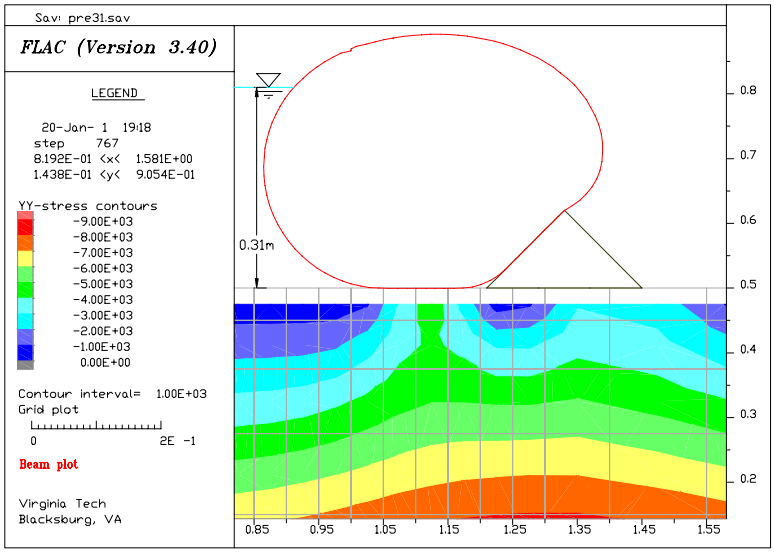

Figure 3.17: Soil stress under the block, block shape 1, block height = 12cm.

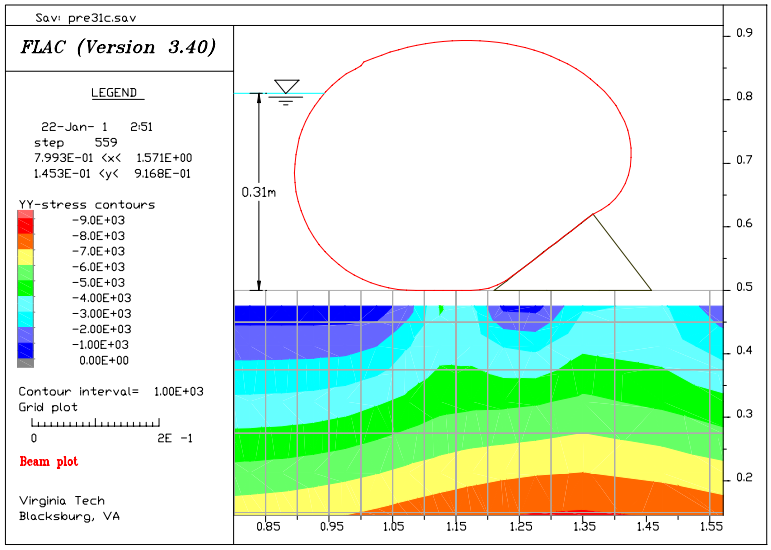

Figure 3.18: Soil stress under the block, block shape 3, block height = 12cm.

The soil stress under the block in Figures 3.17 and 3.18 are similar. This means that block shapes 1 and 3 are more stable than block shape 2. Therefore, they are recommended for further tube stability analysis, which includes computer models with pore water effect, and experimental tube stability testing.

Figures 3.17 and 3.18 have the same floodwater level and the same block height. It is interesting to note that the soil stress under the tube in Figure 3.17 is higher than the soil stress under the tube in Figure 3.18. In addition, the soil-tube contact length is also longer in Figure 3.17. Therefore, the shape-1-block is good for coarser soil because higher stress in the interface and longer contact length between the tube and the soil help in resisting the seepage. Shape-3-block is better for the soil that has weak friction resistance because the shape-3-block has a gentler slope facing the tube. The tube will put less horizontal load component but more vertical load components on the block. More vertical load also means higher sliding resistance of the block.

3.7.4 Tube height

If the block height is sufficient, an increase in floodwater level will lead to an increase of tube height, as is evident by Figure 3.5, Figure 3.7, and Figure 3.9. The floodwater level rises from 0.23m in Figure 3.5 to 0.28m in Figure 3.7 and leads to an increase of tube height from 0.364m to 0.380m. When the tube begins to roll over the block, the increase of floodwater level has very little impact on the tube height. For instance, the tube height in Figure 3.5 is 0.365m, and the tube height in Figure 3.6 is 0.358m. The tube height is in fact lowered by the increase of floodwater level. Please note that the tube height at failure is not reported in Table 3.1. The 0.358m shown in the above is recorded for showing how the tube height behaves after the tube starts to roll.

3.8 Further studies

Further investigation is carried out to study the soil, tube, and block stresses. The variation of the tube volume under different floodwater levels will also be studied to check the validity of the assumption made in section 3.2. Block shape 1 with block height equal to 0.12m is used here since it was used in the field experiment. Its configuration is simple and easy to construct. The procedures of modeling are the same as mentioned previously. Four floodwater levels are considered, and they are 0.1m, 0.2m, 0.25m, and 0.3m. Floodwater levels at 0.31m and 0.32 have been considered previously.

3.8.1 Tube shape and contact length

Figure 3.19 shows how the tube shape changes when the floodwater increases from zero to 0.32m. The solution for the 0.32m case was not converged. The shape in Figure 3.19g shows that the tube is rolling over the block. It was taken after the calculation was ended manually. Since a large portion of the tube has rolled over the block and the FLAC's calculation has not yet converged, the author assumes that the converged solution or the system equilibrium will never be achieved. This means that the whole tube will eventually roll over the block, and the tube is unable to resist the external water load at a floodwater level equal to or greater than 0.32m.

As shown in Figure 3.19a through Figure 3.19f, the contact length (if the longitudinal distance is omitted) between tube and soil is shortened when the floodwater level is increased. Figure 3.20 shows that the decreasing rate of the contact length between tube and soil increases when the floodwater level increases. The contact length increases rapidly after the floodwater exceeds 0.3m, and it reaches zero at the 0.32m floodwater level.

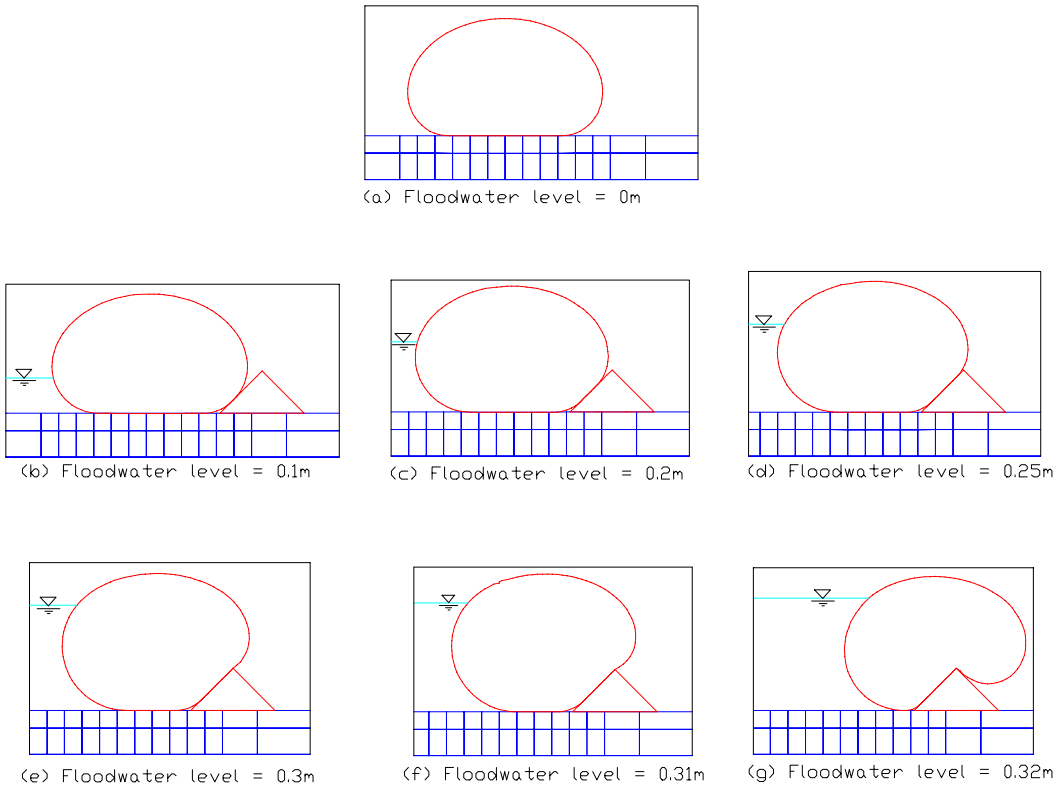

Figure 3.19: Tube shapes at different floodwater levels

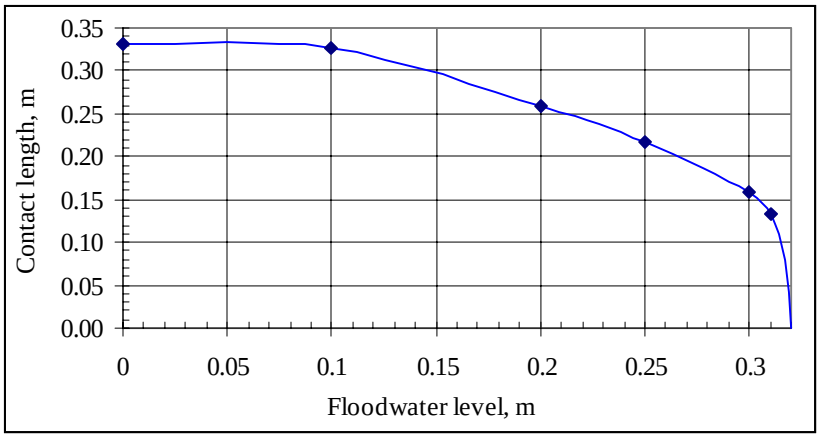

Figure 3.20: Contact length versus floodwater level

3.8.2 Stresses at the interfaces

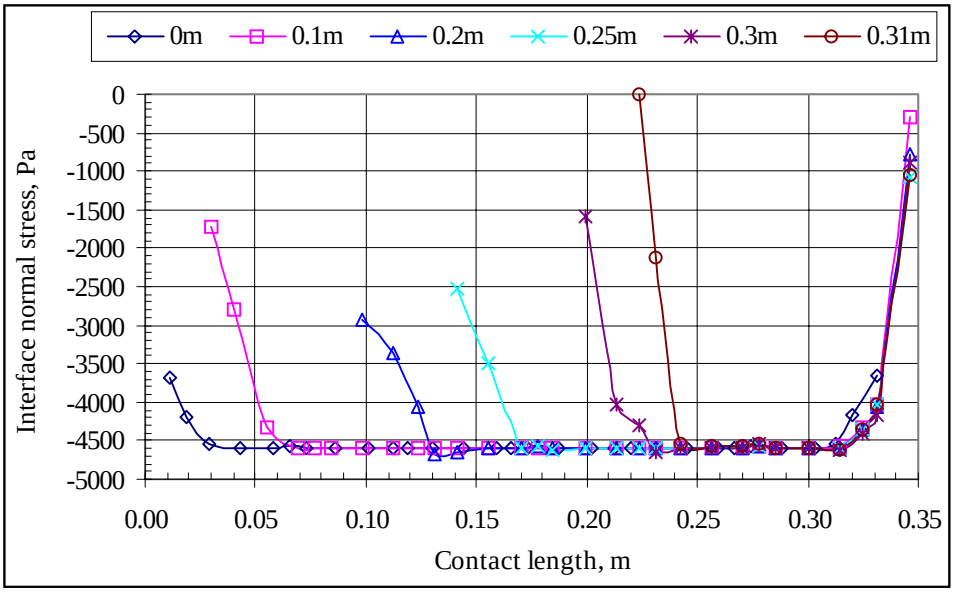

Figure 3.21: Vertical stresses at the interface between tube and soil

As the floodwater level increases, the vertical stresses in the interface between tube and soil remain approximately constant. Figure 3.21 shows the vertical compressive stresses at the interface for various floodwater levels. Again, it shows that as the floodwater level increases, the contact length becomes shorter.

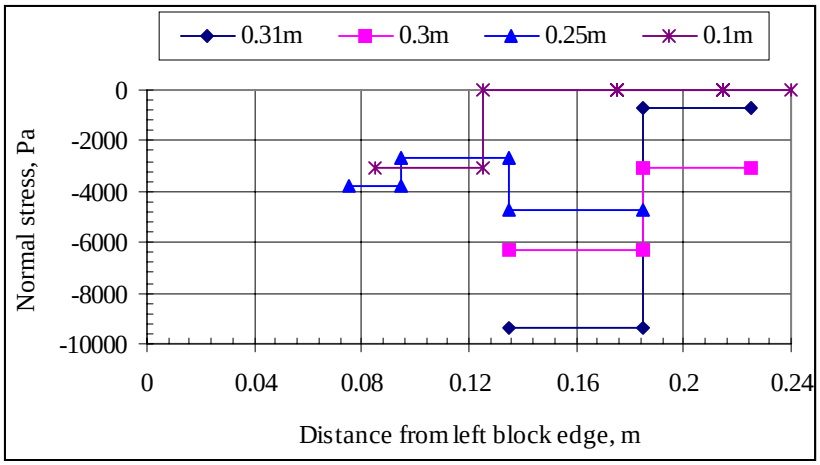

Figure 3.22: Stresses at the interface between block and soil at different floodwater levels

Figure 3.22 shows the stresses at the interface between the wooden block and the foundation soil at various floodwater levels. Since only three beam segments are used to represent the base of the block, the results obtained are only for indication and they are not accurate. It is obvious that the stresses at the interface increase when the floodwater level increases. The location under stress shifts toward the right when the floodwater level increases.

Figure 3.23 shows the schematics of the wooden block with a tube loaded on the left side of the frame. It shows the node locations for the block. The FLAC results indicate that only node 201 is under stress when the floodwater level equals or exceeds 0.3m. This means that only the right side of the block base is effectively in contact with the foundation soil at high floodwater levels. Block shape 3 may be a better choice because it has a gentler slope facing the tube. More vertical load and less horizontal load act on this block shape when the floodwater level increases. This can reduce the possibility of failure in sliding.

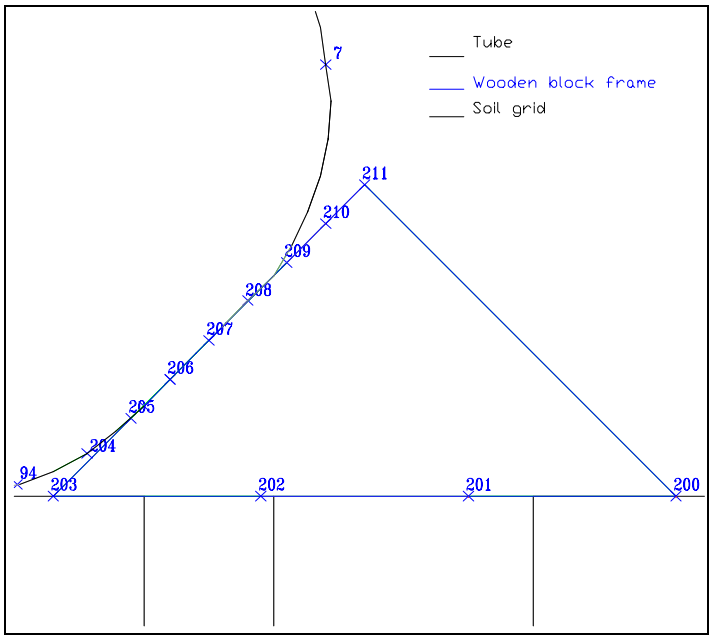

Figure 3.23: Schematics of a wooden block frame

3.8.3 Soil stresses at the bottom of the tube and at the bottom of the wooden block

Although as shown in Figure 3.21, the soil stress under the tube is almost constant at various floodwater levels, the tube area under that stress decreases when the floodwater level increases. This is illustrated in Figure 3.24 through Figure 3.28. By comparing the vertical soil stress contours in Figure 3.24 through Figure 3.28, one can easily notice that high stress contours shift from the soil under the tube to the soil under the block as the floodwater level increases.

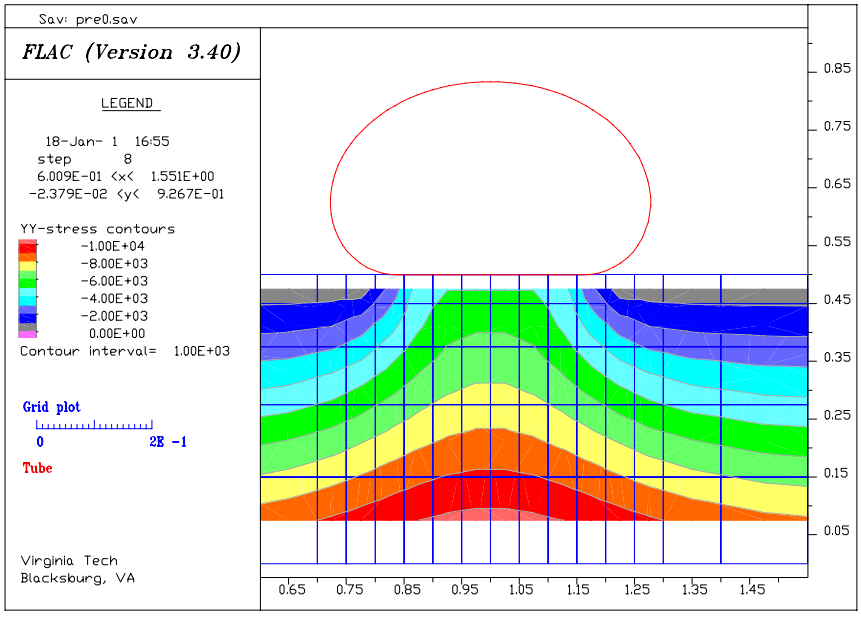

Figure 3.24: Vertical soil stress contours for zero floodwater level

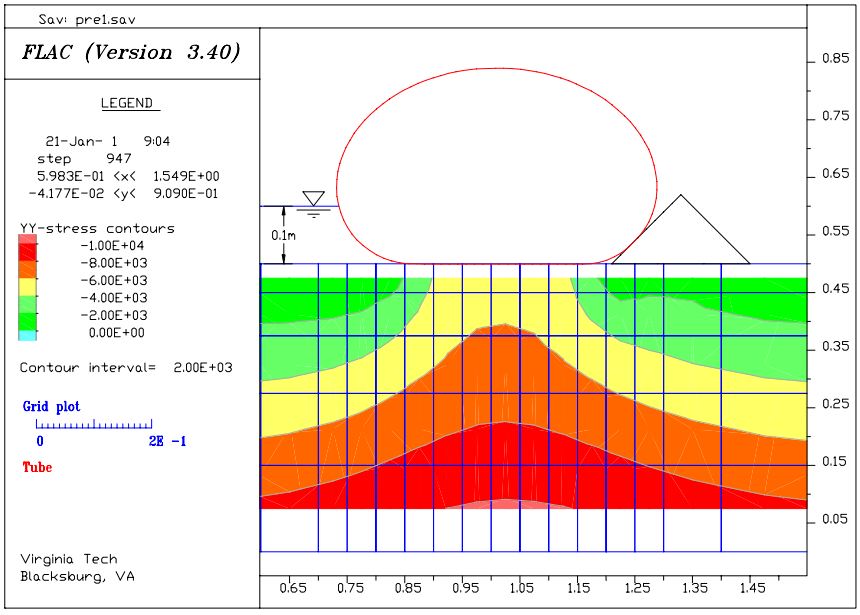

Figure 3.25: Vertical soil stress contours for floodwater level equals to 0.1m

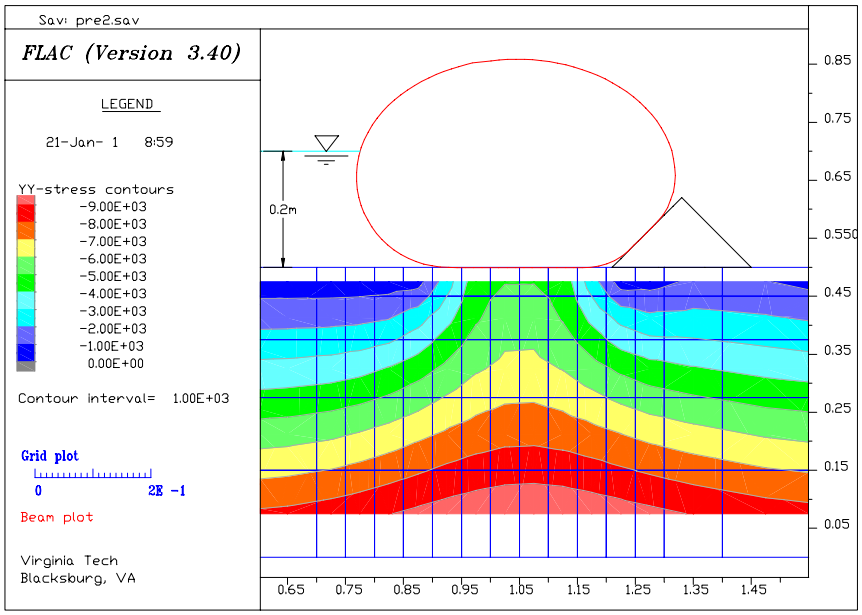

Figure 3.26: Vertical soil stress contours for floodwater level equals to 0.2m

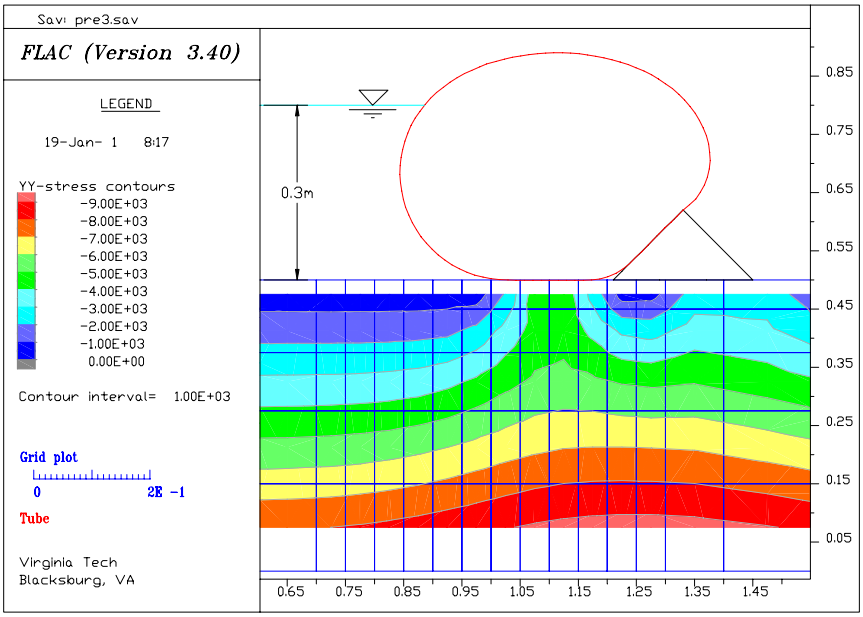

Figure 3.27: Vertical soil stress contours for floodwater level equals to 0.3m

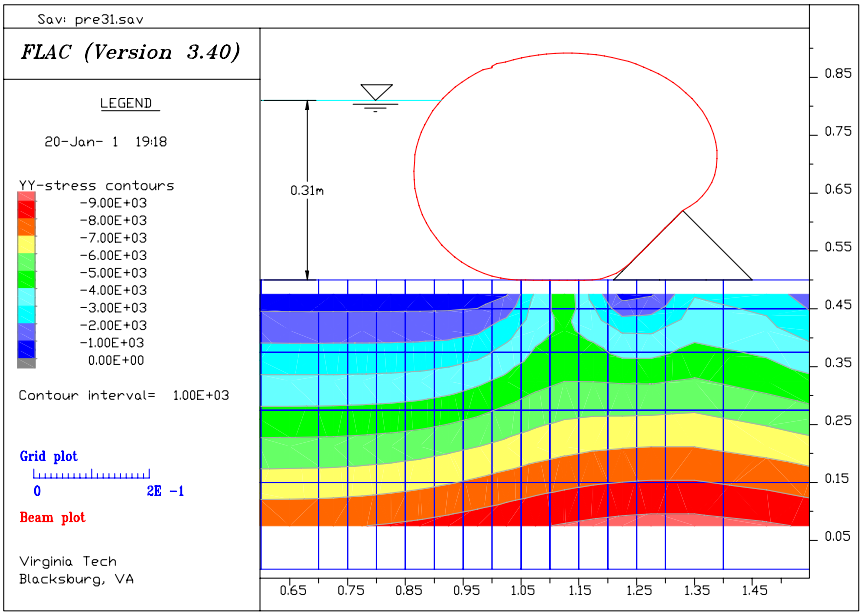

Figure 3.28: Vertical soil stress contours for floodwater level equals to 0.31m

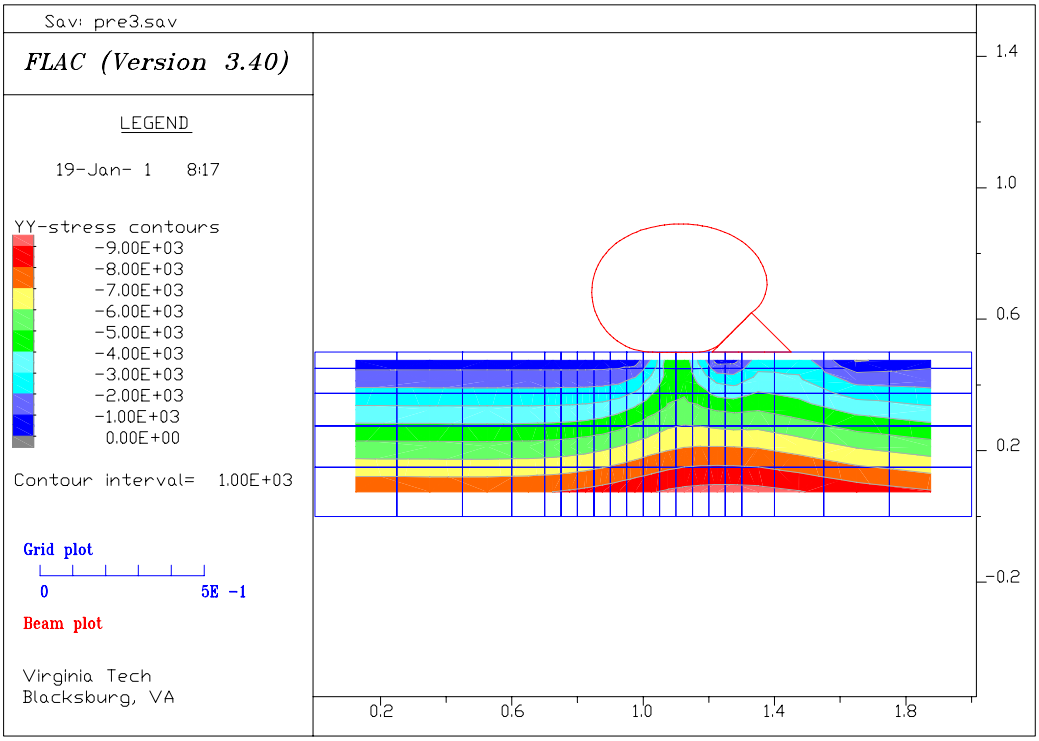

Figure 3.29: Full view of vertical soil stress contours at 0.3m floodwater level.

Figure 3.29 shows the extent of the tube loading effect on the soil. The contours are flattened at the ends of the soil grid mesh. This indicates that the loading of the tube no longer affects the soil stress there. It also means that the length of the grid mesh is sufficient.

Figure 3.30 shows a clearer picture of the transferring of vertical soil stresses from the bottom of the tube to the bottom of the block. The soil stresses shown are at a depth of 0.025m below ground level. When the floodwater level increases from zero to 0.31m, the left dome of the curve becomes skinnier whereas the right dome of the curve increases its height. This explains that the high stresses in the soil as well as the tube itself are mobilizing away from the floodwater side as the floodwater level increases.

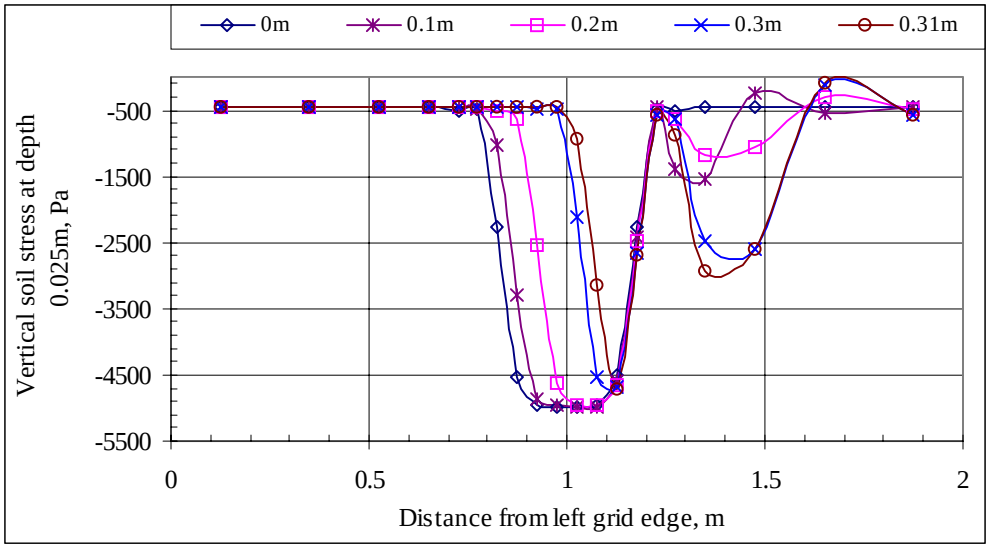

Figure 3.30: Vertical soil stresses corresponding to floodwater levels

3.8.4 Tensile forces in the tube

Figure 3.31 shows the tensile force in the tube versus the position on the tube for various floodwater levels. When the floodwater level increases, the tensile forces in the tube decrease. The figure also shows that the highest tensile stress in the tube occurs when there is no floodwater.

The slopes of the curves are basically constant, or in other words, the tensile stresses are constant for the portions of the tube that are not in contact with either soil or block. But the tube tensile stresses in the tube for the zero floodwater level case behave differently. The maximum tensile force occurs at two locations, which are around nodes 70 and 2. These are the tube sides right before they contact with the soil. The lowest stress in this tube occurs at the bottom of the tube.

The tensile stresses in the tube for the tube-soil contact region and the tube-block contact region distribute differently. It is clear that friction between the tube and the soil, and between the tube and the block, plays an important role.

As marked on the curves, the left side of the tube begins contact with the soil at node 74 at zero external water, and this first contact point moves to node 89 when the floodwater level rises to 0.31m. The stresses in the part of the tube that is in contact with the soil increase from the left end to the right end, except for the 0m and 0.1m floodwater level cases. This is because in the 0m and 0.1m cases, the friction between the tube and the soil is restraining the beam from stretching, whereas in the cases where the floodwater level is higher than 0.1m, the friction between the tube and the soil is restraining the length of the beam elements from shortening.

There is another example that illustrates that the friction restrains the tube from shortening. As can be seen from the curves in Figure 3.31, the tube's tensile force remains constant from node 97 to node 102. These nodes are located between the tube-soil and tube-block interfaces. They are not in contact with the soil or the block, and thus the stresses in the tube are constant. But after these nodes, from nodes 1 to 8, the friction between the block and the tube tries to keep the tensile stresses in the tube from dropping until the tube is no longer in contact with the block.

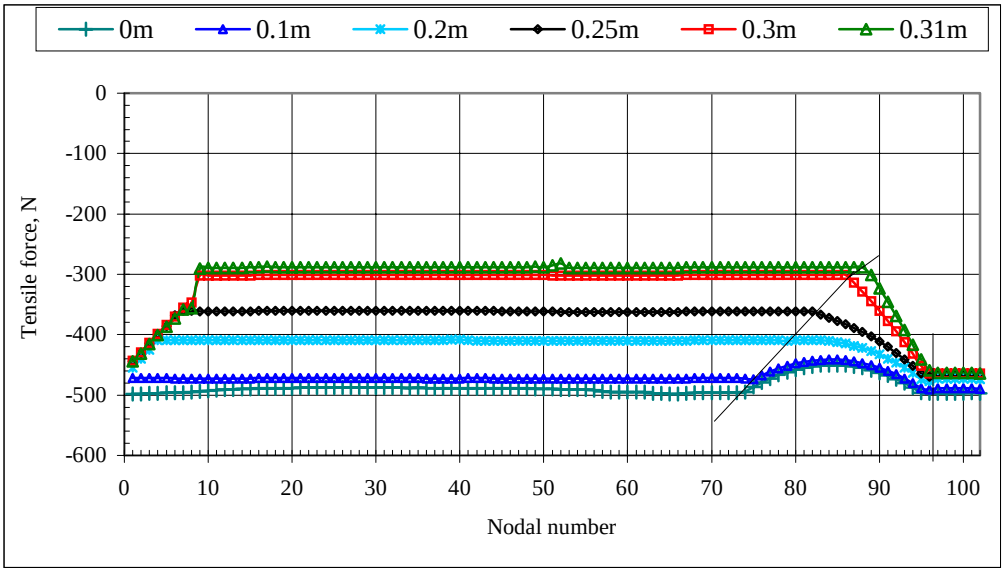

Figure 3.31: Tensile force versus nodal number (position)

3.8.5 Shear forces and moments in the tube

Figure 3.32 shows the shear forces in the tube for various floodwater levels. If the erratic values in this figure are ignored, the shear forces in the tube are basically very close to zero. These forces are relatively small when compared with the tension forces shown in Figure 3.31.

The same situation is found in Figure 3.33. The moments in the tube are basically zero, if the erratic values in the figure are ignored. Therefore, it is reasonable to neglect the shears and moments in the analysis.

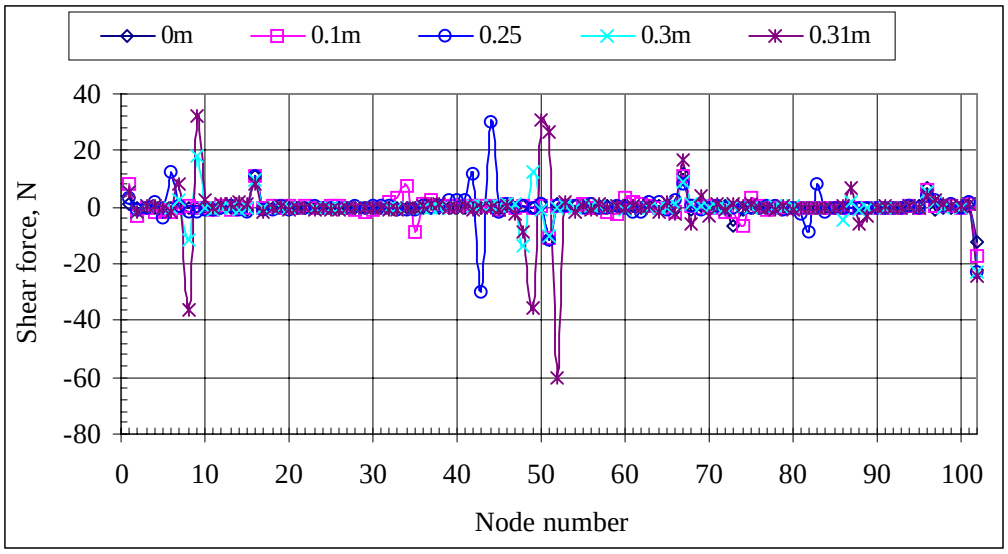

Figure 3.32: Shear force versus nodal number

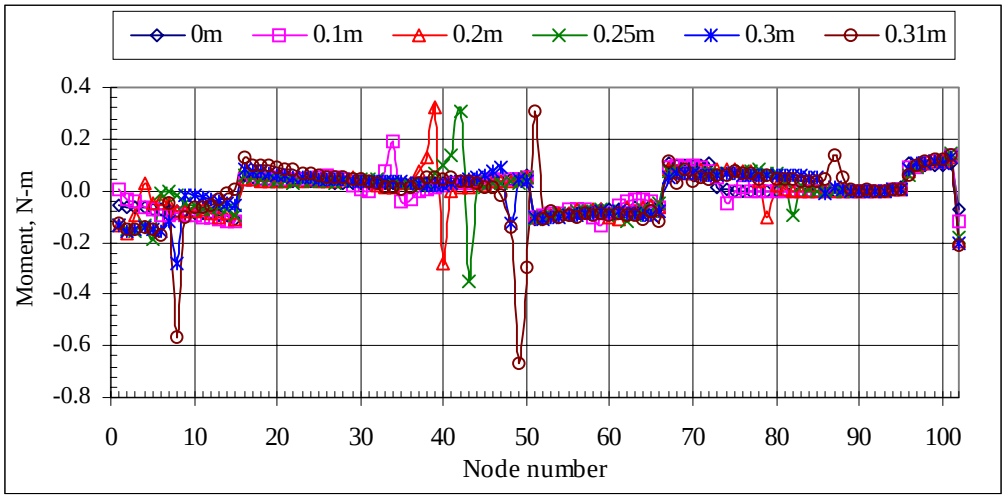

Figure 3.33: Moment versus nodal number

3.8.6 Volume of the tube at various floodwater levels

The volume of the water in the tube is not constant throughout every case. Figure 3.34 shows that when the floodwater level increases, the water volume in the tube increases until the floodwater reaches 0.3m. Then the volume begins to decrease until the tube rolls over the block.

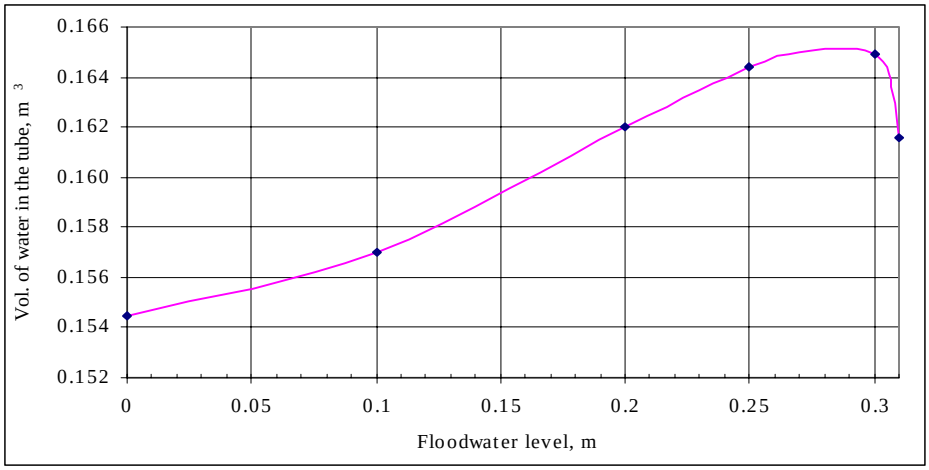

Figure 3.34: Volume of water in the tube versus external floodwater level

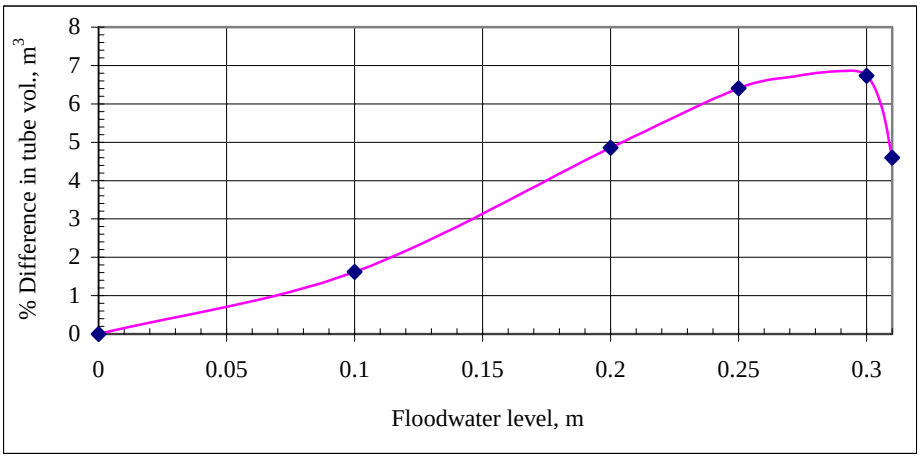

Figure 3.35: Percent difference in tube volume versus floodwater level

Figure 3.35 compares the water volume in the tube at various floodwater levels with the water volume in the tube without external floodwater. The curve shows that the water volume in the tube increases continuously until the floodwater level reaches 0.3m. At this floodwater level, the water volume in the tube is 6.7% more than its initial volume.

In the actual field situation, the tube filling inlets may be sealed or closed before the floodwater comes. Under this condition, the pressure in the tube may not be constant. Leaving the tube filling inlet open to a constant water head source causes larger tube volume, and induces higher stresses in the wall of the tube. The larger tube volume means that the tube is heavier, and the heavier tube is more stable, so it is less likely to fail in sliding.

3.8.7 Tube's height and width

Figure 3.36 shows that when the floodwater level increases, the height of the tube increases while the width of the tube decreases.

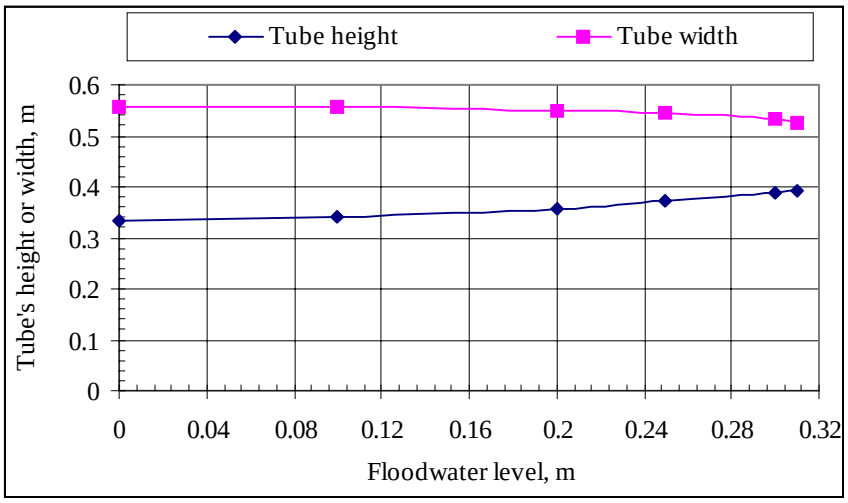

Figure 3.36: Tube's height and tube's width versus floodwater level

3.8.8 Stresses in wooden block frame

The nodal numbers in the following figures are referred to the nodal numbers shown in Figure 3.23. Figure 3.37 illustrates that the wooden block is in tension at node 200 because the friction between the beams (nodes 201, 202 and 203) and the soil resists the tensile force caused by the beam (nodes 211 and 200) on the opposite side of the tube, which is in compression and tries to shear off from node 200. When the water level is low, the upper left side of the block (facing the tube side) is in tension. But, when the water level is high, the whole side is in compression. The magnitude of the axial force tends to increase when the floodwater level increases.

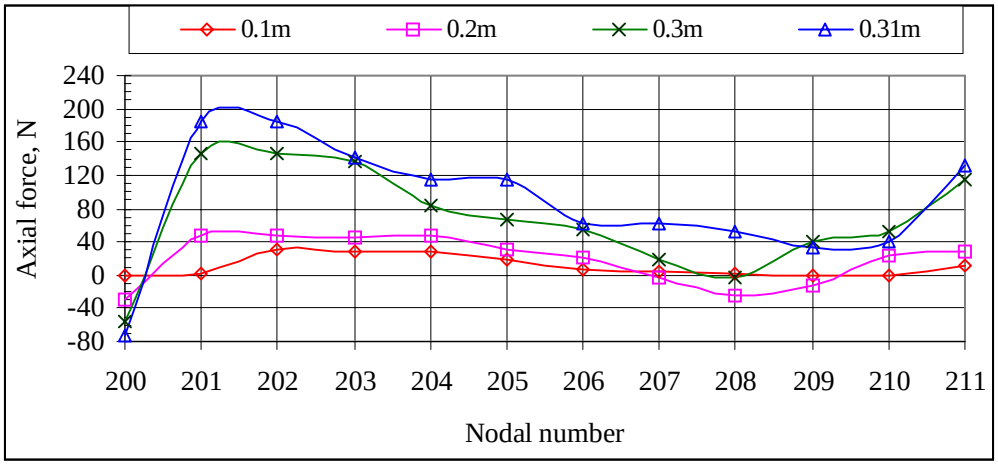

Figure 3.37: Axial force in the wooden block frame at different floodwater level

Figure 3.38 presents the bending moments in the wooden frame at different levels of floodwater. Again, a higher floodwater level tends to cause higher bending moments in the block frame as well as higher shear forces, which are shown in Figure 3.39.

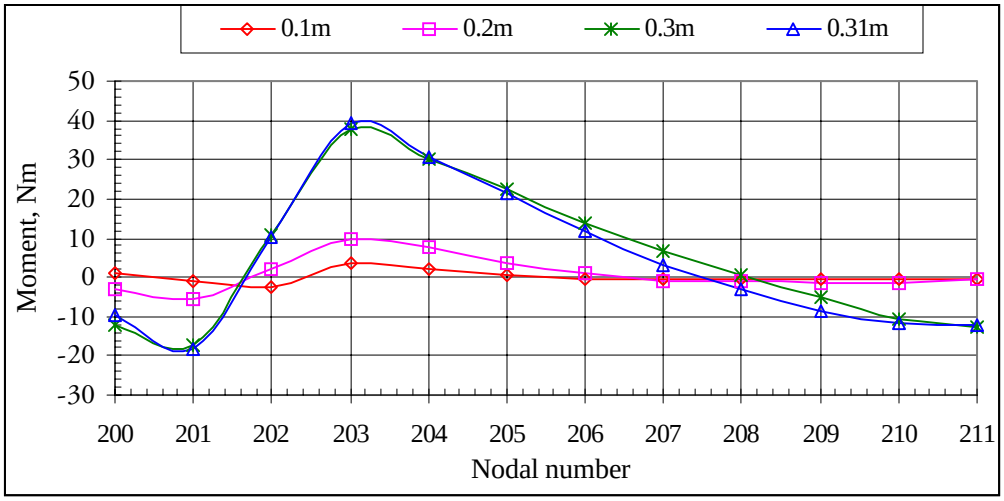

Figure 3.38: Bending moments in the wooden frame at various floodwater level

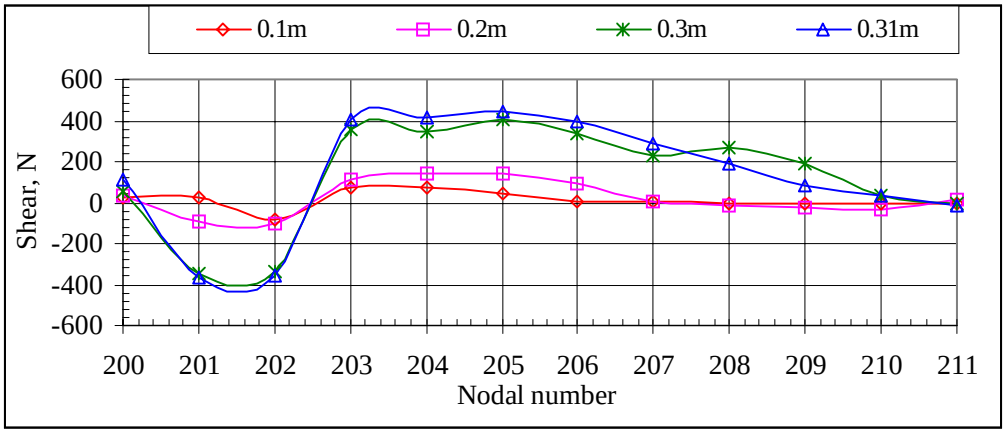

Figure 3.39: Shear forces in the block frame at various floodwater levels

3.9 Comments

Since the sandy soil is highly permeable, the excess pore water pressure in the soil might not build up during the loading of the tube. But the uplift force induced by the floodwater must not be ignored. This uplift force could generate uplift forces at the bottom of the tube and worsen the rolling problem. In addition, this uplift force may decrease the frictional resistance between the tube and the ground, and thus reduce the sliding resistance capacity of both the wooden block and the tube.

Seepage may create a piping problem, especially if the foundation soil is cohesionless. When the floodwater level is higher, the potential head is also higher and the contact length between the tube and the soil is shortened. This may cause the fine soil particles to be washed away and cause the porosity of the soil to increase and eventually form a small stream under the tube. The next chapter will address uplift and seepage problems.

Chapter 4

Stability of a single tube with the effect of pore pressure

4.1 Introduction

This chapter covers the computer simulation of the stability of a single tube with the effect of pore pressure. The modeling procedures are similar to the modeling mentioned in chapter 3. The soil mesh is first created, and then a tube is placed on the top of it. This tube is filled with water, and a wooden block is placed on the right side of the tube. Floodwater is flowing from the left side of the grid, and the placements of the tube and the block are meant to stop the floodwater flowing towards the right side of the tube. Finally, the floodwater level is increased until the system fails.

The main objective of the simulation is to find the maximum floodwater level that causes the system to fail. The system fails when the tube rolls over the block or when both the tube and the block slip. Piping under the tube may also lead to the bearing failure of the system.

4.2 Soil

Brendan Fitzpatrick and Dave Nevius, two graduate students, with initial assistance from Marcos Freeman, an undergraduate student, carried out the experimental work on the stability of a single tube. In order to compare the numerical analysis results with the experimental results, every effort is made for the numerical model to match the actual site conditions, the actual soil, and the tube properties.

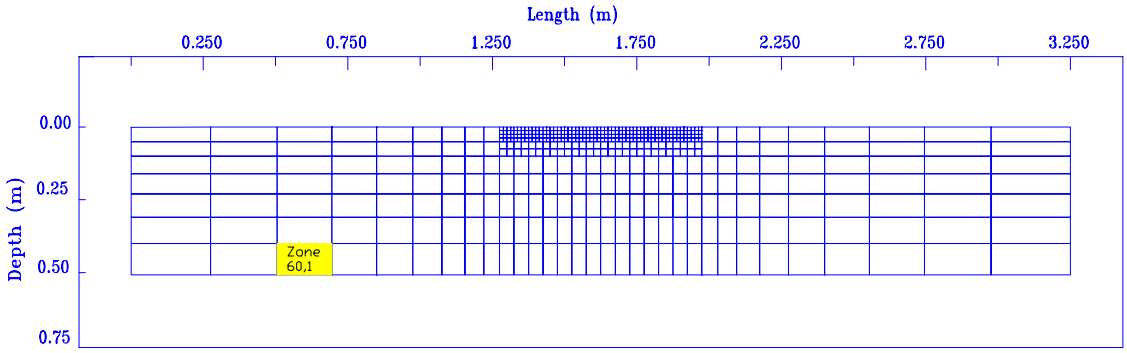

Figure 4.1: Soil grid mesh

The soil mesh used is shown in Figure 4.1 and the FLAC code that makes up this mesh is included in Appendix A. The main soil mesh is 3.25m long and 0.508m deep. It consists of a fine mesh, a medium fine mesh, and a coarse mesh. As shown in Figure 4.1, the fine mesh (0.0125m square zone) and the medium fine mesh are attached at the center of the coarse soil mesh. The length of the fine mesh is 0.7m for the 6cm block height case and 0.8m for the 12cm block height case. For the coarse mesh, the distances between the grids increase gradually as they are further away from the fine mesh. The soil properties of the main soil mesh are:

*Medium sand

Dry density: $\rho_D = 1600$ kg/m^3 (100 pcf)

*Internal angle of friction, $\phi = 36^\circ$

Cohesion, C = 0

Tension, $\sigma^t = 0$

*Dilation angle, $\psi = 7^\circ$

Poisson's ratio, $\upsilon = (1-\sin\phi)/(2-\sin\phi) = 0.292$ (Dr. Bob Makwa's lecture)

*Standard penetration blow count, N = 25

$E = 500{,}000(N+15) = 2\times10^7$ Pa (McGregor and Duncan, 1998)

Bulk modulus, $K = E/(3(1-2\upsilon)) = 1.6\times10^7$ Pa

Shear modulus, $G = E/(2(1+\upsilon)) = 7.7\times10^6$ Pa

Porosity, n = 0.4

Permeability, $k_h = 2\times10^{-5}$ m/s

Water density, $\rho_w = 1000$ kg/m^3

Mobility, $k = k_h/(g\rho_w) = 2.04\times10^{-9}$ m^2/Pa-sec

Water bulk modulus, $K_w = 10^2$Pa ($K_w = 2\times10^8$ Pa was tried, but it did not work)

The * means that the value is assumed.

According to the FLAC manual (1998), the pure water bulk modulus (K_w) is equal to $2x10^9$ Pa. But there might be some air present in the soil and this air reduces the value of K_w. Therefore, K_w equal to $2x10^8$ Pa is assumed initially.

The FLAC manual's recommended procedures are used to determine the maximum value of K_w that can be used in the model. It is recommended that the fluid versus soil solid stiffness, R_k, be less than 20.

Fluid versus soil solid stiffness, $R_k = \dfrac{\dfrac{K_w}{n}}{K + \dfrac{4G}{3}} < 20$

If $K_w = 2x10^8$ Pa, $R_k = 19$.

If the fluid stiffness is much greater than the solid soil modulus, FLAC will increase the nodal mass during mass scaling. Since the mechanical time step is taken as unity in FLAC, the result of the increase in nodal mass is to slow down the convergence to the solution.

In this model, R_k is 19, which is less than 20. This means that $K_w = 2x10^8$ Pa should work. But, unfortunately, the test shows that it did not work as expected. As shown in Figure 4.2, $K_w = 2x10^8$ Pa causes the flow to penetrate through the assigned impermeable surface (the ground between the tube and the block). This ground is considered to be impermeable because a FISH Function, makeApplys, applies the discharge of 10^{-20}m/s on the top grid, beginning from the left fine grid and ending at the first fine grid under the right edge of the block. On the left side of the tube, whenever the ground is not in contact with the tube, a FISH Function, modifyApplys, changes the 'apply discharge' to 'apply pore pressure'. These two FISH Functions can be found in applypp.dat, which is included in Appendix A.

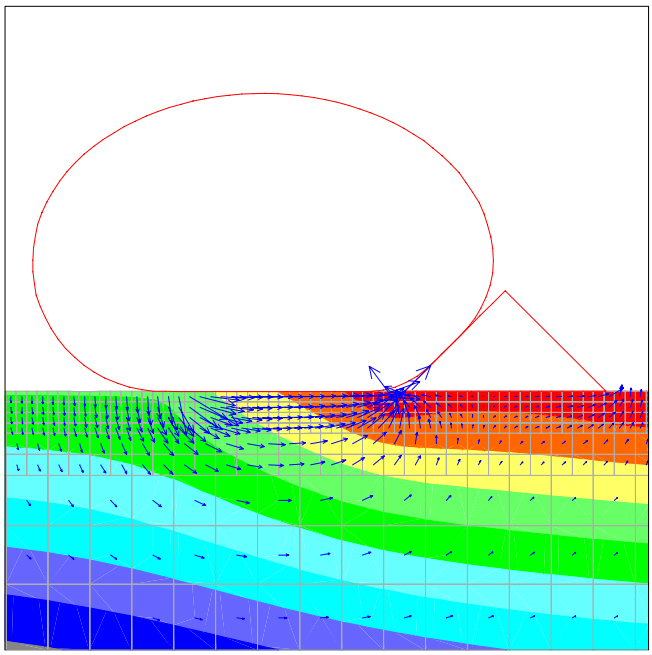

Figure 4.2: Problem of using high K_w

The following inequality is obtained from the FLAC manual (1998) to determine the lower bound of K_w that can be used for this model:

$$K_w \geq 0.3 L_z \rho_w g = 37\text{Pa}$$

where L_z = smallest zone length = 0.0125m

Since sand is porous, it is reasonable to use a smaller value of K_w . Here $K_w = 10^2$ Pa is chosen, based on the assumption that the increase of pore pressure caused by the loading of the water-filled tube is dissipated immediately, and the load is only resisted by the soil's effective stress.

The value $K_w = 10^2$ Pa works in the system and is used for all the groundwater flow-related analyses. The value $K_w = 10^5$ Pa was also used to check if there are any irregularities in using a low K_w. When comparing the tube shapes and the flow contours between Figure 4.3 and Figure 4.4, visually they are no different. This indicates that $K_w = 10^2$ Pa and $K_w = 10^5$ Pa give essentially the same results.

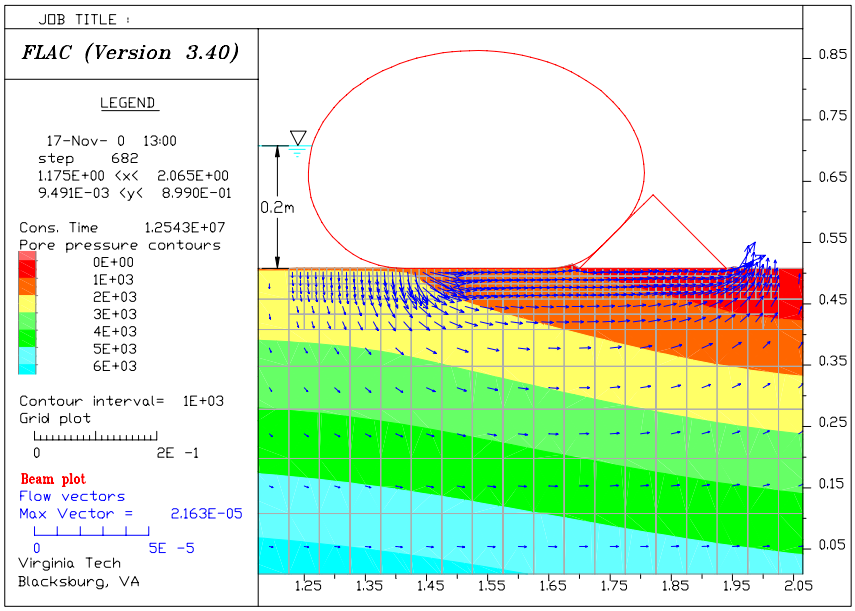

Figure 4.3: Results for using $K_w = 10^5$ Pa

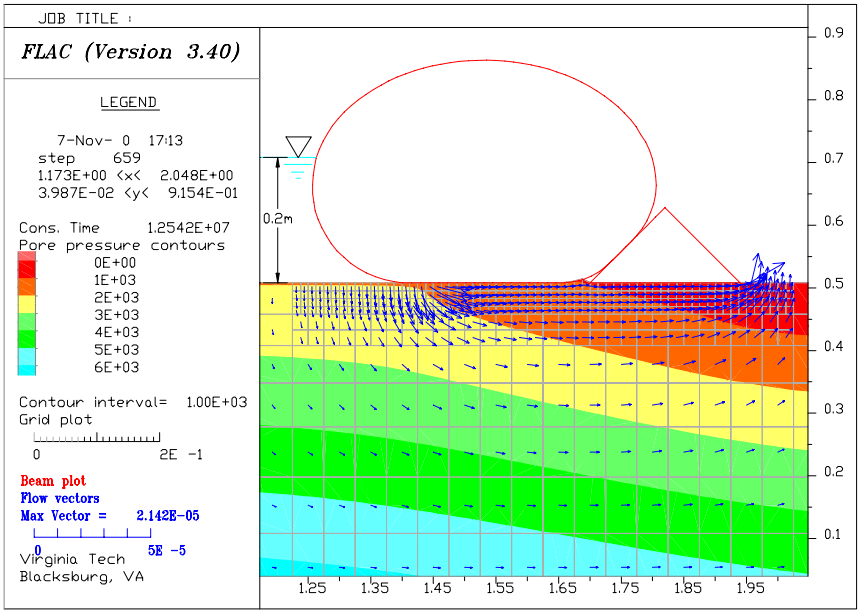

Figure 4.4: Block height = 0.12m, floodwater level = 0.2m, $K_w = 10^2$ Pa

The vertical soil stress due to the soil self-weight at the bottom of the mesh is -9,964Pa, which is computed by equation B2.1. Its corresponding horizontal pressure is 4,107Pa, which is

computed by equation B2.4. A FISH code is written to initialize these soil stress components at the bottom of the mesh, and decrease them linearly to zero at the top of the mesh. It is assumed that the soil is fully saturated; hence, a file called Ininv.dat from the FISH library was modified to initialize the hydrostatic pressure or pore pressure throughout the soil mesh.

The vertical soil stresses, pore pressure, and horizontal soil stresses in zone 60,1 in Figure 4.1 are checked to see whether the written FISH code and FLAC code do the calculation accurately. For the manual calculations, pore pressure, total vertical stress, effective vertical stress, and total horizontal stress are computed by using equations B2.1, B2.2, B2.3, and B2.4, respectively. The effective horizontal stress is equal to the total horizontal stress plus the pore pressure. The depth at zone 60,1 is 0.454m and the FLAC and manual results are tabulated as follows:

Table 4.1: Soil self-stresses computed by FLAC and by hand.

	FLAC	Manual
Total vertical stress (Pa)	-8,905	-8907
Pore pressure (Pa)	4454	4454
Effective vertical stress (Pa)	-4451	-4454
Effective horizontal stress (Pa)	-1835	-1836
Total horizontal stress (Pa)	-6288	-6290

Table 4.1 shows that the FLAC and manual results agree very well. The 1Pa or 2Pa differences between the two results may be due to the round-off numbers that were used in the manual calculations.

4.3 Tube

The tube formulation is the same as described in section 2.3. Brendan has actually tested some of the properties of tube material. These tested properties are shown as follows:

Modulus of elasticity, $E = 1.724 \times 10^9$ Pa
Thickness, t = 0.457 mm

The model here is modeling a 1 m strip of the tube. The cross-sectional area, A, is 0.000457 m^2, and the moment of inertia, I, is 7.95×10^{-12} m^4. Since the tube is very light and it is believed that the effect of its weight on the results is negligible, its density, ρ, is assumed to be zero. The same interface properties as mentioned in section 3.4 are used.

4.4 Block

Block shape 1 that was described in section 3.5 is used, and the block properties remain the same. Block heights of 0.06m and 0.12m are considered. The wooden block is placed on the right side of the tube to stop the tube from rolling.

4.5 Filter

It is suspected that the system may fail in piping instead of rolling or sliding. To check whether piping will occur, no filter is used in the cases that are modeled in this chapter. Filter placements will be covered in chapter 5.

4.6 Loading of the floodwater

The water pressure or pore pressure shown in Figure 4.5 is applied. The pore pressure on the right of the tube is fixed at zero to simulate the water draining away as soon as it flows out from the soil. The pore pressure equals the floodwater pressure that is applied on the ground at the left of the tube. The mechanical pressure is also applied at the same place and at the same time to simulate the water load or to prevent the top grid from swelling up.

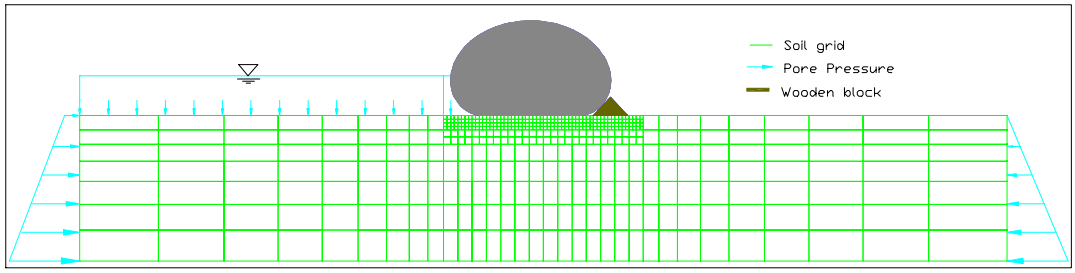

Figure 4.5: Placements of tube, filter, and block, and loading of floodwater

A special FISH code is written to apply the pore pressure and the mechanical pressure on the fine grid surface at the left of the tube. The code detects the first contact node between the foundation soil and the tube, and then it applies the pore pressure and mechanical pressure on the top of the fine soil grid at and to the left of the first contact grid nodes. When the tube is pushed to the right by the floodwater, these pressures follow right behind the tube. This is to simulate the floodwater filling in the space that is caused by the separation between the tube and the ground.

4.7 Results

Two cases are considered in this chapter, the 0.06m block height case and the 0.12m block height case. The floodwater or external water level is increased until the system fails. The results for the 0.06m block height and the 0.12m block height are discussed in sections 4.7.1 and 4.7.2, respectively.

4.7.1 0.06m block height case

Figure 4.6 shows the floodwater at the critical level for the system to fail by rolling the tube over the block. This critical floodwater level is 0.23m. At this critical water level, the block is still able to resist the tube from rolling over the block. When the floodwater is increased by one more centimeter, the tube rolls over the block. Figure 4.7 shows the tube rolling over the block at a floodwater level equal to 0.24m. The solution for the 0.24m case was not converged. Figure 4.8 illustrates that if the calculation for the 0.24m case is continued, the tube will roll over the block. The right side of the tube penetrates into the soil grid because the tube-soil interface at that location was not assigned.

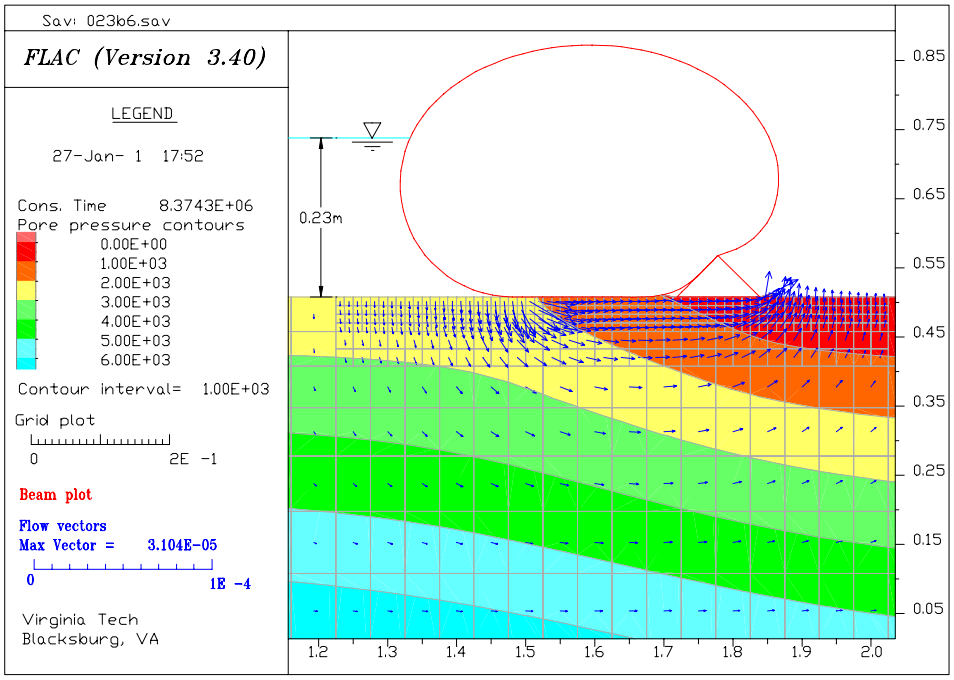

Figure 4.6: Block height = 6cm, floodwater level = 0.23m

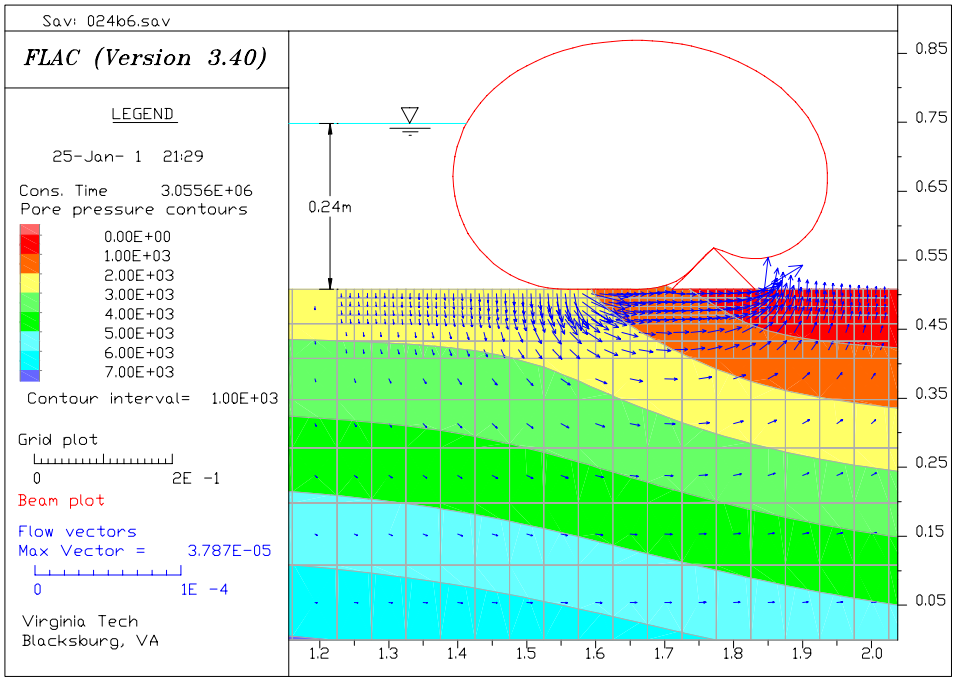

Figure 4.7: Block height = 6cm, floodwater level = 0.24m

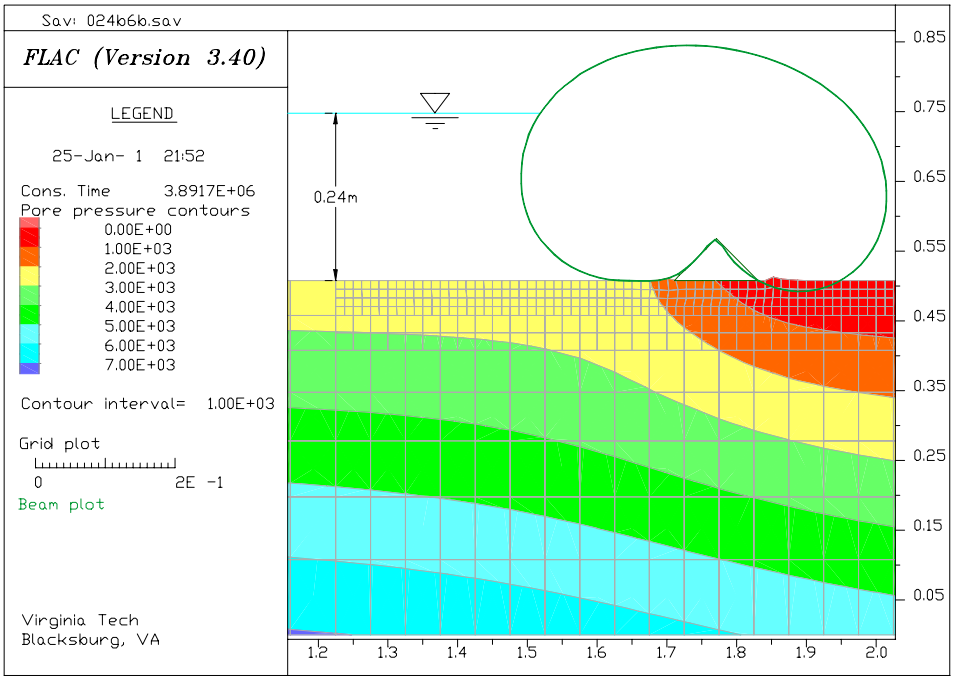

Figure 4.8: Rollover view, block height = 6cm, floodwater level = 0.24m

When comparing these results to the results that are shown in Table 3.1, the critical floodwater levels are the same. The tube shape shown in Figure 4.6 is also the same as that shown in Figure 3.5. The reasons why the pore pressure in the soil does not affect the rolling of the tube are covered in section 4.8.

The swelling of the soil grid on the right side of the block can be seen in Figure 4.8. Therefore, it is suspected that another failure mode may occur earlier than the rolling failure mode. In order to visually check on any other type of failure mode that may occur earlier than the 0.24m-floodwater level, a magnified view of Figure 4.6 is made. This view is shown in Figure 4.9, and the view is concentrated on the interfaces between tube block and soil.

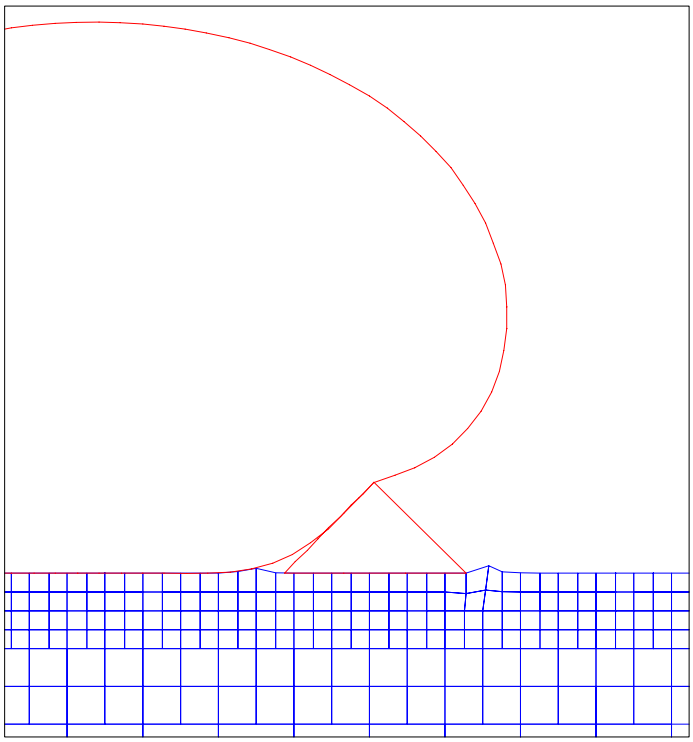

Figure 4.9: Magnified view of Figure 4.6

It can be seen in Figure 4.9 that the soil surface next to the edge of the right side of the block swelled up like a little bump. Since the pore pressure on this surface is assigned to be zero, swelling should not happen on this soil surface. The best guess for the reason of the swelling problem is that piping has occurred in the soil.

This explains that the system may fail in piping before it fails by rolling the tube over the block. The piping failure criterion in Naval Facilities Engineering Command (1982, pp. 259-271) is used to confirm the piping failure. This criterion states that the factor of safety against piping is $F = \frac{\gamma_b}{i\gamma_w}$.

Failure occurs when $F < 1$, i.e., $i\gamma_w > \gamma_b$, (4.1)

where γ_w = unit weight of water

γ_b = buoyant soil unit weight of soil

i = vertical hydraulic gradient $= \frac{U_b}{d\gamma_w} - 1$ (4.2)

U_b = water pressure at the base; in this case it is the pore pressure at the center of the zone (i=50, j=7), right under the edge of the right side of the block.

d = the distance between the center of the zone (i=50, j=7) and the ground surface.

The soil in the model is assumed to be homogeneous sand. Upward groundwater flow through the sand at the toe of the block can cause a piping problem. The soil particles will be washed out from the bottom of the block if $i\gamma_w > \gamma_b$.

For the 0.23m floodwater level and 0.06m block height case:

U_b = 165Pa

d = 0.00625m.

$$i = \frac{U_b}{d\gamma_w} - 1 = \frac{165}{0.00625 \times 1000 \times 9.807} - 1 = 1.69$$

$$i\gamma_w = 1.69 \times 9807 = 16593 > \gamma_b = ((1600 + 0.4(1000)) - 1000) * 9.807 = 9807$$

Since $i\gamma_w > \gamma_b$, piping occurs at the right edge of the block. As the soil particles are washed out from the bearing soil underneath the block, the soil underneath the block becomes more porous and thus the flow increases. As the flow increases, more soil will be washed out and streams may form under the block. This problem will get worse through time and eventually the system could fail in a bearing failure mode.

4.7.2 0.12m block height case

As has been discussed in the previous section, the piping problem causes the system to fail before the floodwater level reaches 0.23m in the 0.06m block height case. Since this problem has been noticed, the floodwater level in the 0.12m-block height case is increased from a low water level. As soon as piping occurs, further analysis will be stopped.

A 0.1m floodwater level is considered first and then increased to 0.2m. The tube shape and flow vectors for the 0.1m and 0.2m floodwater levels are shown in Figure 4.10 and Figure 4.4, respectively. For these cases, the zone number just below the right edge of the block is i=59, j=7. For the 0.1m floodwater case, FLAC reports U_b=113Pa, and equation 4.2 gives i=0.844. Thus, $i\gamma_w = 0.844(9807) < \gamma_b = 9807$, which shows that piping does not occur at a floodwater level equal to 0.1m or less.

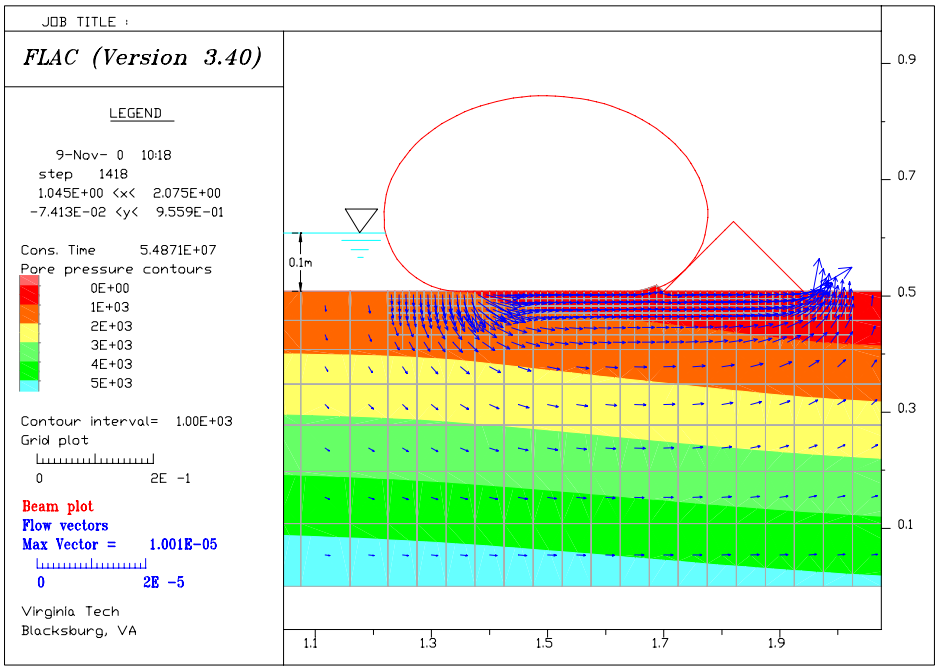

Figure 4.10: Block height = 0.12m, floodwater level = 0.1m

When the floodwater level rises to 0.2m, piping occurs. With FLAC reporting U_b =130Pa, i is equal to 1.12. Then, $i\gamma_w = 1.12(9807)$, which is greater than $\gamma_b = 9807$. Therefore, piping does occur under the block. Based on the results for the 0.1m and 0.2m floodwater level cases, one can say that piping occurs at a floodwater level somewhere between 0.1m and 0.2m, and one can also conclude that piping occurs at a much shallower floodwater level than rolling of the tube.

In order for the system to be more efficient, it is really necessary to find methods that can prevent the piping problem so that a higher floodwater level can be achieved. The solution to

this problem will be addressed in Chapter 6, in which a filter will be placed under the right edge of the tube and under the block.

Figures 4.11 and 4.12 illustrate the piping problem for floodwater levels equal to 0.25m and 0.3m, respectively. In these two figures, the ground surface on the right side of the block is obviously swelling up. This simply indicates that piping has occurred. The soil surface swells up when the pressure due to the total weight of the soil is smaller than the pore pressure in the soil. Also note that in the 0.3m-floodwater case, FLAC reported that a zone (i=59, j=7) just at the right edge of the block was too distorted and FLAC was unable to continue the execution.

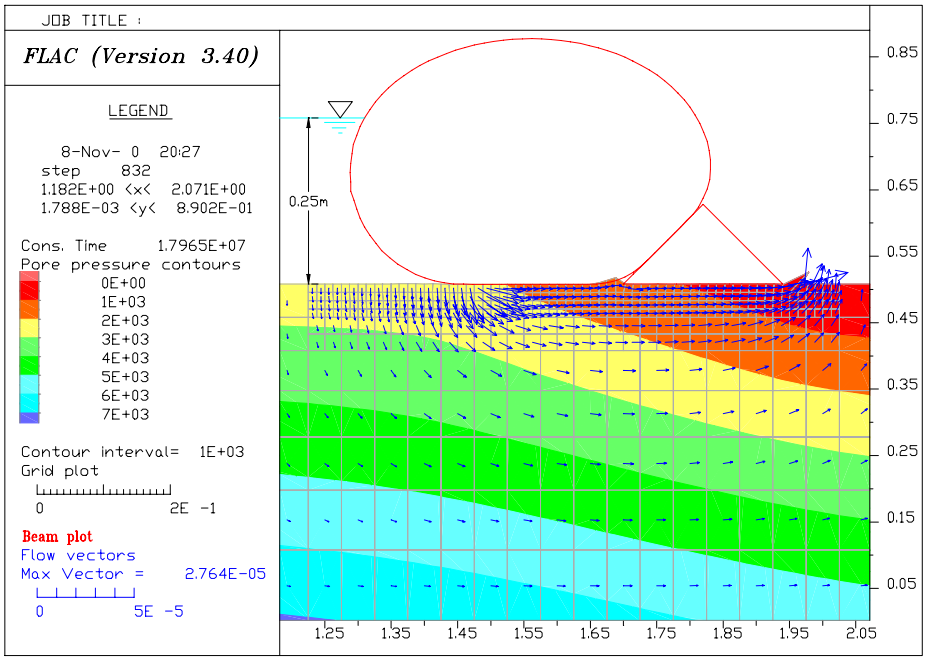

Figure 4.11: Block height =12cm, Floodwater level =0.25m.

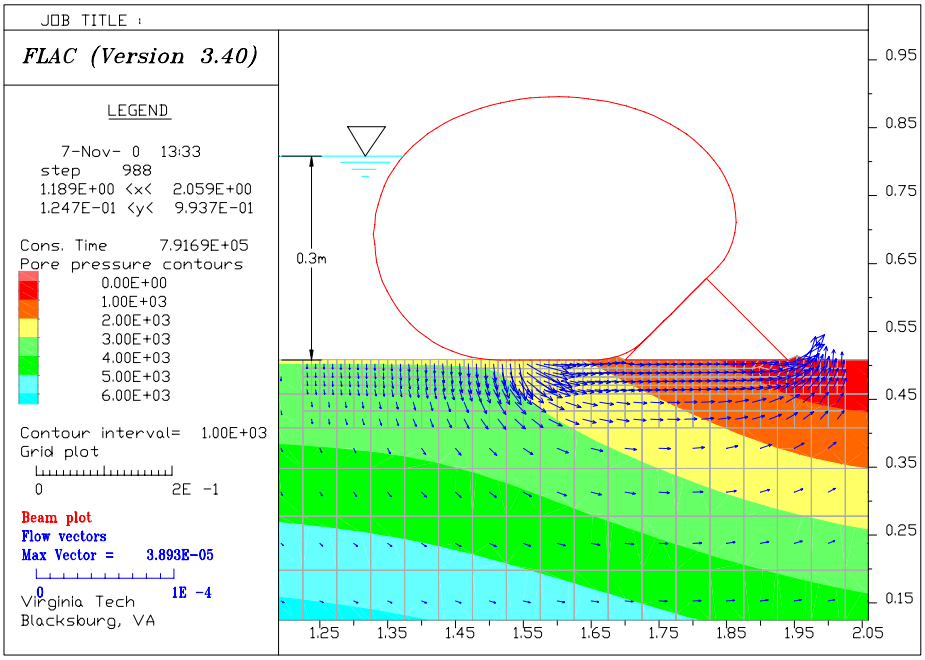

Figure 4.12: Block height = 12cm, Floodwater level = 0.3m

4.8 Proof that pore pressure in the soil has no effect on the rolling failure mode

The total stresses at the tube-soil interface are retrieved from FLAC for cases with the pore pressure (pp) effect and without the pp effect. The floodwater level and block height for these cases are 0.1m and 0.12m, respectively. The interface stresses are plotted in Figure 4.13.

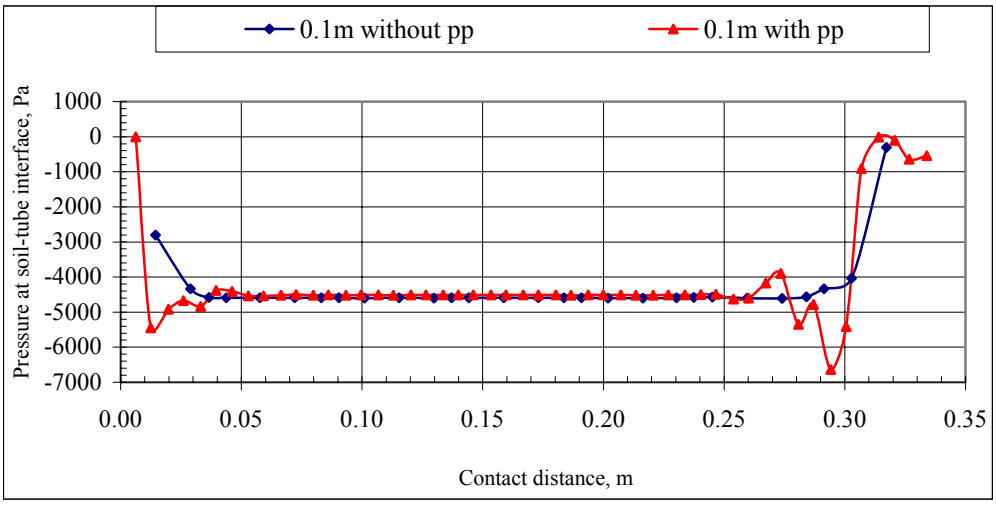

Figure 4.13: Comparison of the total stresses at the soil-tube interfaces.

Figure 4.13 shows that the total vertical stresses at the interface are approximately equal with the pp effect and without the pp effect. Since the total reaction stresses under the tube are the same, the rolling behavior of the tube for both cases should not be different. This explains why the pore pressure in the soil has no effect on the rolling failure mode.

The point spacings for the curves with the pp effect and without the pp effect are not equal, because the soil grid used for the pp effect case is finer than the soil grid for the case without the pp effect.

The pressure at the first point on the left of each curve is smaller than the pressure in the middle of the curve. This is the first contact point from the left between the tube and the soil. The total stress at the interface at this point is –1.5 Pa for the case with pore pressure effect, and this stress is less than the pp of 980.7 Pa or 0.1m water pressure head.

According to equation B2.3, the effective compressive stress at this point would be 979.2Pa tension. The sign conventions in FLAC are: positive for pp, and negative for compression at the interface. Since no tensile strength is assigned for the interface, this indicates some isolated numerical problem at this location.

However, it is believed that the outcome won't be much different, since only one structural node out of 25 structural nodes in contact with the soil grid did not perform as expected. One can always increase the accuracy by increasing the number of structural nodes and using a finer grid. The price of higher accuracy is a longer computational time.

The soil-tube contact extends further to the right for the case with the pp effect than the case without the pp effect. This is because for the former case, the pp in the soil causes the topsoil grid to swell up if there is no mechanical stress on the soil surface. As shown in Figure 4.13, the total interface stresses due to these swelled-up grids are usually small. It is believed that these stresses help to resist the rolling or sliding of the tube, since they are acting upward and to the left.

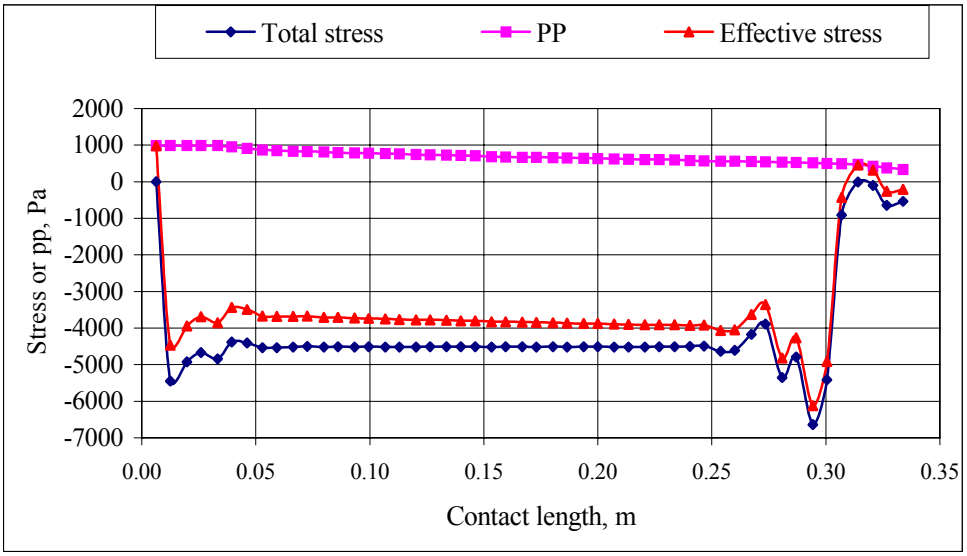

Figure 4.14: Components of interface stresses

The total stress in the case with pp effect consists of effective stress and pp. Figure 4.14 shows the plot of these three stresses for the 0.1m-floodwater case. The soil will feel only the effective stress and will act accordingly with its magnitude.

4.9 Discussion

Although this system seldom fails in sliding in the sandy soil condition, the pore pressure does affect the sliding resistance of the system. The comparison between the results shown in Table B.6 and Table B.7 in Appendix B proved that the sliding resistance is reduced by the effect of pore pressure at the interface.

As has been proven in section 4.7.1, if the piping problem is avoided, the controlling failure mode will be the rolling mode and the critical floodwater levels will be the same as for those cases that have been analyzed in chapter 3.

Chapter 5

Comparison Between Numerical Results and Experimental Results

5.1 Introduction

This chapter attempts to compare the numerical results that are obtained in Chapter 3 and Chapter 4 with the experimental results that are obtained by Fitzpatrick et al. (2001). It will be shown that the placement of a filter under the tube and the block can solve the piping problem. The total groundwater flow will be monitored, and the settlements of the soil will be obtained. Groundwater flow and settlement results are not obtained in the experimental tests.

5.2 Comparison between the experimental results and the results obtained in Chapter 3 and Chapter 4

As mentioned in section 4.9, if piping does not occur, rolling will be the next failure mode if a sandy foundation soil is used in the model. Based on this assumption, the critical floodwater levels shown in table 3.1 are the numerical results. For ease of comparison, the critical floodwater levels for 6cm and 12cm block height cases are tabulated in Table 5.1 together with the experimental critical floodwater levels.

Table 5.1: Numerical and experimental critical floodwater levels

Block height	6cm	12cm
Experimental critical floodwater level	22.9cm	27.3cm
Numerical critical floodwater level	23cm	31cm

Table 5.1 shows that the numerical critical water levels for both 6cm and 12cm block height cases are higher than the experimental critical floodwater levels. For the 6cm block height case, the critical floodwater level for the numerical model is almost the same as the experimental result. Please note that the increment of floodwater level in the numerical analysis is 1cm. This

means that the numerical critical floodwater level is greater than or equal to 23cm but less than 24cm.

When the block height is 12cm, the critical water level for the computational analysis is at least 14% higher than the experimental result. This may be due to the assumption that the internal pressure head is constant in the numerical calculations.

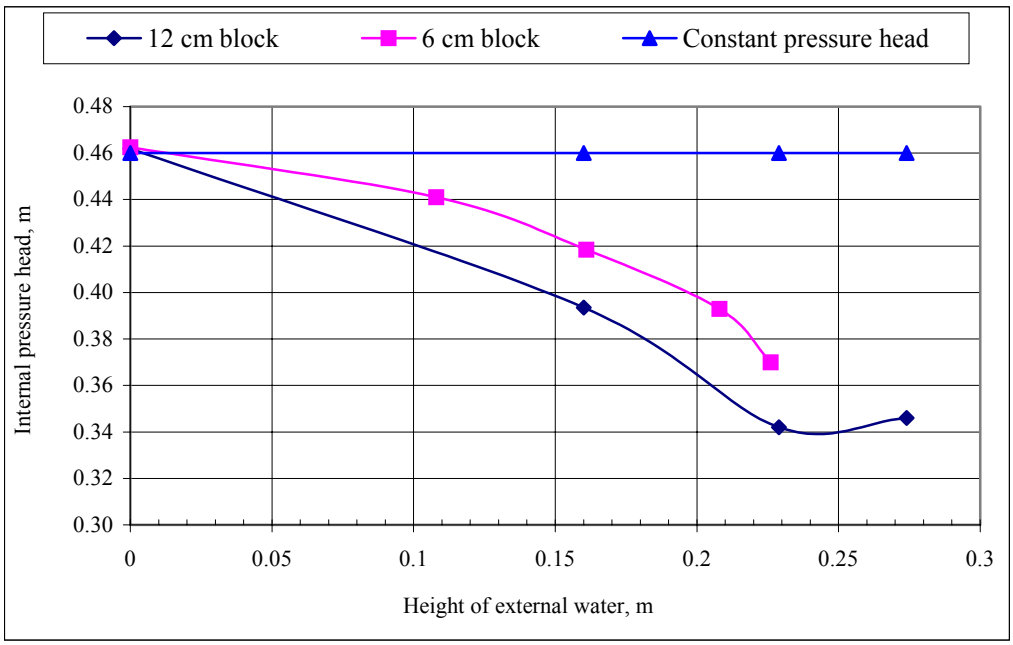

Figure 5.1: Internal pressure head for numerical model and experimental model

In the computational analysis, the tube is assumed to be connected to a fixed water source at 0.46m head throughout the tests. This gives a constant internal pressure head as shown in Figure 5.1. In the field experiment, the tube was sealed after it had been filled. The internal tube pressures were monitored and they are plotted in Figure 5.1. These plotted curves are sloping downward as the floodwater height increases. This explains why the sealed tube and unsealed tube could behave differently.

The internal pressure head of the experimental tube decreases when the floodwater increases because a constant water head was not supplied. When the floodwater pushes the elliptical tube to the right, the block on the right side of the tube pushes back and causes the tube to be rounder

and have a larger volume. But, since there is no additional water available, the tube volume will not change too much. If the tube volume is held constant, a tendency for volume increase causes the pressure head in the tube to drop, and decreases the tension in the wall. As the tensile stress in the wall of the tube decreases, the tube becomes more flexible and softer. Therefore, it is easier for the tube to conform to another shape, and its resistance to rolling over the block is reduced.

To compare the computational results with the experimental results under approximately the same situations, the numerical models must be close to the situations in the field. Therefore, more calculations on the 6cm and 12cm block height cases are carried out.

5.3 New calculations

The soil properties, tube properties, block properties, and the procedures of modeling are exactly the same as those described in Chapter 4. But, instead of maintaining a constant internal pressure head, the field measured internal pressure heads are used in the new calculations. To account for the thickness of the filter that was used in the experiment, the heights of the block are increased to 6.5cm and 12.5cm. For convenience and consistency, the block heights are still called 6cm and 12cm block heights.

As presented in Table 5.2, when the numerical models use the same internal tube pressures as in the experimental models, the critical floodwater levels between them are almost the same. The numerical critical floodwater levels are slightly lower than the experimental critical floodwater levels in both 6cm and 12cm block height cases.

Table 5.2: Comparison of critical floodwater levels.

Block height	6cm	12cm
Experimental critical floodwater level	22.9cm	27.3cm
Numerical critical floodwater level	22cm	26.5cm

However, both numerical and experimental critical floodwater levels are not exact. For example, the tube does not actually fail in the field and it could withstand even higher floodwater levels. The critical floodwater level is estimated based on the deformed shape and the experience of Brendan and Dave. In the numerical calculations, the increment of floodwater level for each case may not be fine enough. For example, in the 6cm block height case, the floodwater levels between 22cm and 22.9cm are not performed. And, in the 12cm block height case, the floodwater levels between 26.5cm and 27.3cm are not carried out. The tube may fail within these ranges of floodwater levels.

It is reasonable for the numerical tube to fail earlier than the experimental tube. In the field, the interfaces between the ends of the tube and the walls of the box are greased to reduce the friction. It is believed that the experimental tube rolls at a higher floodwater level partly because these interfaces are not frictionless, but still provide some restraint on the rolling of the tube. In addition, the experimental tubes probably exhibit some three-dimensional effects.

5.4 The relationship between rolling failure and internal water pressure

The new calculations conclude that the internal pressure head in the tube does affect the rolling behavior of the tube. As shown in Table 5.2, the critical floodwater levels in both 6cm and 12cm cases are about the same in the numerical and experimental results. When comparing to the numerical results that are presented in Table 5.1, the numerical results presented in Table 5.2 agree very well with the experimental results. This also indicates that when the internal tube pressure increases, so does the resistance against the rolling of the tube.

5.5 Filter

The results of the analysis mentioned in sections 4.7.1 and 4.7.2 illustrate that a filter is required to be placed on the right side of the tube and under the block to prevent piping problems at the right edge of the tube and at the right edge of the block. The filter is meant to prevent or retain the soil particles from being washed out from the ground. If the filter is not provided, the soil

particles just below the right edge of the block or tube will be lost due to the piping problem, and eventually will lead to a bearing failure of the whole system.

It is believed that with the help of the filter, the resistance against the floodwater can be upgraded to the next level of failure mode. This can be either the rolling or sliding failure mode.

The fine grids shown in Figure 4.5 are specifically designed for creating the filter. In fact, this filter is made up of the top fine grid zones. The left edge of the filter is approximately placed 9.5cm to the left of the left block edge for the 6cm block height case, and 11.2cm to the left of the left block edge for the 12cm block height case. The right edge of the filter is at the boundary between the fine grid mesh and the coarse grid mesh. The position of the left filter edge is about the same as it was in the field. To make the zones as porous as the filter, the permeability and the porosity in these zones are increased to 1mm per second and 60%, respectively.

The filter in the field is made up of geonet and geotextile. The geonet was placed on the top of the geotextile, which rested on the ground. The total thickness of the geonet plus geotextile was measured in the field, and it is equal to 0.5cm. The filter in the numerical model is buried in the soil and its top is at the ground level. It is believed that the difference in elevation between the filters in the field and in the computer model will not affect the results significantly, since only a small portion of the tube is resting on the filter. Since the block in the field is placed on the filter, the block height in the numerical model is increased by 0.5cm to account for the height of the filter.

5.6 Inflow and outflow

A file called Qratio.fis from the FISH library is called into FLAC immediately after the water pressures are applied on the grid boundaries. This file is able to measure the total inflow rate and outflow rate. The execution of FLAC is paused periodically for a ground water converging test. During the test, the total flow time and the total inflow and total outflow rates are recorded and compared.

Figure 5.2 shows the convergence of inflow and outflow for the 6cm block height case with a floodwater level equal to 0.1073m. In this figure, the inflow curve illustrates that the total inflow rate decreases when the flow time increases, and the outflow curve illustrates that the total outflow rate increases when the total flow time increases. Both curves eventually meet and become a horizontal line. When the curves have converged, the flows are in equilibrium, and these constant flows are called the steady-state flows.

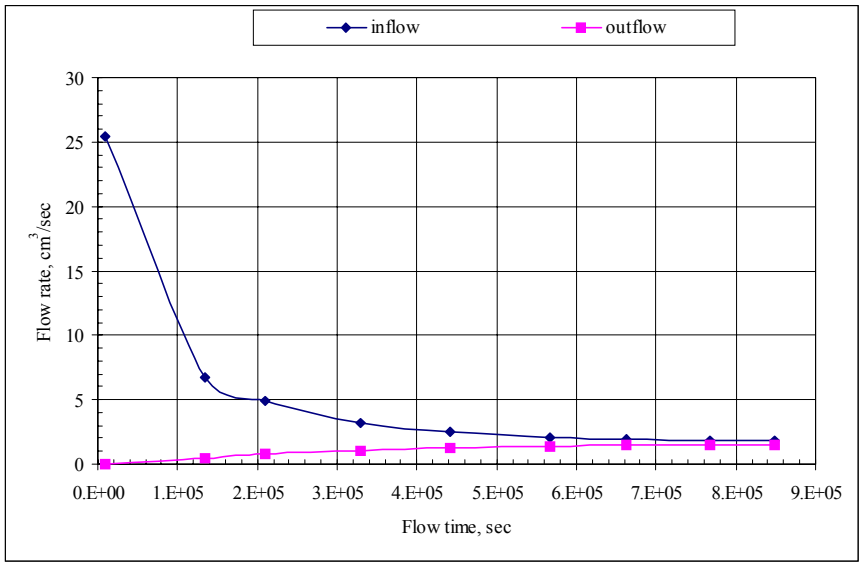

Figure 5.2: An example of the convergence of groundwater flow

5.7 Tubes with no external water

Figure 5.3 shows the comparison of the tube shape between the experimental result and the new computational model result when there is no external water. Both experiments and computational analysis used 0.465m internal tube pressure head, with the same tube circumference. The experimental tube cross-sections at the central cross section and at the cross section halfway between the center and end on the right side are plotted together with the numerical tube cross section. Their shapes compare fairly well, although the experimental tube is slightly higher and wider than the numerical model tube.

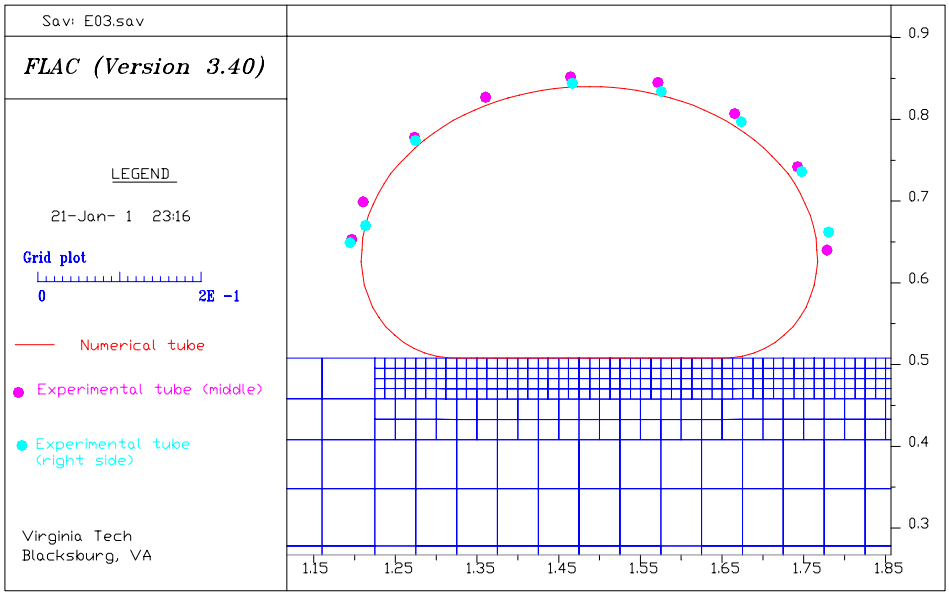

Figure 5.3: Tube shape without external water, internal pressure = 0.465m.

5.8 Modulus of elasticity

Dr. Plaut and the author carried out a tension test on a 3.2cm wide strip of the tube material, and found out that the modulus of elasticity (E) of the tube is 0.13Gpa. Brendan Fizpatrick and Dave Nevius did the tension tests also and obtained E equal to 0.17Gpa and 0.32Gpa for the 12.7cm and 20.3cm wide strips, respectively. It is expected that the value of E obtained from the widest strip matches best to the actual value of E for the tube. All these values are much lower than the value of 1.72GPa used in the numerical model. Therefore, tests on the tube's sensitivity to the value of E were carried out.

Tubes with different moduli of elasticity are inflated with the same initial tube circumference (1.4732m), internal tube pressure head (0.465m), and foundation soil. FISH functions, tubecir and tubea are written to compute the new circumference and cross-sectional area of the tubes, respectively. They can be found in the data file, tube_a.dat, which is included in Appendix A. The results of the tests are presented in Table 5.3.

Table 5.3: Tube's circumference and cross-sectional area associated with different values of modulus of elasticity.

E (Gpa)	Circumference (m)	Volume (m^3)
1.72	1.474	0.1541
1.0	1.475	0.1543
0.5	1.476	0.1546
0.3	1.478	0.1549
0.13	1.484	0.1560

Table 5.3 shows that the circumference of the inflated tube is insensitive to the magnitude of E. If the actual value of E is above 0.3Gpa, the tube is almost inextensible. There is also no significant change in the tube's cross-sectional area when E changes from 1.72Gpa to 0.3Gpa. Thus, the conclusion can be made that the effect of the use of a high value of E in the numerical model is insignificant.

5.9 Piping

5.9.1 Piping for 6cm block height case

For the experimental models, Brendan and Dave reported that there was no sign of piping under the tube and the block when the floodwater level increased from a low level to the critical level. For the numerical models, the same method that has been presented in section 4.7.1 is used to check the piping problem.

Since the tube fails in rolling at the floodwater level equal to 0.229m, the piping problem is checked near the critical floodwater case, and the floodwater level is set at 0.22m. For this case the zone number just below the right edge of the block is i=50, j=7. FLAC reports U_b=96.7Pa at the center of this zone. Equation 4.2 gives i=0.578, and equation 4.1 gives $i\gamma_w = 5665 < \gamma_b = 9807$. Since $i\gamma_w$ is less than γ_b, piping does not occur at floodwater levels equal to or less than 0.22m.

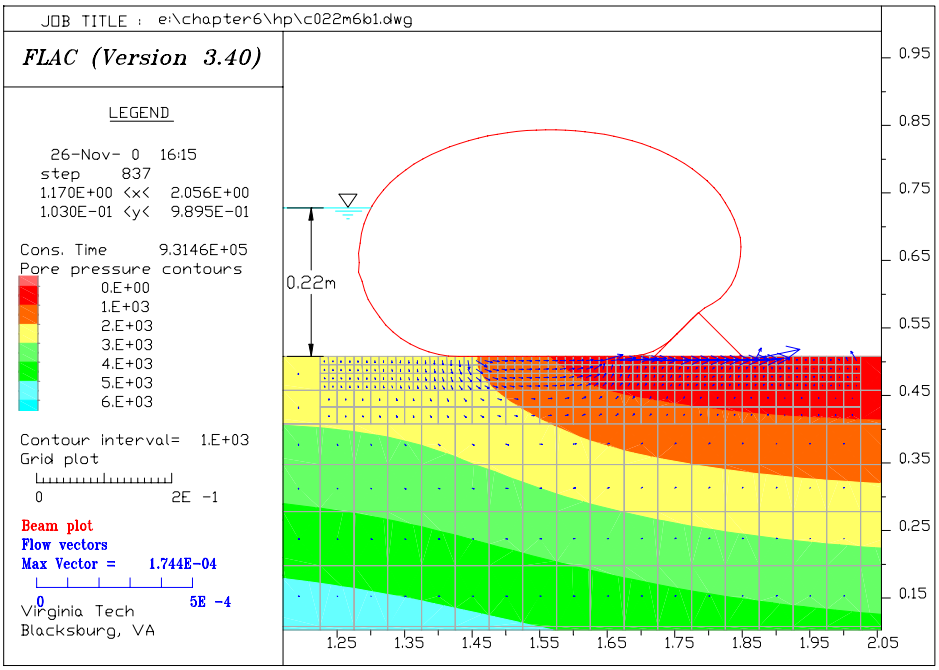

Figure 5.4: Block height = 6cm, floodwater level = 0.22m, internal pressure = 0.397m

Figure 5.4 illustrates the function of the filter at the critical floodwater level. It can be seen in the figure that the flow vectors in the filter are larger than in the soil because the ground water surrounding the filter is flowing into the filter. This clearly indicates that the filter is acting like a drain, which diverts the flow of ground water and reduces the pore pressure in the soil under the right edge of the tube and under the block. Therefore, piping was prevented after a filter was placed under part of the tube and block.

5.9.2 Piping for the 12cm block height case

The piping condition on the soil beside the right side of the block is investigated for the case with floodwater level of 0.265m. Equations 4.1 and 4.2 are used again as piping failure criteria. FLAC reports that the U_b at the center of the zone number just below and to the right of the block (i=59, j=7) is 84Pa, which gives i=0.37 and $i\gamma_w = 0.37(9807) < \gamma_b = 9807$. Therefore, piping does not occur. When a filter was not used, as was mentioned in section 4.7.2, piping occurs before the 0.2m floodwater level is reached. This clearly illustrates that the filter is one of the critical components in the system.

5.10 Rolling

5.10.1 6cm block height case

Figure 5.5 shows that the tube is rolling over the block at a floodwater level of 22.9cm. But, it does not roll at a floodwater level of 22cm as shown in Figure 5.4. No test has been done between the floodwater levels of 22cm and 22.9cm. The numerical critical floodwater level is between 22cm and 22.9cm.

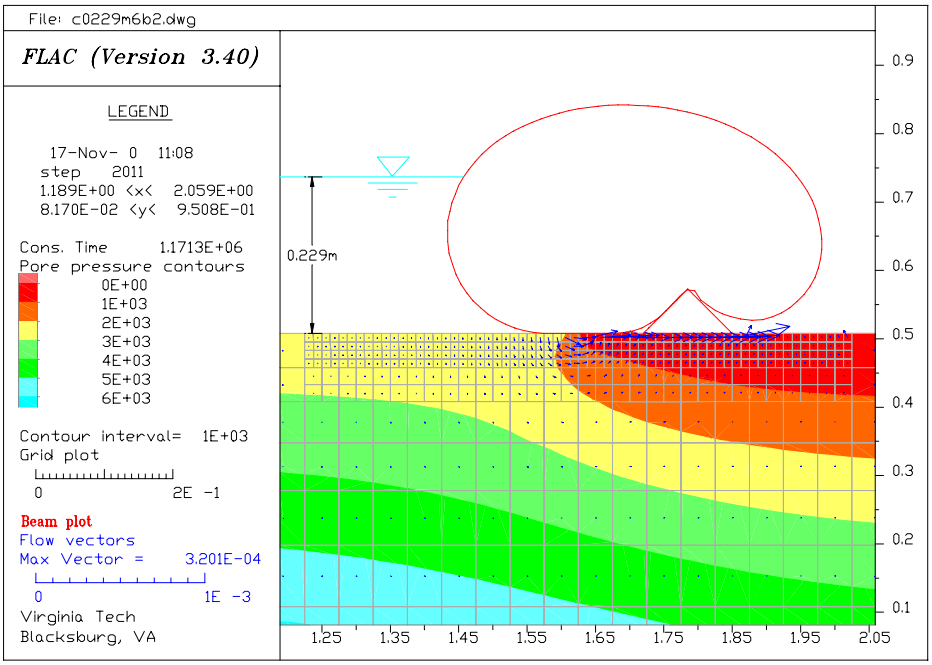

Figure 5.5: Block height = 6cm, floodwater = 0.229m, internal pressure = 0.397m

5.10.2 12cm block height case

The tube in the 0.12m block height fails in rolling also. Figure 5.6 shows the tube with a floodwater level of 0.265m, and Figure 5.7 shows that the tube is rolling over the block when the level is 0.273m. The critical floodwater level for the experimental tube is 0.273m, while the critical level for the numerical tube is between 0.265m and 0.273m.

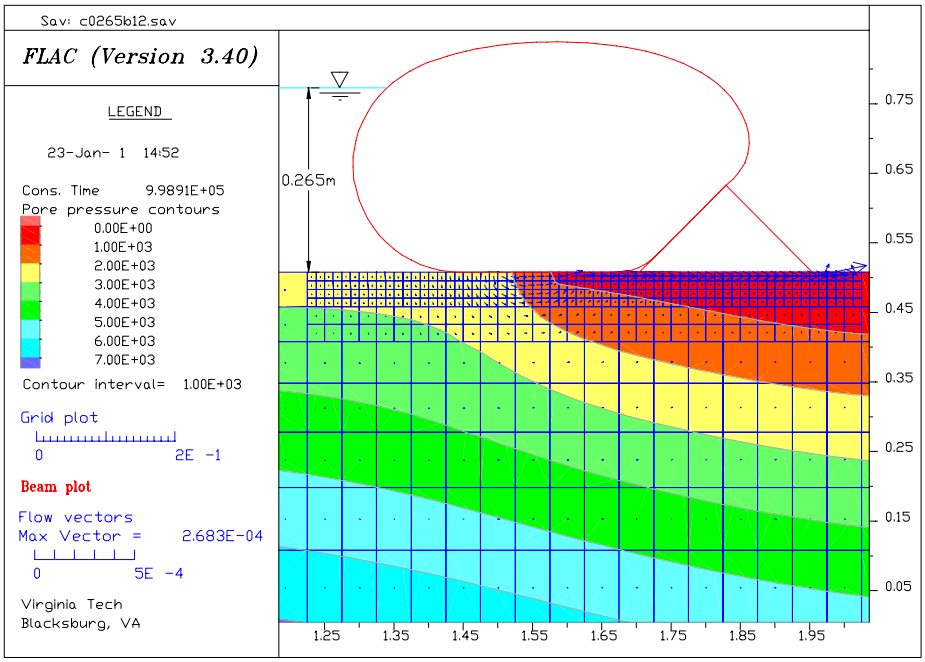

Figure 5.6: Block height = 0.12m, floodwater level = 0.265m, internal pressure = 0.349m

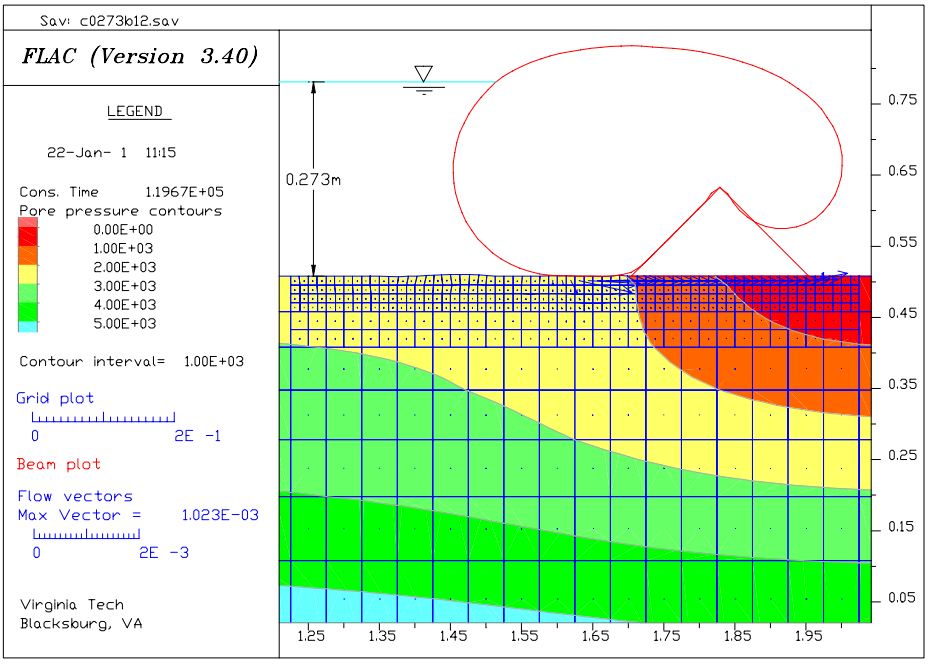

Figure 5.7: Block height = 0.12m, floodwater level = 0.273m, internal pressure = 0.349m

5.11 Pore pressure

In the field, the standpipes were installed at 4 inches (10.16cm) below the ground surface and across the length of the box (FitzPatrick et al., 2001, p.22). These standpipes are meant to measure the pore pressures of the soil at the level of the standpipes. The water levels in the standpipes are measured from the ground surface.

For convenience, the pore pressures from FLAC were retrieved at 10cm below the ground surface because there is a horizontal grid line at this level in the numerical models. The field recorded pore pressure heads are increased by 10cm, which is about the distance from the ground surface to the standpipes in the ground. Both the field measured pore pressures and the FLAC calculated pore pressures are plotted in Figure 5.8 for the 6cm block height case, and in Figure 5.9 for the 12cm block height case.

These figures show that the field and computational curves agree very well with each other. The pore pressure at the ends of the numerical curves is about constant, whereas the pore pressure at the right end of the experimental curve for the 6cm block height case continues to decrease. This is because in the field the water that seeps through the sand under the tube and the block is drained at the end of the box, and at some distance below the ground surface, but in the numerical case, the water is drained only if it comes out to the soil surface on the right side of the wooden block.

The pore pressure drops sharply under the contact area of the tube and block with the soil. For example, in the 12cm block height case, the slope of the pore pressure curves drops sharply between 1.36m and 1.98m. This is the region in which the tube and block rest on the soil when the floodwater is at 0.158m. For the 0.227m floodwater level case, this contact distance is between 1.38m and 1.98m.

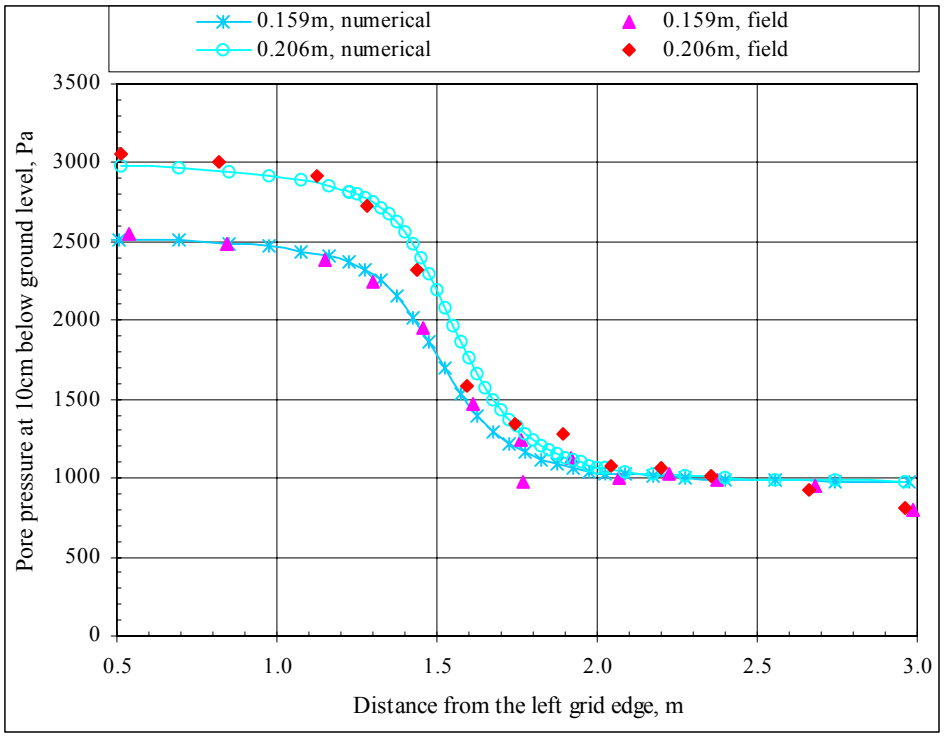

Figure 5.8: Pore pressure for the 6cm block height case

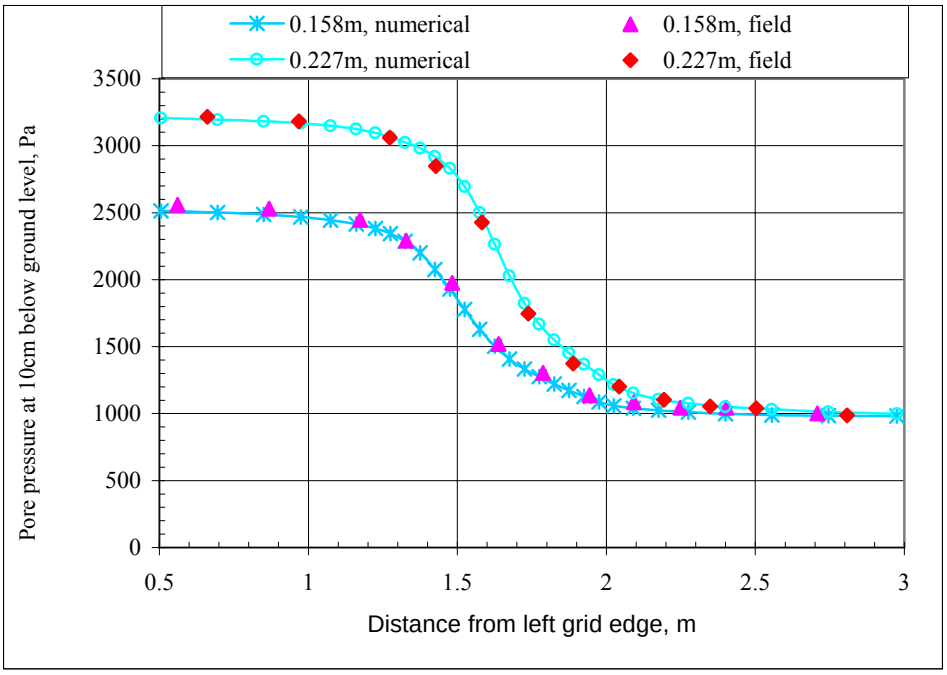

Figure 5.9: Pore pressure for the 0.12m block height case

5.12 Groundwater flow rates

The total groundwater flow rates in the computational models are obtained after the inflows and outflows have converged. These flow rates are shown in Figure 5.10. The curves in Figure 5.10 shows that the flow rate increases almost linearly when the floodwater level increases. This is because the differential hydraulic head under the tube increases when the floodwater increases. But, when the tube is about to roll over the block, the flow rate increases with increasing rate. This is because when the floodwater level increases, the contact length between the tube and the soil decreases. When the tube-soil contact length decreases, the drain path of the floodwater to flow to the other side of the tube is reduced. This is also the reason why the curve for the 6cm block height is above the curve for the 12cm block height case. For the 6cm block height case, the tube contact length is shorter than for the 12cm block height case at the same floodwater level because the tube is closer to its critical rollover condition with the lower block. Thus, the flow path is shorter for the 6cm block height case.

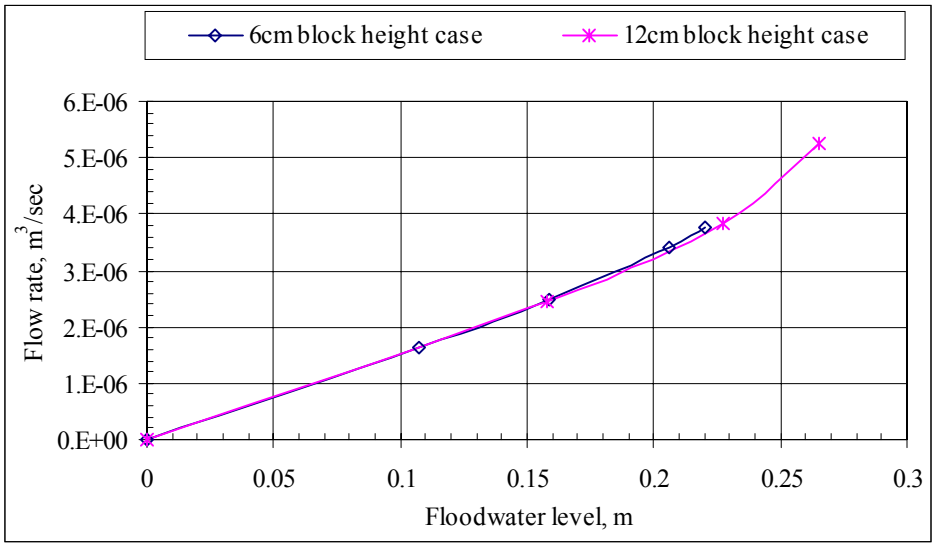

Figure 5.10: Total groundwater flow rate versus floodwater level

5.13 Tube deformations

5.13.1 6cm block height case

Figure 5.11 shows the deformed tube shapes as the floodwater level increases from zero to the level that causes the tube to roll over the block. It can be seen from the plot that the deformation

of the tube is insensitive to the rise of floodwater when the floodwater level is low. But, the sensitivity of the tube deformation increases when the floodwater level is higher, and it becomes very sensitive when the floodwater approaches the critical floodwater level.

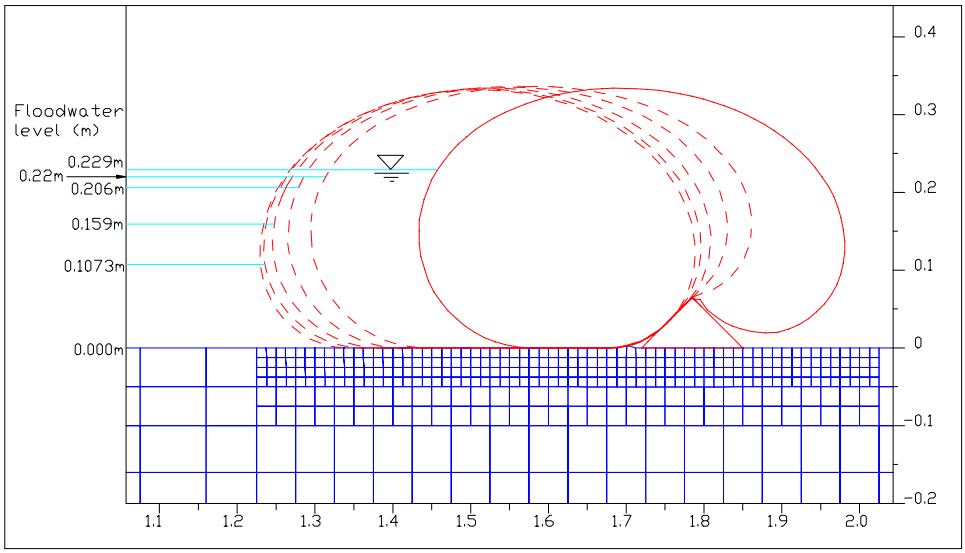

Figure 5.11: Deformation of tube

A specific point on the tubes for both the computational model and experimental model is tracked for its horizontal deformation as the floodwater level increases. For the computational model, this specific point, sp1, is the highest node of the tube when there is no floodwater. The point sp1 in the experimental tube is located somewhere on the top when the tube is not subjected to floodwater load. This point moves to the right when the floodwater rises. The horizontal deformations of the experimental tube are measured in three locations: one at the middle and one at approximately a quarter point from each end. It is believed that the middle section of the experimental tube will behave similarly as the two-dimensional numerical tube. Thus, the experimental results obtained for the middle section of the tube are selected for all the comparisons throughout this chapter unless otherwise stated.

Both the computer and the field results are plotted in Figure 5.12. These curves do not match perfectly, but agree fairly well. The field tube deforms less than the computational tube at lower floodwater levels because the end restraints help the experimental tube resist rolling. When the floodwater level is higher than 0.15m, the tube in the field deforms more than the computational

tube. This could be due to a slight movement of the block in the field. One important reason why the tube in the field deforms more horizontally is that the tube in the field was under cyclic floodwater load, and the tube in the computational model is not. For example, when the floodwater level was lowered from 0.206m to 0.101m, and back to 0.205m, the tube moved 16mm to the right. The modulus of elasticity of the tube (E) used in the numerical models is larger than the value used in the experiment, which can also be one of the reasons why the numerical tube deforms less. A tube with a higher value of E is stiffer and less flexible.

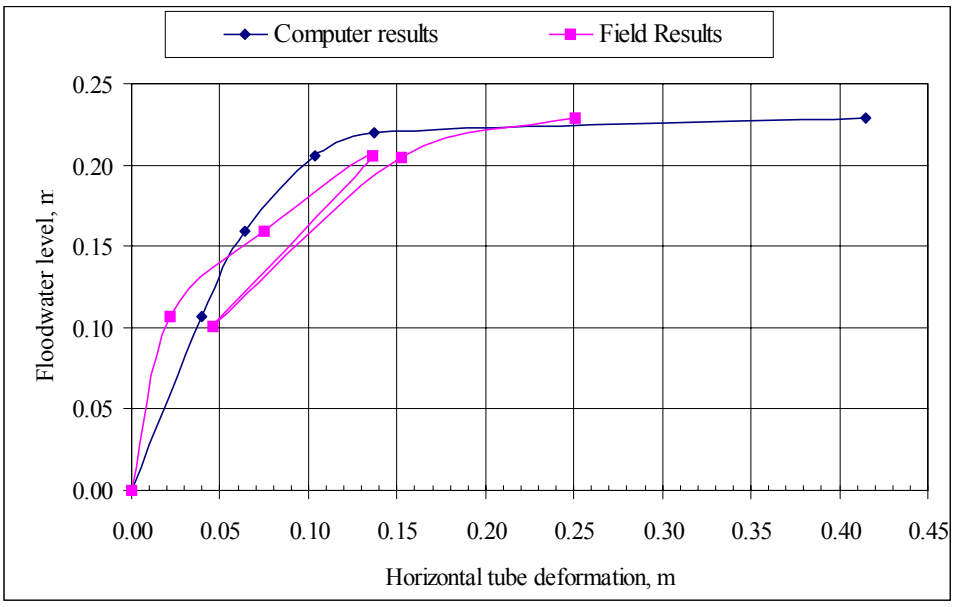

Figure 5.12: Horizontal deformation of the tube for the 6cm block height case

The horizontal deformation of the computer model at the floodwater level of 0.229m is invalid because the tube has already failed, but the experimental result at this floodwater level is valid. These are the last points of the curves in Figure 5.12.

Figure 5.13 shows the movement of the 'sp1' node calculated by FLAC, and by the experiment. This point moves to the right when the floodwater level rises. But, in the vertical movement, the numerical tube and experimental tube behave differently before the tube reaches 0.159m floodwater level. The numerical tube rises very slowly until it reaches the floodwater level of 0.159m. In contrast, the experimental tube drops sharply when the floodwater level increases from zero to 0.107m, then it remains almost constant until the floodwater level is equal to

0.159m. When the floodwater level exceeds 0.159m, both numerical and experimental tubes behave similarly. They both drop first, and then rise after the floodwater level is higher than 0.206m.

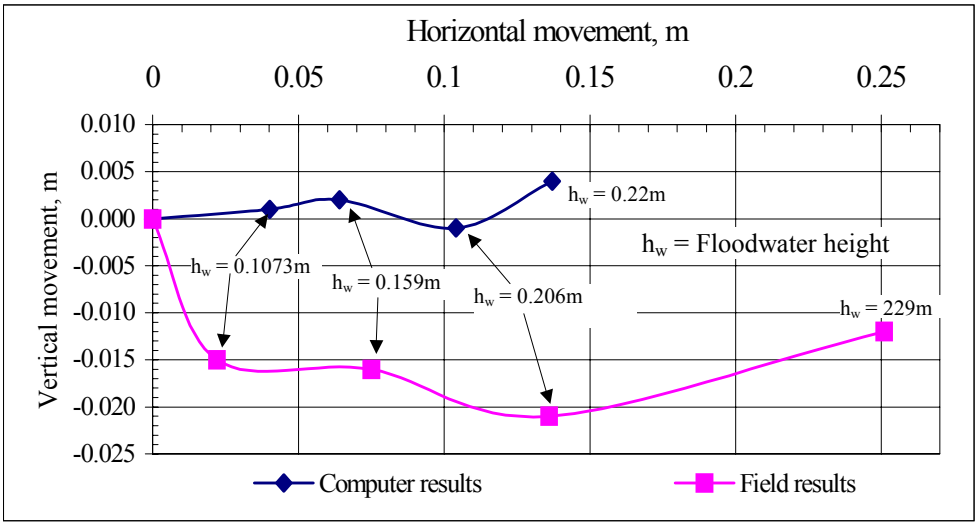

Figure 5.13: The movement of a point on the tube, 6cm block height case

5.13.2 12cm block height case

Figure 5.14 compares the horizontal tube deformations for the 12cm block height case. It can be seen that the field curve almost matches the numerical curve. The numerical tube deforms only a little more than the experimental tube at low floodwater levels. When compared to the curves in Figure 5.13, these curves agree a lot better. This is because the experimental tube here was not subjected to the cyclic loading from zero to 0.273m of floodwater level. The slope for the numerical curve becomes horizontal after 0.265m (the last point) floodwater level. This infinite deformation represents the failure of the numerical tube in rolling at the 0.273m floodwater level. The deformation data at the 0.265m floodwater level were not recorded for the experimental tube. It is expected that if this point exists, it will be very close to the numerical tube's point.

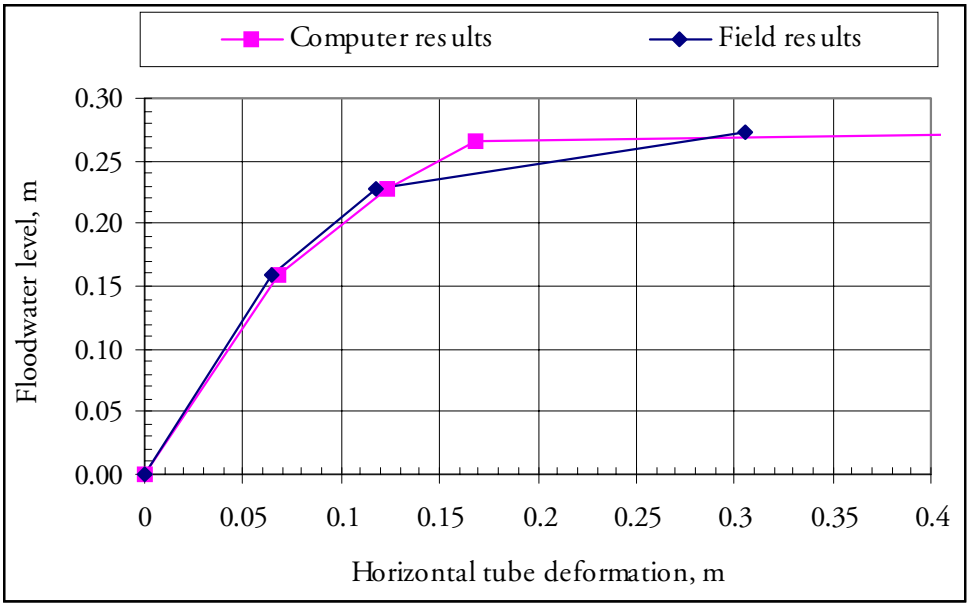

Figure 5.14: Horizontal deformation of the tube for the 12cm block height case

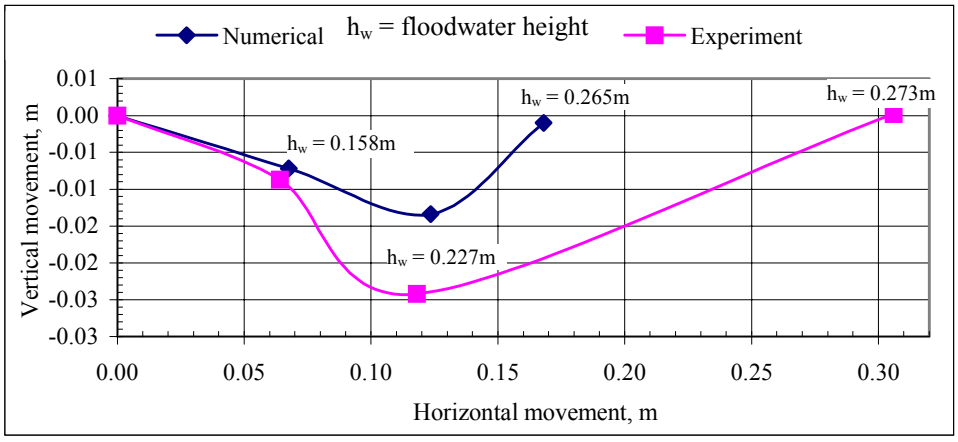

Figure 5.15: The movement of a point on the tube, 12cm block height case

For the 12cm block height case, the movement of 'sp1' behaves similarly between the numerical and experimental tubes. Both tubes drop when the floodwater level increases from zero to 0.227m, and then rise until they roll over the blocks. At zero floodwater level, the experimental tube is higher than the numerical tube, as is evident in Table 5.4 for the 6cm block height case, and in Table 5.6 for the 12cm block height case. This is the main reason why the vertical movement of the numerical tubes does not agree well with the vertical movement of the experimental tubes.

5.14 Tube height and width

5.14.1 6cm block height case

Table 5.4 and Figure 5.16 show that the numerical tube height agrees fairly well with the experimental tube height. The tube height remains almost constant when the floodwater level increases from zero to the critical level. This is because the internal pressure of the tube decreases when the floodwater level increases. Section 5.14.2 will present a comparison of the tube heights between the constant internal pressure case and the variable internal pressure case.

Table 5.4: Tube height, width, and height over width ratio

		Numerical results			Experimental results		
Floodwater level	Internal pressure	Tube height	Tube width	$\frac{\text{height}}{\text{width}}$	Tube height	Tube width	$\frac{\text{height}}{\text{width}}$
0m	0.465m	0.332m	0.559m	0.594	0.353m	0.578m	0.611
0.107m	0.445m	0.333m	0.562m	0.593	0.338m	0.589m	0.574
0.159m	0.422m	0.334m	0.564m	0.592	0.337m	0.588m	0.573
0.206m	0.396m	0.331m	0.565m	0.586	0.332m	0.590m	0.563
0.220m	0.387m	0.336m	0.566m	0.594	-	-	-
0.229m	0.387m	Fails in rolling			0.341m	0.589m	0.579

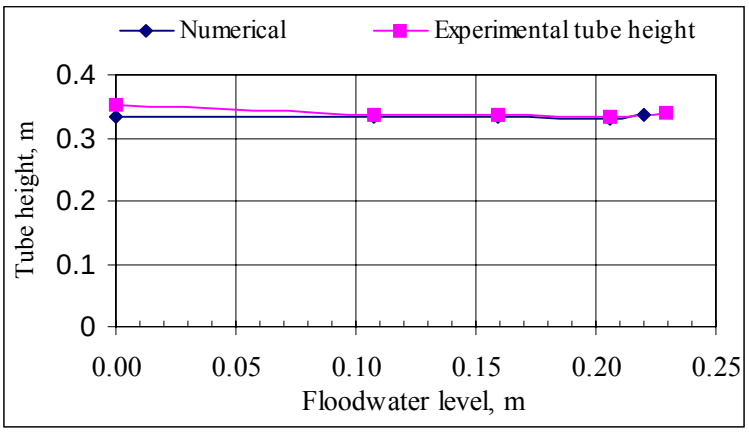

Figure 5.16: Tube height vs. floodwater level for the 6cm block height case

Figure 5.17 shows that the width of the computational tube increases almost linearly as the floodwater increases. But the changing pattern for the width of the experimental tube is not simple. It increases up to a certain floodwater level and then remains constant until the system fails. Figure 5.17 also indicates that the experimental tube is about 3.5% wider than the computational tube.

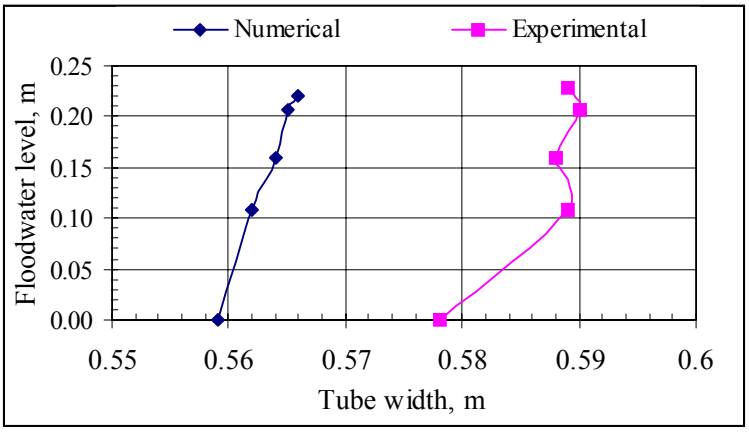

Figure 5.17: Tube width vs. floodwater level for the 6cm block height case

The computational tube height to tube width ratio that is shown in Figure 5.18 is almost constant at any floodwater level. This ratio is around 0.59 as can be read from Table 5.4. For the experimental model, this ratio drops when the floodwater level increases to 0.107m, and then it remains roughly constant at 0.57, which is slightly lower than the computational result. Anyway, the computational and experimental results agree well with each other.

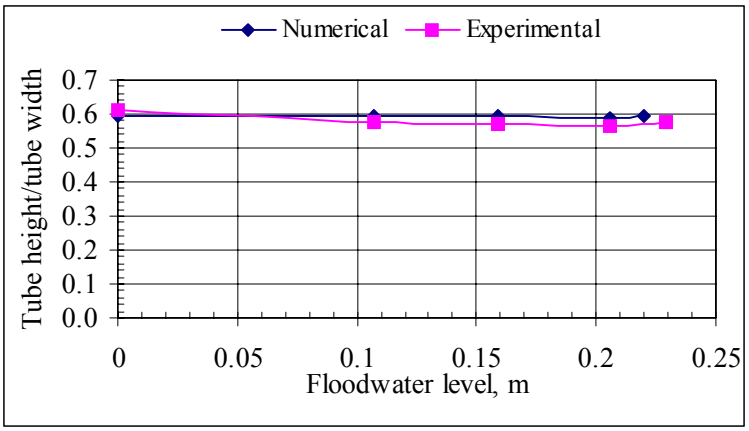

Figure 5.18: Tube height over tube width ratio vs. floodwater level for the 6cm block height case

5.14.2 12cm block height case

Table 5.5 presents the tube height and width at different floodwater levels for the cases with constant internal tube pressure head, which is 0.46m. Table 5.6 presents the tube height and width from the results obtained by the numerical and experimental analyses side by side. The field measured internal tube pressure heads are used in these numerical analyses.

Table 5.5: Tube height and width for the tube with constant internal pressure

Floodwater level	Tube height	Tube width	$\frac{\text{height}}{\text{width}}$
0	0.334m	0.556m	0.601
0.1	0.339m	0.557m	0.609
0.2	0.359m	0.550m	0.653
0.25	0.373m	0.544m	0.686
0.3	0.390m	0.534m	0.730
0.31	0.392	0.525	0.747
0.32	Fails in rolling		

Table 5.6: Tube height and width for the tube with variable internal pressure

		Numerical results			Experimental results		
Floodwater level	Internal pressure	Tube height	Tube width	$\frac{\text{height}}{\text{width}}$	Tube height	Tube width	$\frac{\text{height}}{\text{width}}$
0m	0.465m	0.332m	0.559m	0.594	0.344m	0.582m	0.591
0.158m	0.397m	0.325m	0.57m	0.570	0.334m	0.597m	0.559
0.227m	0.346m	0.319m	0.578m	0.552	0.332m	0.602m	0.551
0.265m	0.349m	0.331m	0.572m	0.579	-	-	-
0.273m	0.349m	Fails in rolling			0.347	0.571	0.608

Tube height and width are different if a different internal pressure is used. The tube height comparison between the experimental tube, the numerical tube with a constant tube pressure

head, and the numerical tube with the field measured pressure heads is shown in Figure 5.19. The height of the tube increases with higher floodwater level if the internal pressure head remains constant (unsealed tube). In contrast, when the field measured pressure is used (sealed tube), the height of the tube decreases when the floodwater level increases, except when it approaches failure: then the tube height increases. The experimental tube behaves similarly to the sealed numerical tube.

Figure 5.20 shows how the tube width changes when the internal tube pressure is constant or variable. The tube becomes narrower at higher water level if the internal tube pressure is constant. But when the field measured pressure is used, which means lower internal pressure is used, the tube is wider at a higher floodwater level. When the floodwater level approaches the critical floodwater level, the internal tube pressure increases, and the tube width decreases. Again, the experimental tube behaves similarly to the sealed numerical tube, except the experimental tube is slightly wider.

When the tube pressure is unchanged, the tube height over tube width ratio increases at a higher floodwater level as shown in Figure 5.21. When the field measured pressure is used, this ratio is decreased at a higher floodwater level, but its variation is small. The curve for the numerical tube almost matches the curve for the experimental tube.

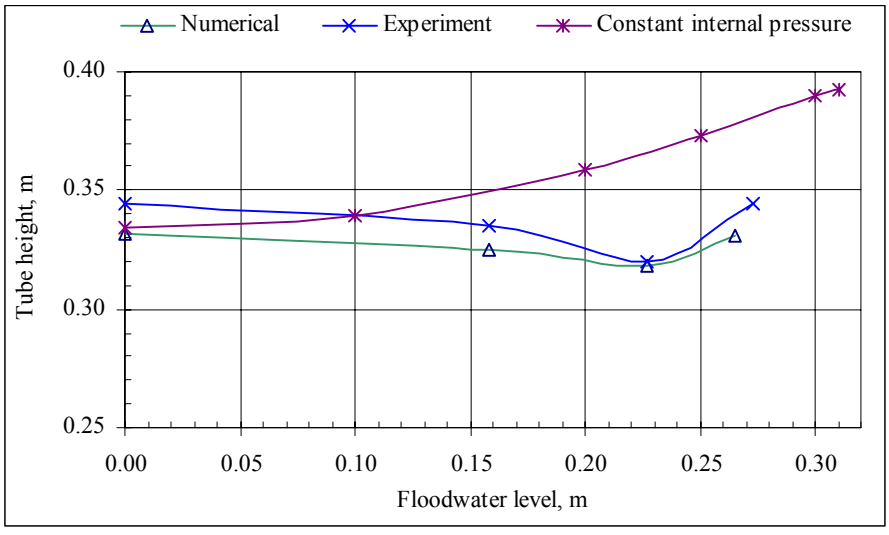

Figure 5.19: Tube height versus floodwater level for the 12cm block height case

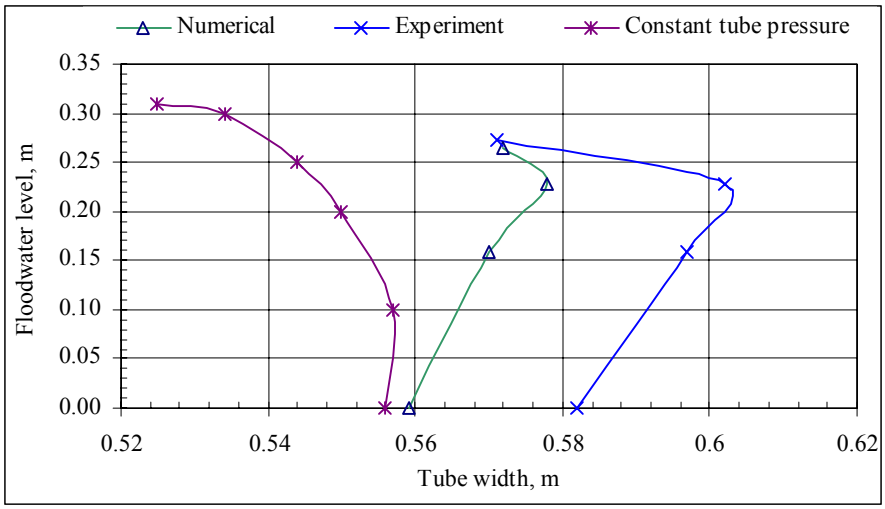

Figure 5.20: Tube width versus floodwater level for the 12cm block height case

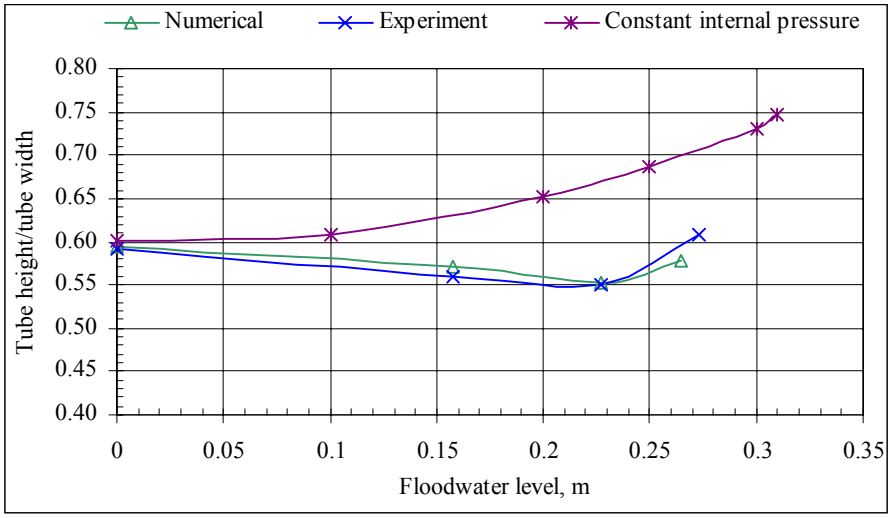

Figure 5.21: Tube height over tube width ratio versus floodwater level for the 12cm block height case

5.15 Tube shapes

5.15.1 6cm block height case

Figure 5.22 compares the tube shapes between the computational and experimental models at different floodwater levels. As shown in Figure 5.22a, the tube shapes at 0.107m floodwater level almost match perfectly except the experimental tube is slightly larger than the computational tube. Figure 5.22b shows the tube shapes at the floodwater level of 0.159m. The

tube shapes still agree well, but the experimental tube rolls slightly more to the right. When the floodwater level is at 0.206m, as shown in Figure 5.22c, the experimental tube rolls more than the numerical tube. But, when the floodwater level is at 0.229m, as shown in Figure 5.22d, the numerical tube rolls over the block while the experimental tube is left behind with a large portion of it overhanging on the block.

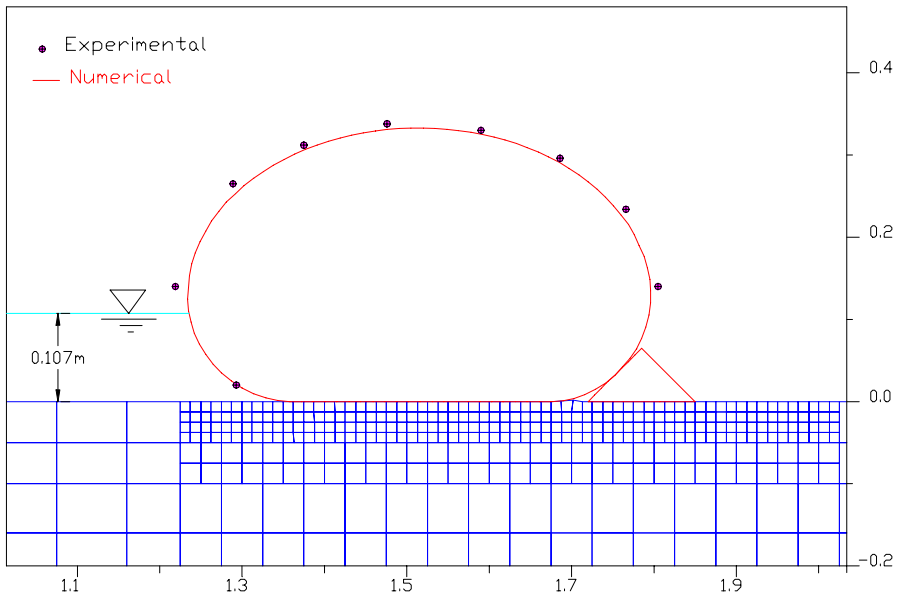

Figure 5.22a: Tube shape at 0.107m floodwater level, block height = 6cm

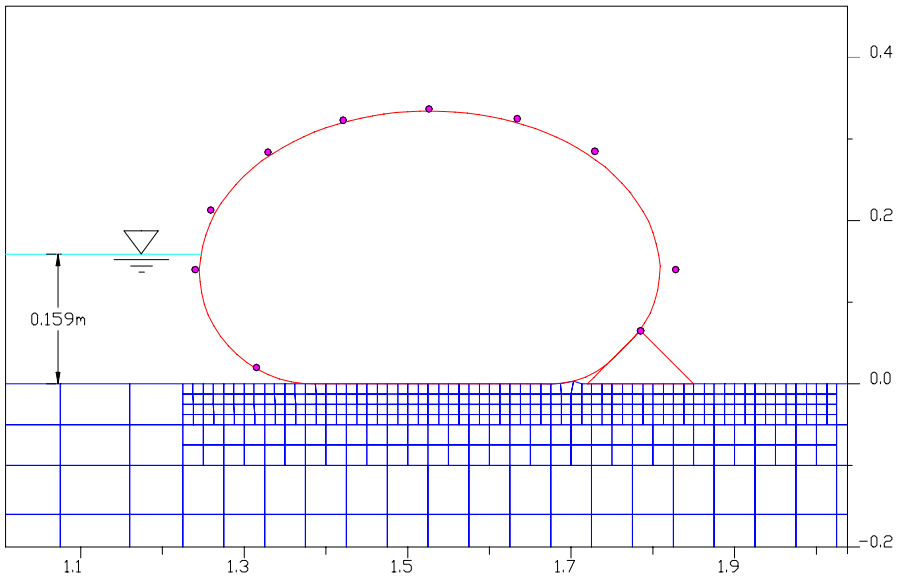

Figure 5.22b: Tube shape at 0.159m floodwater level, block height = 6cm

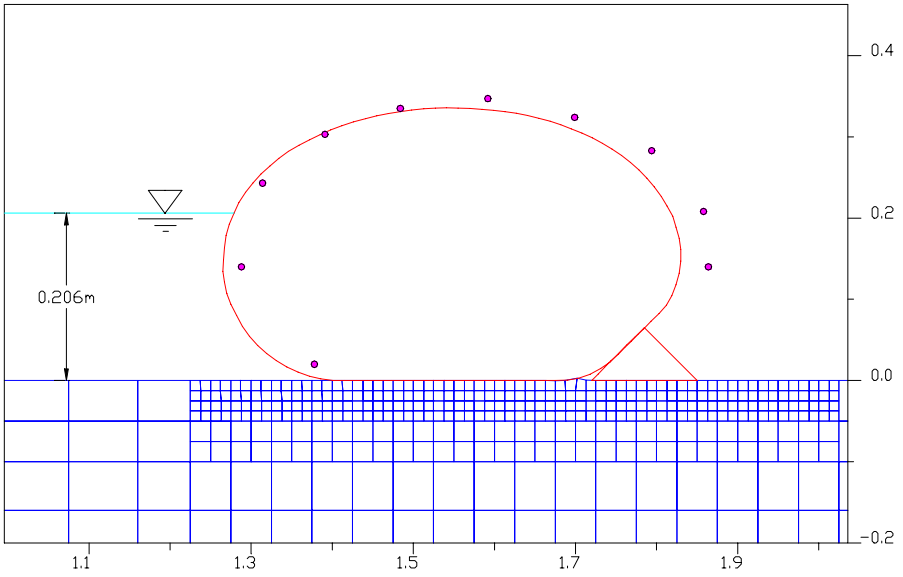

Figure 5.22c: Tube shape at 0.206m floodwater level, block height = 6cm

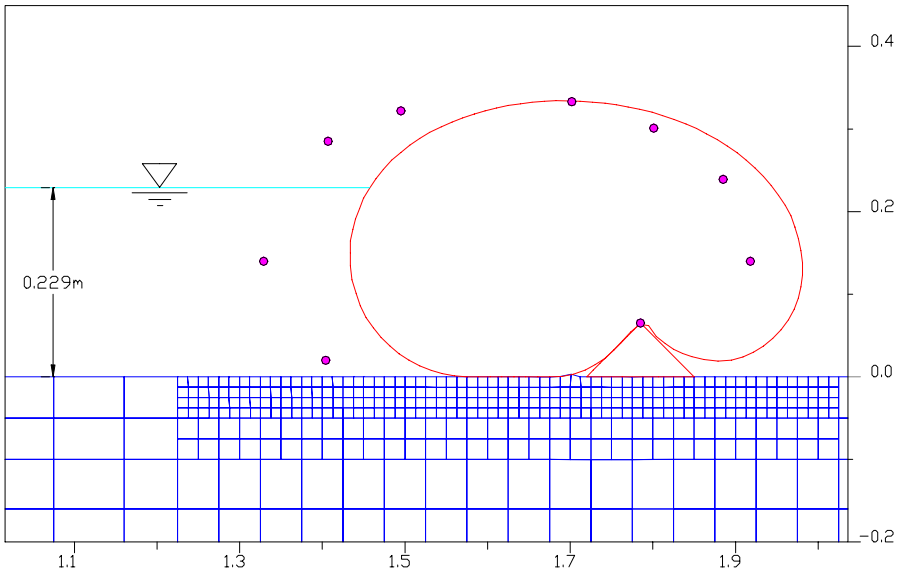

Figure 5.22d: Tube shape at 0.229m floodwater level, block height = 6cm

5.15.2 12cm block height case

Figure 5.23a through Figure 5.23c compare the numerical tube shapes with the experimental tube shapes for the 12cm block height case. Figure 5.23a shows that the experimental tube at floodwater level of 0.158m is slightly wider and higher. As shown in Figure 5.23b, when the floodwater level increases to 0.227m, the height of the numerical tube matches that of the experimental tube. But, the experimental tube is still a little wider than the numerical tube. The shapes compare well.

Figure 5.23c shows that the numerical tube is rolling when the floodwater level is at 0.273m, whereas the experimental tube was still stable with part of it overhanging on the block. It can be seen that the numerical tube penetrates into the block a little bit. This is because the interface between tube and block at that location was not assigned.

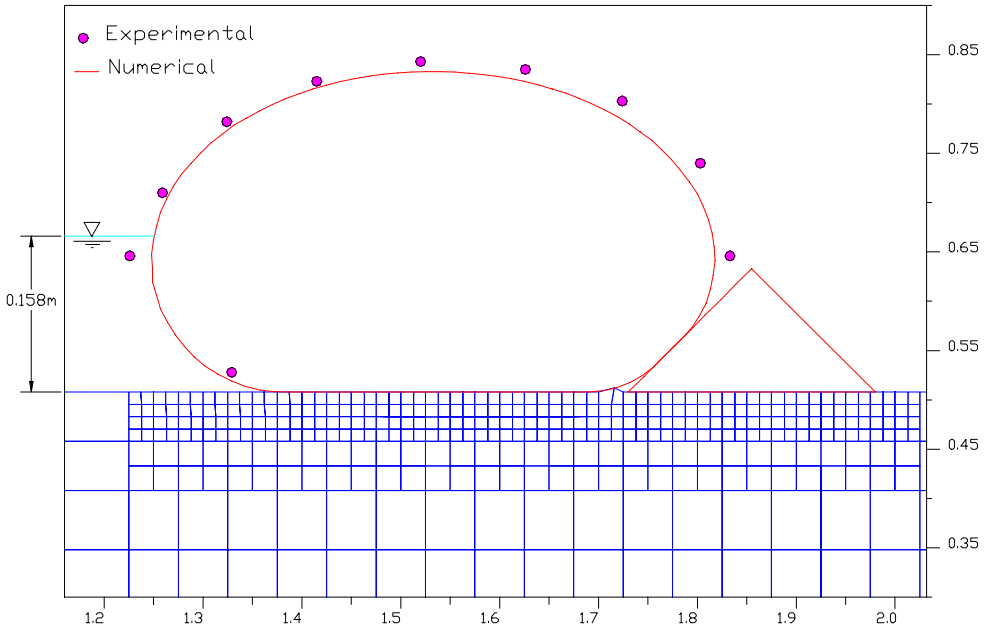

Figure 5.23a: Tube shape at 0.158m floodwater level, block height = 12cm

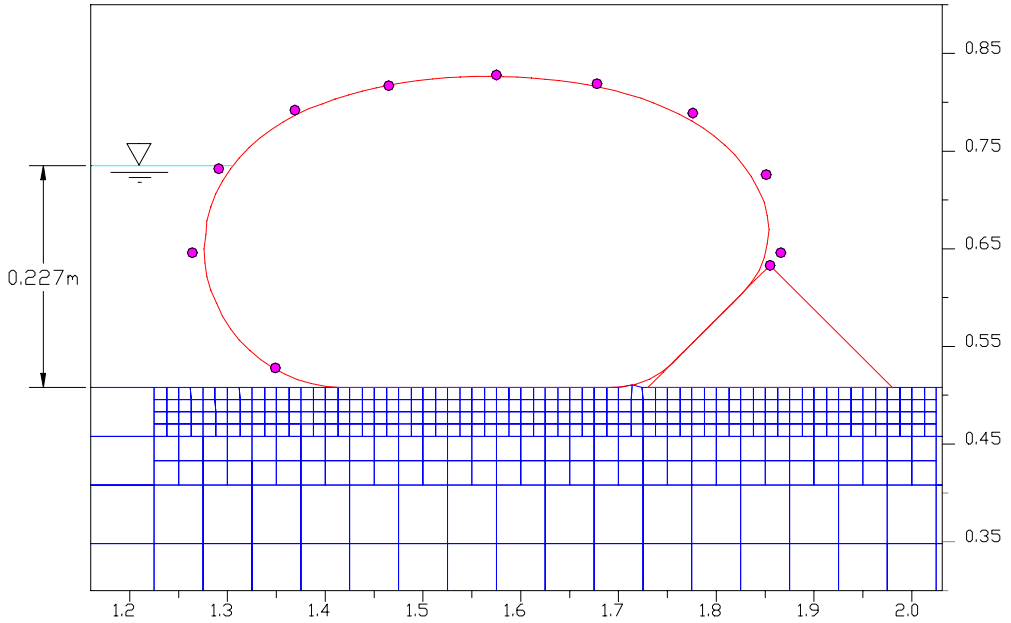

Figure 5.23b: Tube shape at 0.227m floodwater level, block height = 12cm

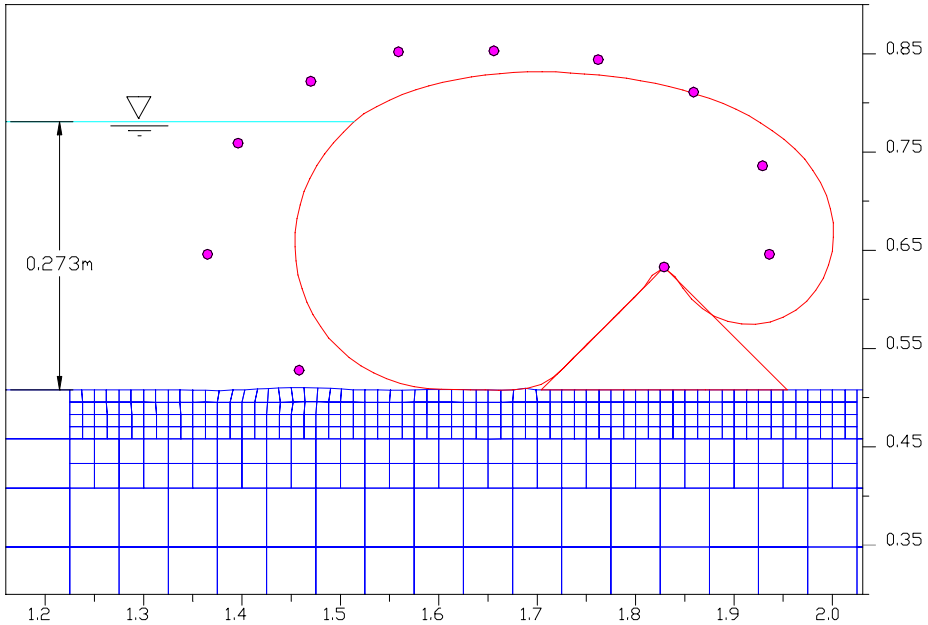

Figure 5.23c: Tube shape at 0.273m floodwater level, block height = 12cm

5.16 Tube's circumference and cross-sectional area

5.16.1 6cm block height case

The tube's circumference and cross-sectional area for the numerical model are presented in Table 5.7 for the case of variable (field measured) internal pressure head. If four significant digits are used, the tube circumference is basically unchanged for all the floodwater levels. The percent difference in tube area associated with floodwater level is computed based on the initial (zero floodwater level) tube area. Figure 5.24 shows that the tube cross-sectional area increases almost linearly when the floodwater increases. But, it decreases sharply after the floodwater level exceeds 0.206m. A large vertical scale is used in Figure 5.24 to make it the same as the vertical scale in Figure 5.25. For the comparison of the tube areas between the fixed internal tube pressure and variable field measured internal tube pressure, please refer to the next section.

Table 5.7: Tube's circumference and cross-sectional area at various floodwater levels

Floodwater level (m)	Internal tube pressure head (m)	Tube circumference (m)	Tube area (m^2)	Difference in tube area (%)
0	0.465	1.474	0.1543	0
0.1073	0.445	1.474	0.1553	0.65
0.159	0.422	1.474	0.1559	1.04
0.206	0.396	1.474	0.1563	1.30
0.22	0.387	1.474	0.1554	0.71
0.229	0.387	Fails in rolling		

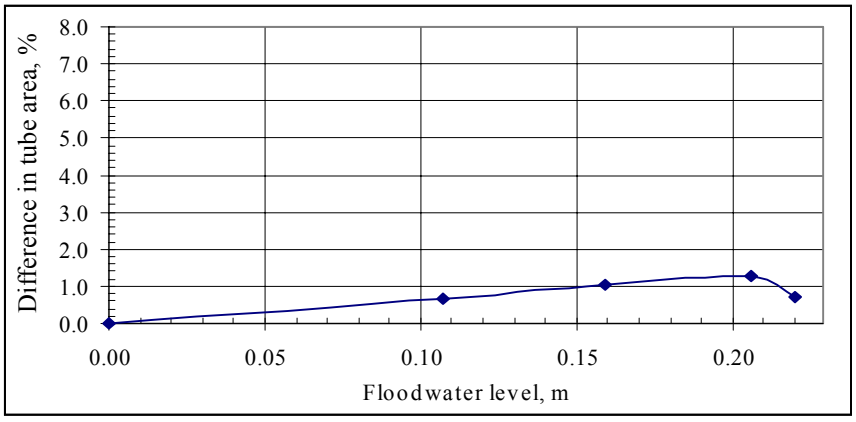

Figure 5.24: Percent difference in area versus floodwater level for the 6cm block height case

5.16.2 12cm block height case

If the internal tube pressure is maintained the same, the results shown in Table 5.8 and Figure 5.25 would be obtained, in which the tube's area and circumference increase as the floodwater level increases. Please note that the results shown in Table 5.8 and Figure 5.25 are obtained from the analyses that were mentioned in section 3.8.

Table 5.8: Tube's circumference and area with constant internal pressure

Internal tube pressure head = 0.46m	Floodwater level (m)	Tube circumference (m)	Tube area (m^2)	Difference in circumference (%)	Difference in tube area (%)
	0	1.471	0.1545	0	0
	0.1	1.476	0.1570	1.62	0.34
	0.2	1.478	0.1620	4.85	0.48
	0.25	1.477	0.1644	6.41	0.41
	0.3	1.472	0.1649	6.73	0.07
	0.31	1.459	0.1616	4.60	
	0.32	Fails in rolling			

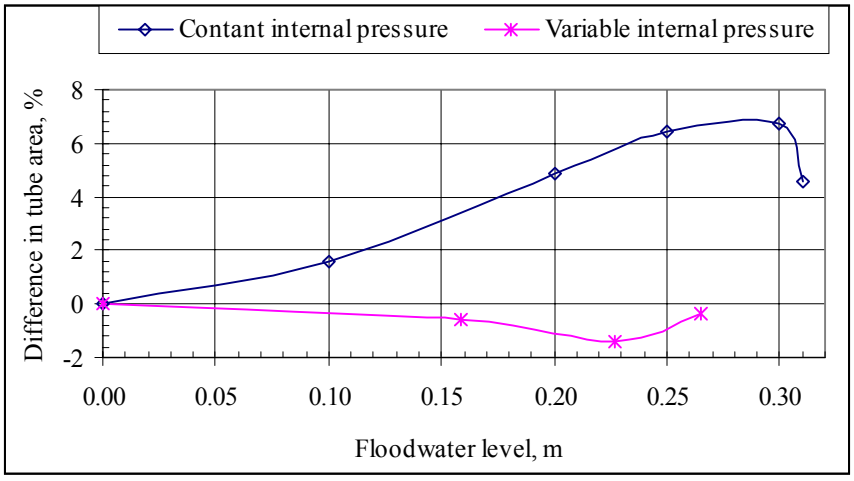

Figure 5.25: Percent difference in tube area for the 12cm block height case

Table 5.9: Tube circumference and area with variable tube pressure

Internal tube pressure (m)	Floodwater level (m)	Tube circumference (m)	Tube area (m^2)	Difference in tube area (%)
0.465	0	1.474	0.1546	0
0.397	0.1583	1.474	0.1537	-0.58
0.346	0.227	1.474	0.1524	-1.42
0.349	0.265	1.474	0.154	-0.39
0.349	0.273	Fails in rolling		

Figure 5.25 shows that when the constant internal pressure head of the tube is used, the tube area increases. At 0.3m floodwater level, the tube area is the largest and it is 6.7% larger than the initial tube area. When comparing this with the tube area obtained by using the field measured internal pressure head (variable internal pressure), the latter is much smaller, and even smaller than the initial area. When the variable internal tube pressure head is used, the maximum variation of the tube area with respect to the initial tube area is 1.3% in Figure 5.24, and –1.4% in Table 5.9. For the sealed tube containing incompressible water, the correct results can be obtained if the initial tube area can be maintained.

5.17 Soil settlements

Figure 5.26 presents an example of the settlement of the foundation soil surface. This is for the 6cm block height case. The settlement for the 12cm block height case is not presented because it is expected to behave similarly as the 6cm block height case. The curves in Figure 5.26 indicate that the settlement of the soil surface under the tube tends to decrease when the floodwater level increases. This occurs because the settlement of the soil is directly related to the effective soil stress instead of the total soil stress. When the floodwater level increases, the pore pressure in the soil under the tube is also increased, but the tube load is constant. As equation B2.2 shows, an increase in pore pressure will reduce the effective soil stress. Lower effective stress in the soil causes smaller settlement.

It can be seen from the plots that the edges of the tube settle more than the rest. For the zero floodwater level, the left edge is around 1.325m and the right edge is around 1.64m from the left edge of the grid mesh. The tube at these locations settles 0.06mm more than at its center.

The plots also indicate that when the tube settles, some sand is displaced to the sides of the tube. This displaced soil is clearly shown on the left side of the plots. One may also notice that as the increased floodwater level pushes the tube to the right, a little soil is displaced behind the tube.

The soil is uplifted or squeezed into the little gap between the tube and the block. As shown in Figure 5.26, this uplifted soil is located at a horizontal distance between 1.685m and 1.725m. The maximum level of uplift is around 2.5mm and touches the bottom of the tube. The plots do not show the whole uplift curves because if they are shown, the details of settlement for all the remaining portions of the soil surface will not be recognizable. This uplift may be the displaced soil caused by the tube settlement or due to the high pore pressure that acts like a hydrostatic pressure, which raises the top grid up and pushes on the tube.

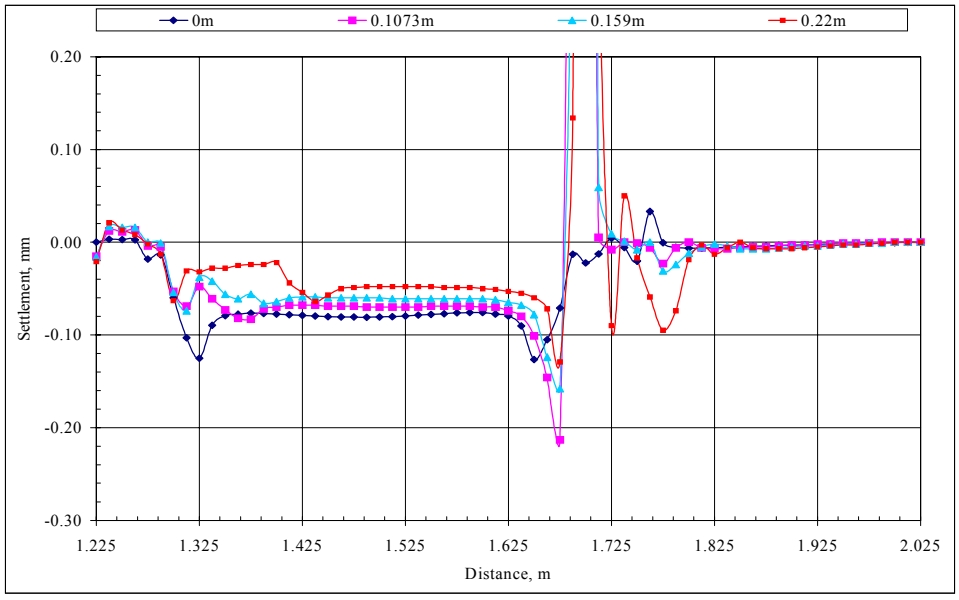

Figure 5.26: Settlements of the foundation soil surface

The base of the block is sitting on the soil between 1.72m and 1.84m along the top of the top grid. The curves in Figure 5.26 indicate that the soil settles more under the middle of the block.

This means that the block base deflects more at its middle. Although the thickness of the wooden block frame is 2.5cm, it is not rigid. The curves also show that the soil under the block settles more when the floodwater level increases.

The settlement for the sand foundation is relatively small in the cases considered in this chapter. The sand considered in the model is medium dense sand with an internal angle of friction, ϕ, equal to 36°. If ϕ were smaller, the settlement of the soil would increase. A very loose sand foundation is not covered in this thesis, but it can be done easily by changing the ϕ and N values in section 4.2, and the soil-tube and wood-soil interface friction angles in section 3.4. Then, simply replace the old bulk modulus (b), shear modulus (s), and internal soil friction angle (ϕ), and tube-soil interface friction angle with the new ones in Grid.dat file, and replace the old wood-tube interface friction angle with the new one in Block.dat file. These two data files are included in Appendix A.

Chapter 6

Conclusions and Recommendations

6.1 Conclusions

As was mentioned in Chapter 1, a water-filled geomembrane tube can be a relatively cheap, efficient, and environmentally friendly system for fighting flooding. Some companies have started to manufacture this type of system. The safety of using this system is critical. This thesis presents some insights on the analyses and designs of a safer water-filled geomembrane tube flood protection system. The following paragraphs present the conclusions of the analyses.

A finite difference program, FLAC, was used to perform the two-dimensional analyses on this water barrier. The analyses found out that the stresses in the tube depend on the consistency or stiffness of the soil, and it is most critical before the floodwater arrives. The stresses in the tube that is resting on soft clay, such as those mentioned in chapter 2, are higher than if it is on medium dense sand.

For an unsealed tube or when the internal tube pressure remains constant, an increase of floodwater level causes higher internal tube pressure, as well as larger tube cross-sectional area, and higher resistance to rolling and sliding than for a sealed tube. For a sealed tube or when the field measured tube pressure is used, the tube rolls at a slightly lower floodwater level than in the experiment. This is because the tube in the field has some restraints at its ends. Anyway, the difference of the critical floodwater levels between the results obtained by FLAC and by experiment is less than 4%. The shape of the cross section and the pore pressure in the soil agree very well with the results obtained in the experiments.

Piping is a major problem for the sandy soil foundation. But placing a filter under part of the tube and block can solve the problem. For the sandy soil, if the piping problem is solved, the tube will fail in rolling instead of sliding provided a proper block, such as shapes 1 or 2, is used.

The pore pressure in the soil has no effect on the rolling failure of the tube because the tube is always heavier than the pore pressure force that pushes under the tube. The pore pressure does reduce the sliding capacity of the system.

6.2 Recommendations for further research

In research, solving one problem opens up more problems that need to be solved. This is how mankind progresses. After one tackles a problem, he or she gains the knowledge to explore further. It is also no different in this research or thesis; it opens up more areas that require further research. These areas are discussed in the following paragraphs.

In this thesis, a block was used to wedge the tube. Future research should consider attaching an apron on the top of the tube and spreading it on the side with external water. The friction between the tube and apron may be able to help the tube withstand external water. Some experimental results are reported in FitzPatrick et al. (2001).

Two tubes enclosed by a tube should be studied. As the internal two tubes are inflated, the friction between the internal tubes and the external tube resists movement relative to each other and may be able to prevent the tubes from rolling. Again, some experiments on this case were conducted (FitzPatrick et al., 2001).

A single tube with external water on one side resting on clay, silt, or grass should be studied, since the ground conditions in the flooding areas varies from place to place. It is possible that sliding failure would be more critical than the rolling and piping failures in the cases that were considered in this thesis.

To increase the height of the barrier, one might want to stack the tubes. Studies on different tube-stacking geometries may be necessary. For example, one could consider two tubes at the base with one tube on top, or three tubes at the ground with two tubes on top and then another tube on top of those. Stability of stacked tubes is very important. The friction between tubes and the friction between tubes and ground will affect the stability of the system. If friction alone is

insufficient to keep this structure in place, these stacked tubes might require some form of anchoring or strapping.

During flooding, boating activities and wind may create waves that may affect the stability of the whole system and the stresses in the tube. It is important that dynamic loading of waves be considered in the future research.

References

Biggar, K. and Masala, S., (1998). Alternatives to Sandbags for Temporary Flood Control, Alberta Transportation and Utilities, Disaster Services Branch, Edmonton, Alberta, and Emergency Preparedness Canada, Edmonton, Alberta.

Bogossian, F., Smith, R. T., Vertematti, J. C., and Yazbek, O. (1982). "Continuous retaining dikes by means of geotextiles," Proceedings, 2nd International Conference on Geotextiles, Las Vegas, Nevada, Vol. I, pp. 211-216.

Das, B.M. (1994). Principles of Geotechnical Engineering, 3rd ed., PWS, Boston, pp. 590-596.

Davis, H. E., Troxell, G. E., and Hauck, G. F. W. (1982). The Testing of Engineering Materials, 4th ed., McGraw-Hill, New York, pp. 391-410.

Duncan, J. M. and Buchignani, A. L. (1987). An Engineering Manual for Settlement Studies, Foundation I course pack '99, Virginia Tech, p. 26.

FitzPatrick, B. T., Nevius, D. B., Filz, G. M., and Plaut, R. H. (2001). Pilot-Scale Tests of Water-Filled Tubes Resisting Floodwaters, Virginia Tech, Blacksburg.

Gere, J. M. and Timoshenko, S. P. (1990). Mechanics of Materials, 3rd ed., PWS, Boston, Massachusetts.

Gutman, A.L. (1979). "Low-cost shoreline protection in Massachusetts," Coastal Structures '79 , Vol. 1, ASCE, New York, pp. 373-387.

Hsieh, J.-C. and Plaut R. H. (1990). "Free vibrations of inflatable dams," Acta Mechanica, Vol. 85, No. 3-4, pp. 207-220.

Itasca Consulting Group (1998). Fast Lagrangian Analysis of Continua (FLAC), Minneapolis, Minnesota. Web site: http://www.itascacg.com

Kazimierowicz, K. (1994). "Simple analysis of deformation of sand-sausages," 5th International Conference on Geotextiles, Geomembranes, and Related Products, Singapore, pp. 775-778.

Koerner, R. M. (1994). Designing with Geosynthetics, 3rd ed., Prentice-Hall, Englewood Cliffs, New Jersey.

Koerner, R. M. and Koerner, G. R. (1996). "Geotextiles used as flexible forms," Geotextiles and Geomembranes, Vol. 14, No. 6, pp. 301-311.

Landis, K. (2000). "Control floods with geotextile cofferdams," Geotechnical Fabrics Report, Vol. 18, No. 2, pp. 24-29.

Leshchinsky, D., Leshchinsky, O., Ling, H. I., and Gilbert, P. A. (1996). "Geosynthetic tubes for confining pressurized slurry: Some design aspects," Journal of Geotechnical Engineering, Vol. 122, No.8, pp. 682-690.

McGregor, A. J. and Duncan, J. M. (1998). Performance and Use of the Standard Penetration Test in Geotechnical Engineering Practice, Virginia Tech, Blacksburg, p. 87.

Mysore, G. V., Liapis, S. I., and Plaut, R. H. (1997). "Vibration analysis of single-anchor inflatable dams," Proceedings of the Fourth International Symposium on Fluid-Structure Interactions, Aeroelasticity, Flow-Induced Vibration and Noise, ASME, New York, Vol. 2, pp. 119-124.

Mysore, G. V., Liapis, S. I., and Plaut, R. H. (1998). "Dynamic analysis of single-anchor inflatable dams," Journal of Sound and Vibration, Vol. 215, pp. 215-272.

Naval Facilities Engineering Command (1982). Soil Mechanics, Design Manual 7.1, Department of the Navy, Alexandria, Virginia, pp. 260-307.

Perrier, H., (1986). "Use of soil-filled synthetic pillows for erosion protection," 3rd International Conference on Geotextiles, Vienna, pp. 1115-1119.

Plaut, R. H. and Klusman, C. R. (1999). "Two-dimensional analysis of stacked geosynthetic tubes on deformable foundations," Thin-Walled Structures, Vol. 34, No. 3, pp. 179-194.

Plaut, R. H. and Suherman, S. (1998). "Two -dimensional analysis of geosynthetic tubes," Acta Mechanica, Vol. 129, No. 1-4, pp. 207-218.

Plaut, R. H., Liapis, S. I., and Telionis, D. P. (1998). "When the levee inflates," Civil Engineering, ASCE, Vol. 68, No. 1, pp. 62-64.

Potyondi, J. G. (1961). "Skin friction between various soils and construction materials," Geotechnique, Vol. 11, No. 4, pp. 339-353.

Sarti, G. and Larsen, J., (1983). "Underwater filling of Longard tubes," Coastal Structures '83, J.R. Weggel, ed., ASCE, New York, pp. 610-618.

Silvester, R. (1986). " Use of grout-filled sausages in coastal structures," Journal of Waterway, Port, Coastal, and Ocean Engineering, Vol. 112, No. 1, pp. 95-114.

Seay, P. A. and Plaut, R. H. (1999). "Three-dimensional behavior of geosynthetic tubes," Thin-Walled Structures, Vol. 32, pp. 263-274.

Sprague, C. J. and Koutsourais, M. M. (1992). "Fabric formed concrete revetment systems," Geosynthetics in Filtration, Drainage and Erosion Control, R. M. Koerner, ed., Elsevier, London, pp. 251-273.

Van Santvoort, G. P. T. M. (1995). Geosynthetics in Civil Engineering, A. A. Balkema, Rotterdam, The Netherlands.

Watson, L. T., Suherman, S., and Plaut, R. H. (1999). "Two-dimensional elastica analysis of equilibrium shapes of single-anchor inflatable dams," International Journal of Solids and Structures, 36, pp. 1383-1398.

Wu, P.-H., Plaut, R. H. (1996) Analysis of the vibrations of inflatable dams under overflow conditions, Thin-Walled Structures, Vol. 26, No. 4, pp. 241-259.

Appendix A

Sample FLAC Programs

This file generates the foundation soil

;Grid.dat

```
config gw ext=5                ;groundwater (GW) mode
set echo off
ca str.fin                     ;call structural link-list file
ca int.fin                     ;call interface link-list file
ca app.fin                     ;call apply mech. and pp link list file
set echo on

grid 97 7                      ;Grid mesh
mod mo i=1,64 j=4,7            ;zone 1
mod mo i=1,32 j=1,2            ;zone 2
mod mo i=66,73 j=6,7           ;zone 3
mod mo i=66,73 j=1,5           ;zone 4
mod mo i=74,89 j=1,5           ;zone 5
mod mo i=90,97 j=6,7           ;zone 6
mod mo i=90,97 j=1,5           ;zone 7

prop d 1600 s 7.7e6 b 1.6e7 f 36 perm 2e-9 poros 0.4 i=1,64 j=4,7       ;1
prop d 1600 s 7.7e6 b 1.6e7 f 36 perm 2e-9 poros 0.4 i=1,32 j=1,2       ;2
prop d 1600 s 7.7e6 b 1.6e7 f 36 perm 2e-9 poros 0.4 i=66,73 j=6,7      ;3
prop d 1600 s 7.7e6 b 1.6e7 f 36 perm 2e-9 poros 0.4 i=66,73 j=1,5      ;4
prop d 1600 s 7.7e6 b 1.6e7 f 36 perm 2e-9 poros 0.4 i=74,89 j=1,5      ;5
prop d 1600 s 7.7e6 b 1.6e7 f 36 perm 2e-9 poros 0.4 i=90,97 j=6,7      ;6
prop d 1600 s 7.7e6 b 1.6e7 f 36 perm 2e-9 poros 0.4 i=90,97 j=1,5      ;7
water dens 1000 bulk 0  ;bulk must be non-zero when the GW mode is on

gen 0,0.408 0,0.508 1.225,0.508 1.225,0.408 i=66,74 j=6,8               ;3
gen 2.025,0.408 2.025,0.508 3.25,0.508 3.25,0.408 i=90,98 j=6,8         ;6
gen 1.225,0 1.225,0.408 2.025,0.408 2.025,0 i=74,90 j=1,6               ;5
ini x=0     i=66                                                        ;4
ini x=0.275 i=67
ini x=0.505 i=68
ini x=0.695 i=69
ini x=0.85  i=70
ini x=0.975 i=71
ini x=1.075 i=72
ini x=1.16  i=73
ini x=1.225 i=74

ini x=2.025 i=90                                                        ;7
ini x=2.09  i=91
ini x=2.175 i=92
ini x=2.275 i=93
ini x=2.4   i=94
ini x=2.555 i=95
ini x=2.745 i=96
ini x=2.975 i=97
ini x=3.25  i=98
```

```
ini y=0     j=1
ini y=0.108 j=2
ini y=0.198 j=3
ini y=0.278 j=4
ini y=0.348 j=5
ini y=0.408 j=6
gen 1.225,0.458 1.225,0.508 2.025,0.508 2.025,0.458 i=1,65 j=4,8        ;1
gen 1.225,0.408 1.225,0.458 2.025,0.458 2.025,0.408 i=1,33 j=1,3        ;2

attach as fr 1,4 to 65,4 bs fr 1,3 to 33,3            ;1 bottom to 2 top
attach as fr 1,1 to 33,1 bs fr 74,6 to 90,6           ;2 bottom to 5 top
attach as fr 1,4 to 1,8 bs fr 74,7 to 74,8            ;1L to 3R
attach as fr 65,4 to 65,8 bs fr 90,7 to 90,8          ;1R to 6L
attach as fr 1,1 to 1,3 bs fr 74,6 to 74,7            ;2L to 3R
attach as fr 33,1 to 33,3 bs fr 90,6 to 90,7          ;2R to 6L
fix x y j=1 i=66,98                                   ;boundary conditions
fix x i=66
fix x i=98
set large
set g=9.807
                                    ;Initializes zone pore pressures
def ini_pp
loop i (1,igp)
  loop j (1,jgp)
    if y(i,j)>wth then              ;wth = height of the water table
      sat(i,j)=0.0
    else
      sat(i,j)=1.0
      gpp(i,j)=-1.0*abs((y(i,j)-wth))*wdens*ygrav
    end_if
  end_loop
end_loop
loop i (1,izones)
  loop j (1,jzones)
    pp(i,j)=0.25*(gpp(i,j)+gpp(i,j+1)+gpp(i+1,j+1)+gpp(i+1,j))
  end_loop
end_loop
end
set wth=0.508                       ;water table = 0.508m
ini_pp
ini syy -9964 var 0 9964            ;initialize total vertical stress
def ini_shor                        ;initialize total horizontal stress
loop i (1,izones)
  loop j (1,jzones)
    sxx(i,j)=k0x*(syy(i,j)+pp(i,j))-pp(i,j)
    szz(i,j)=k0z*(syy(i,j)+pp(i,j))-pp(i,j)
  end_loop
end_loop
end

set k0x=0.4122                      ;horizontal earth pressure coefficient
set k0z=0.4122
ini_shor

set flow off
```

This file creates a tube

;tubeload.dat

```
ini xdis=0 ydis=0                   ;reset displacement = 0
def setup                           ;using FISH to create a tube
      nbeam = 102                   ;102 beam elements
      L1 = 1.4732/nbeam             ;length of each beam
      L2 = (nbeam - 30)/2
      L3 = L2/2
      xcenter  = 1.4875
      ycenter  = 0.508
      x1 = xcenter + L3*L1
      y1 = ycenter
      ang1 = 0
      ang2 = pi/16

      loop n (1,15)                 ;create 15 beams on the right
            ang1 = ang1 + ang2
            x2 = x1 + L1*cos(ang1)
            y2 = y1 + L1*sin(ang1)

            command
                  stru beam beg x1,y1 end x2,y2
            endcommand

            x1 = x2
            y1 = y2
      endloop

      loop n (1,L2)                 ;create top beams
            x2 = x1 - L1
            y2 = y1
            command
                  struct beam beg x1,y1 end x2,y2
            end_command
            x1 = x2
            y1 = y2
      endloop

      ang1 = 0                      ;reset ang1 to zero
      loop n (1,15)                 ;create 15 beams on the left
            ang1 = ang1 + ang2
            x2 = x1 + (-1)*L1*cos(ang1)
            y2 = y1 + (-1)*L1*sin(ang1)
            command
                  stru beam beg x1,y1 end x2,y2
            endcommand
            x1 = x2
            y1 = y2
      endloop

      loop n (1,L2)                 ;create bottom beams
            x2 = x1 + L1
            y2 = y1
            command
```

```
                  stru beam beg x1,y1 end x2,y2
            endcommand
            x1 = x2
            y1 = y2
      endloop
end
setup
                                    ;Beam properties
struct prop 1 e=1.72e9 a=0.000457 i=7.95e-12

;specify the properties for the tube-ground interface
int 1 as from no 1,102 to no 66 bs from 1,8 to 48,8
int 1 ks 5e7 kn 1e8 fric 28

def nlist1                          ;Retrieve nodal information list
      ip = imem(str_pnt + $ksnode)
      loop while ip # 0
            idnum = imem(ip + $kndid)
            if idnum = node_num then
                  nlist1 = ip
                  exit
            endif
            ip = imem(ip)
      endloop
end
def makeNlist                       ;set up nodal addresses
      array nlist(nbeam)
      loop n (1,nbeam)
            node_num = n
            nlist(n) = nlist1
      endloop
end
makeNlist

def ar1                             ;declare arrays
      float x1 y1 nLx n2x n3x nLy n2y n3y s1 s2 s21 s22 s3
      array x1(nbeam) y1(nbeam) nLx(nbeam) n2x(nbeam) n3x(nbeam)
      array nLy(nbeam) n2y(nbeam) n3y(nbeam) s1(nbeam)
      array s2(nbeam) s21(nbeam) s22(nbeam) s3(nbeam)
end
ar1

def n_coor1                                 ;get nodal coordinates
      ymax = 1
      loop n (1,nbeam)                      ;scan through every node
            n1 = nlist(n)
            x1(n) = fmem(n1 + $kndx)        ;retrieving nodal coor fr flac memo
            y1(n) = fmem(n1 + $kndy)
            if y1(n) >= y1(ymax)            ;find the highest node
                  ymax = n
            endif
            if x1(n) <= x1(xmin)            ;find the left extreme node
                  xmin = n
            endif
      endloop
end
n_coor1
```

```
def n_load1                    ;apply load on the nodes
      n_coor1
      ;wh1 = ?                 ;wh1 = specified water head in meter
                               ;to be input by the use
      wu1 = 9.807e3            ;wu1 = water unit weight,
                               ;which is 1000kg/m^3 x 9.807m/s^2
      wp1 = wh1*wu1            ;wp1 = water pressure
      whilestepping            ;this command causes n_load1 to be executed
                               ;every step
      wh1min = 0.18                 ;min water head to start
      up1 = wh1min + 0.00005*ct1    ;ramp
      wp2 = up1*wu1                 ;wp2 = water pressure
      wp3 = min(wp1,wp2)            ;wp3 = water pressure
      ct1 = ct1 + 1                 ;counter

      loop a (1,nbeam)
        n1 = nlist(a)
        p1 = wp3-(y1(a) - 0.508)*wu1      ;Nodal hydrostatic pressure
        If a = 1 then
          s1(a) = sqrt((x1(2)-x1(nbeam))^2+(y1(2)-y1(nbeam))^2)
          s21(a) = sqrt((x1(a)-x1(nbeam))^2+(y1(a)-y1(nbeam))^2)
          s22(a) = sqrt((x1(a)-x1(a+1))^2+(y1(a)-y1(a+1))^2)
          s2(a) = (s21(a)+s22(a))/2
          nLx(a) = p1*s2(a)*(y1(2)-y1(nbeam))/s1(a)
          nLy(a) = -1*p1*s2(a)*(x1(2)-x1(nbeam))/s1(a)
        else
          If a = nbeam then
            s1(a) = sqrt((x1(1)-x1(nbeam-1))^2+(y1(1)-y1(nbeam-1))^2)
            s21(a) = sqrt((x1(a)-x1(a-1))^2+(y1(a)-y1(a-1))^2)
            s22(a) = sqrt((x1(a)-x1(1))^2+(y1(a)-y1(1))^2)
            s2(a) = (s21(a)+s22(a))/2
            nLx(a) = p1*s2(a)*(y1(1)-y1(nbeam-1))/s1(a)
            nLy(a) = -1*p1*s2(a)*(x1(1)-x1(nbeam-1))/s1(a)
          else
            s1(a) = sqrt((x1(a+1)-x1(a-1))^2+(y1(a+1)-y1(a-1))^2)
            s21(a) = sqrt((x1(a)-x1(a-1))^2+(y1(a)-y1(a-1))^2)
            s22(a) = sqrt((x1(a)-x1(a+1))^2+(y1(a)-y1(a+1))^2)
            s2(a) = (s21(a)+s22(a))/2
            nLx(a) = p1*s2(a)*(y1(a+1)-y1(a-1))/s1(a)
            nLy(a) = -1*p1*s2(a)*(x1(a+1)-x1(a-1))/s1(a)
          endif
        endif

      n3x(a) = nLx(a) + n2x(a)
      n3y(a) = nLy(a) + n2y(a)

        fmem(n1 + $kndap1) = n3x(a)       ;write new nodal loads back to
        fmem(n1 + $kndap2) = n3y(a)       ;flac's memory
      endloop
end
n_load1
set large                                 ;large strain mode
set grav 9.807
```

This file creates a block

;block.dat

```
def wblk1               ;creating a block
      L5 = 0.065        ;height of the block
      L5x = 1.7029
      L6x = L5x + L5*2
      L7x = L5x + L5
      L7y = 0.508 + L5

      command                              ;create wood block
            struct node 200 L6x,0.508      ;right edge
            Struct node 203 L5x,0.508      ;left edge
            struct node 211 L7x,L7y        ;top edge
            struct beam beg no 200 end no 203 seg 3 prop 2
            struct beam beg no 203 end no 211 seg 8 prop 2
            struct beam beg no 211 end no 200 prop 2
            struct prop 2 e=10.8e9 a=0.025 i=2.1e-3 den=450
                                   ;interface b/w wood and ground
            int 2 as from no 200,201 to no 203 bs from 39,8 to 52,8
            int 2 ks 5e7 kn 1e8 fric 28
                                   ;interface b/w wood and tube
            int 3 as from no 10,9 to no 96 bs from no 203,204 to no 211
            int 3 ks 5e8 kn 1e9 fric 15
      endcommand
end
wblk1
```

This file applies the floodwater load on the tube

;fwload.dat

```
def cspt1                      ;to find 1st contact point between-
int hai haj                    ;tube and soil
whilestepping
ip = int_pnt                   ;point to interface link-lists
loop while ip # 0

inum = imem(ip + $kicid)       ;retrieving interface ID
if inum = 1                    ;Only scan interface 1
  pa = imem(ip + $kicapt)      ;retrieve no number, A side
  loop while pa # 0            ;scan through non-zero nodes
    intns = fmem(pa + $kidfn) ;retrieve interface normal force
    if intns # 0               ;if normal force not equal to 0
      sod = imem(pa + $kidi)   ;retrieve structural node ID
    endif
  pa = imem(pa)
  endloop

  pa = imem(ip + $kicbpt)      ;retrieve grid number, B side
  loop while pa # 0            ;loop through non-zero grid
    intns = fmem(pa + $kidfn) ;retrieve interface normal force
    if intns # 0               ;if normal force not equal to 0
      hai = imem(pa + $kidi)   ;retrieve grid i
      haj = imem(pa + $kidj)   ;retrieve grid j
      exit
    endif
  pa = imem(pa)
  endloop
endif

ip = imem(ip)
endloop
end
cspt1

def fwload1              ;to apply floodwater load on the tube
wh3 = ycenter + wh2      ;wh3 = water level elev.
                         ;wh2 = floodwater level to be input by user
whilestepping
  loop a (ymax,sod)
    p2 = (wh3-y1(a))*wu1*1    ;Nodal hydrostatic pressure
    if wh3 < y1(a) then
      n2x(a) = 0
      n2y(a) = 0
    else
      n2x(a) = -1*p2*s2(a)*(y1(a+1)-y1(a-1))/s1(a)
      n2y(a) = p2*s2(a)*(x1(a+1)-x1(a-1))/s1(a)
    endif
  endloop
end
fwload1
```

This file applies the pore pressure on the ground

;applypp.dat

```
ca a:Qratio.fis                     ;ca FISH library file for
                                    ;groundwater flow rate calculation
def fwp1
      wh2 = 0.159                   ;flood water level
      pwp2 = wh2*1e3*9.807          ;pwp on left surface
      pwp2a = -1*pwp2
      pwp3 = 0.508*1000*9.807       ;pwp at right bottom
      pwp3a = -1*pwp3
      pwp4 = pwp2 + pwp3            ;pwp at left bottom
end
fwp1

def fwp2
command
  ini sat 1
  ini pp pwp4 var 0 pwp3a i=66      ;pwp on the left side
  fix pp i=66
  ini pp pwp3 var 0 pwp3a i=98      ;pwp on the right side
  fix pp i=98
  apply pp 0 var 0 0 i=49,65 j=8    ;pwp on the right surface
  ini pp 0 var 0 0 i=90,98 j=8      ;pwp on the right surface
  fix pp i=90,98 j=8
  apply pp pwp2 var 0 0 i=66,74 j=8 ;pwp on the left surface
  apply pr pwp2 var 0 0 i=66,74 j=8
endcommand
end
fwp2

set flow on

def makeApplys  ;Create apply lists for potential left over by
                ;the tube
  fjgp = jgp
  loop ii (1,47)
    ii1 = ii + 1
    command
      apply syy=-1.0 from ii,fjgp to ii1,fjgp
      apply disch=1e-20 from ii,fjgp to ii1,fjgp
    endCommand
  endLoop
end
set echo off
makeApplys
set echo on
cyc 100 update=1  ;initial equilibrium

def modifyApplys
                  ;extend the applied pwp area by 1 zone every 10 steps
 while_stepping
 count = count + 1
 if count > 10
   count = 0
```

```
    if hai >= hai5
     hai5 = hai5 + 1
    endif
     pnt = app_pnt                  ;point to apply stress list
      loop while pnt # 0
       if imem(pnt+$kapi1) < hai5   ;Start i
        fmem(pnt+$kapv6) = pwp2a    ;apply mech. stress
       endif
       pnt = imem(pnt)
      endLoop
     pnt = appgw_pnt                ;point to apply pwp list
      loop while pnt # 0
       if imem(pnt+$kapi1) < hai5
        imem(pnt+$kapx)  = 3        ;change to applied pp from discharge
        fmem(pnt+$kapv1) = pwp2
       endif
       pnt = imem(pnt)
      endLoop
            flags(hai5,jgp) = or(flags(hai5,jgp),512) ; set pp fix flag
            flags(1,jgp) = or(flags(1,jgp),512)       ; for 1st grid
 endif
end
solve sratio 0.01 update=1
```

This file calculates tube cross-sectional area and circumference

;tube_a.dat

```
def tubea               ;Calculate the tube area
  tube_a = 0
   loop a(1,nbeam)
    If a = nbeam then
      tube_a = (x1(a)-x1(1))*(y1(a)-0.508 + y1(1)-0.508)/2 + tube_a
    else
      tube_a = (x1(a)-x1(a+1))*(y1(a)-0.508 + y1(a+1)-0.508)/2 +tube_a
    endif
   endloop
end
tubea

def tubecir             ;Calculate the tube circumference
      tube_cir = 0
      loop a(1,nbeam)
            tube_cir = s22(a) + tube_cir
      endloop
end
tubecir

print tube_a
print tube_cir
```

Appendix B

Program Validation Tests

B1 Soil stresses caused by surface load without pore water pressure effect

The vertical soil stress in the center of each highlighted zone that is marked from 1 through 5, as shown in Figure B.1, is computed by three methods. These methods are the direct FLAC results, spread load method, and Boussinesq equation.

B1.1 Soil stresses computed by FLAC

A simple mesh shown in Figure B.1 is created to check if FLAC gives correct stresses in the soil and at the interface. This mesh is 5m high and 20m long. It consists of a hundred 1m x 1m grid zones. The same soil properties as in section 4.2 are used, except the soil dry density is 1889kg/m^3, and without ground water. This soil with its own weight is compacted into equilibrium, and the vertical and horizontal stresses are obtained and shown in Table B.1.

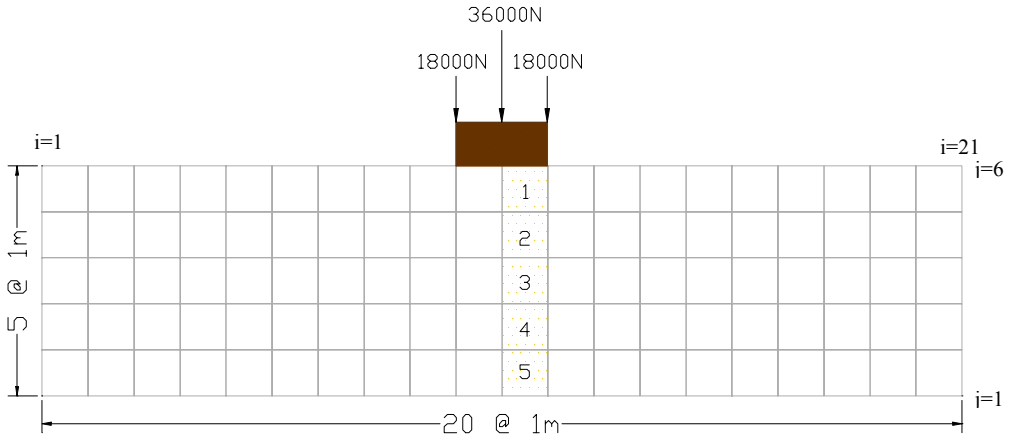

Figure B.1: Soil mesh for testing the subsurface stress due to the surface load

Table B.1: FLAC calculated vertical and horizontal soil self stresses

Depth (m)	Vertical self stress, σ_v (Pa)	Horizontal self stress, σ_h (Pa)	σ_h/σ_v K_1
0.5	-9260	-3830	0.4136
1.5	-27780	-11490	0.4136
2.5	-46290	-19150	0.4137
3.5	-64790	-26800	0.4136
4.5	-83270	-34450	0.4137

Table B.1 shows that the ratio of the horizontal self stress over the vertical self stress, K_1, is 0.41, which is the same as the value of the at-rest horizontal soil pressure coefficient calculated by using the equation

$$K_o = 1\text{-}\sin\phi' \qquad \text{(B1.1)}$$

For $\phi' = 36°$, $K_o = 0.41$ for the normal consolidated soil.

To ensure that the FISH functions written for section 4.2 are correct, a test is carried out with the same soil and beam properties mentioned above, except the initial soil stresses are initialized by the method that was mentioned in section 4.2 instead of calculated by FLAC. The results are presented under the "initial" columns in Table B.2, and they are very close to the results presented in Table B.1. These indicate that FLAC uses K_o for calculating the horizontal soil stresses due to the soil's self weight.

Table B.2: The initial and total stresses.

	Vertical Stress, σ_v			Horizontal Stress, σ_h			σ_v/σ_h ratio	
Depth (m)	Initial (Pa)	Total (Pa)	Change (Pa)	Initial (Pa)	Total (Pa)	Change (Pa)	Initial K_1	Change K_2
0.5	-9270	-35210	-25940	-3800	-13840	-10040	0.41	0.39
1.5	-27800	-47280	-19480	-11400	-13450	-2050	0.41	0.11
2.5	-46330	-61500	-15170	-18990	-18980	-10	0.41	0.0007
3.5	-64860	-77580	-12720	-26590	-27390	-800	0.41	0.063
4.5	-84620	-95740	-11120	-34690	-37620	-2910	0.41	0.26

Now, a mass is placed at the center of the soil mesh. This mass is represented by two thick (1m) beam elements with a very high modulus of elasticity ($1x10^{15}$ Pa), so one can assume that the mass is rigid. These beam elements are connected to form a straight line. Point loads are applied

vertically at each node as shown in Figure B.1. The total applied load is 72,000N, and the resulting total soil stresses are presented in Table B.2.

The initial soil stress is caused by the soil self weight, and the total soil stress is caused by the soil self weight plus any other loads. The change in soil stress caused by the surface load is computed manually, and is equal to the total soil stress minus the initial soil stress. K_2 is the ratio of the change of horizontal stress over the change of vertical stress. K_2 is small compared to K_1, and even smaller than the active horizontal soil pressure coefficient, $K_a = \frac{1-\sin\phi'}{1+\sin\phi'} =$ 0.26, except for the depths 0.5m and 4.5m. These indicate that FLAC varies the effective horizontal earth pressure coefficient for any load added on the soil.

The normal stresses at the interface between the mass and the soil are retrieved and shown in Table B.3. The side A of the interface is on the beam element side, which has three nodes, and each of them is alternated with one of the interface elements from the side B (grid mesh side). The beam node 1 is the right edge, and node 3 is the left edge of the mass. Each grid node at side B has two indices, i and j. Index i is the vertical grid numbering system that begins from the left towards the right. Index j is the horizontal grid numbering system that begins from the bottom towards the top of the mesh. FLAC reports the normal stress and the contact length at each node. The normal reaction is the product of normal stress and contact length, and it is computed manually.

The results show that the total normal reaction (2N) at the interface is slightly lower than the total applied load. This is because the results output by FLAC are not exact since they are rounded off to four significant figures.

Table B.3: FLAC's normal reaction at the interface

	Node	Normal Stress (Pa)	Contact Length (m)	Normal Reaction (N)
Side A	3	-4.254×10^{7}	9.583×10^{-5}	-4077
	2	-2.769×10^{4}	4.999×10^{-1}	-13842
	1	-4.253×10^{7}	9.583×10^{-5}	-4077
Side B	i j			
	10 6	-3.616×10^{4}	5.000×10^{-1}	-18080
	11 6	-2.769×10^{4}	4.999×10^{-1}	-13842
	12 6	-3.616×10^{4}	5.000×10^{-1}	-18080
	Σ		2	-71998

B1.2 Soil stresses computed by using spread load method

Figure B.2 illustrates the spread load method. A single point load of 72,000N is applied on the top of the mass. To maintain the system in equilibrium, the vertical stress beneath the mass is assumed to be equal to the applied load divided by the spread area at the depth of interest. As shown in Figure B.2, the slope for each side of the spread is 2:1, and it is assumed that the length perpendicular to the paper is one meter, so the spread area at the depth of interest is the width of the mass plus the depth. The computed vertical stresses are shown in Table B.4.

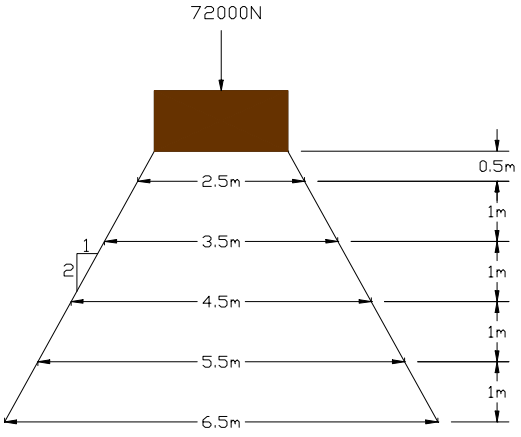

Figure B.2: Spread load method

Table B.4: Soil stresses computed by spread load method

Depth (m)	Spread Area (m^2)	Vertical Stress (Pa)
0.5	2.5	28800
1.5	3.5	20571
2.5	4.5	16000
3.5	5.5	13091
4.5	6.5	11077

B1.3 Soil stresses computed based on the Boussinesq equation

The above mentioned subsurface stress produced by the loading of a 2m wide mass strip is also checked by the Boussinesq equation (Naval Facilities Engineering Command, 1982, pp. 7.1-166). The formulas that are used are referred to the stress diagram shown in Figure B.3.

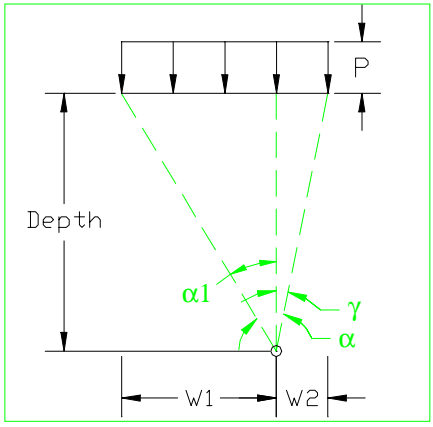

Figure B.3: Stress diagram used by Boussinesq equation

$$\text{Vertical stress} = \frac{P}{\pi}[\alpha + \sin\alpha\cos(\alpha - 2\gamma)] \quad \text{(B1.2)}$$

$$\text{Horizontal stress} = \frac{P}{\pi}[\alpha - \sin\alpha\cos(\alpha - 2\gamma)] \quad \text{(B1.3)}$$

$$\text{where } P = \frac{72{,}000}{W1 + W2}\ \text{Pa} \quad \text{(B1.4)}$$

$$W1 = 1.5\text{m}$$

W2 = 0.5m

α, $\alpha 1$, γ are in radians

Table B.5 below shows the results obtained by using these formulas.

Table B.5: Soil stresses computed using Boussinesq equation

Depth (m)	α (rad)	γ (rad)	Vertical stress (Pa)
0.5	2.034	0.785	32480
1.5	1.107	0.322	21854
2.5	0.738	0.197	15713
3.5	0.547	0.142	12019
4.5	0.432	0.111	9650

B1.4 Comments

Figure B.4 compares the vertical soil stresses computed by the above mentioned three methods. They are all very close to each other, especially the vertical stresses computed by FLAC and the spread load method. The vertical stresses computed by the Boussinesq equations are larger at a shallow depth and are smaller at a greater depth when compared to the other two methods. The maximum difference in stresses between the FLAC and Boussinesq results is less than 23%. Also note that the soil conditions used by the FLAC and the other methods are not exactly the same. For example, the Boussinesq method assumes an elastic foundation while FLAC takes nonlinear soil behavior into account. Also, the Boussinesq method assumes uniform pressure throughout the contact area between the soil and the mass, whereas the FLAC analyses assume a uniform displacement of the mass. The soil stresses at the edge of the mass will be smaller than those at the center-bottom of the mass, because the soil movement at the edge is greater. Therefore, FLAC's results are to be considered more accurate than those of the other two methods.

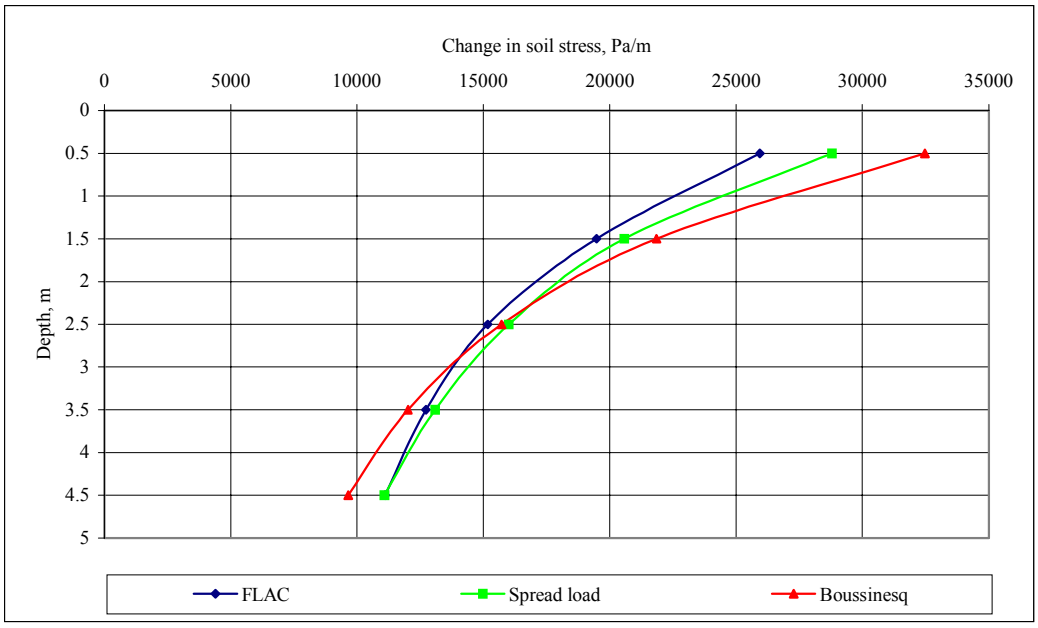

Figure B.4: Change of vertical soil stress versus depth

B2 Normal and shear stresses at the interface caused by surface loads with and without pore water pressure effect

B2.1 Soil stresses without surface load

The same soil properties as mentioned in section B.1 are used. The pore pressures and effective vertical and horizontal stresses computed by FLAC for Zones 2 and 3 in Figure B.1 are checked. The results are shown in Table B.6. These results are checked with the results calculated manually by the following formulas:

$$pp = g\rho_w h \tag{B2.1}$$

$$\sigma_v = (\rho + \eta\rho_w)hg \tag{B2.2}$$

$$\sigma_v' = \sigma_v - pp \tag{B2.3}$$

$$\sigma_h = K_o\sigma_v' + pp \tag{B2.4}$$

where pp = pore pressure

g = gravitational pull, which is equal to 9.81m/s^2

ρ_w = water density, which is 1000 kg/m^3

h = depth of soil in meters

σ_v = total vertical soil pressure

ρ = dry soil density, which is 1889kg/m^3

η = porosity of soil, which is 0.3

σ_v' = effective vertical soil pressure

σ_h = total horizontal soil pressure

$\phi' = 36°$

K_o = lateral earth pressure coefficient, which is 0.4122

Table B.6: Self-stress of the soil without surface load

		Manual				FLAC			
Depth (m)	Zone, i,j	σ_v (Pa)	pp (Pa)	σ_v' (Pa)	σ_h (Pa)	σ_v (Pa)	pp (Pa)	σ_v' (Pa)	σ_h (Pa)
1.5	11,5	-32211	14715	-17496	-21927	-32210	14720	-17500	-21930
2.5	11,4	-53685	24525	-29160	-36545	-53690	24530	-29160	-36540

B2.2 Pore pressure at the interface

A square mass is placed on the soil as shown in Figure B.5. Two beam elements are used to construct each side of this mass. The same beam and interface properties as in section B1 are used. A constant pore pressure head of 2m is applied on the soil surface at the left of the mass. An equal amount of mechanical stress has to be applied at the same time and the same place to prevent the top horizontal grid line from swelling up. A zero pore pressure is applied on the soil surface at the right side of the mass to allow water to flow out from the soil freely. The interface between the beam element and the grid is impermeable (Itasca, 1998).

To speed up the test, the mechanical calculation mode is turned off before turning on the groundwater flow to distribute the pore pressure appropriately. The final pore pressure distribution and the groundwater flow are shown in Figure B.5. Figure B.6 shows the pore

pressure on the soil surface. The steep slope occurs where the mass is located (between 10m and 12m). The surface pore pressure drops from 19620Pa at 10m to zero at 12m. The pore pressure at 11m is 9810Pa, which is the average pore pressure between 10m and 12m. Since the width of the mass is 2m, the pore pressure force at the interface is 19,620N.

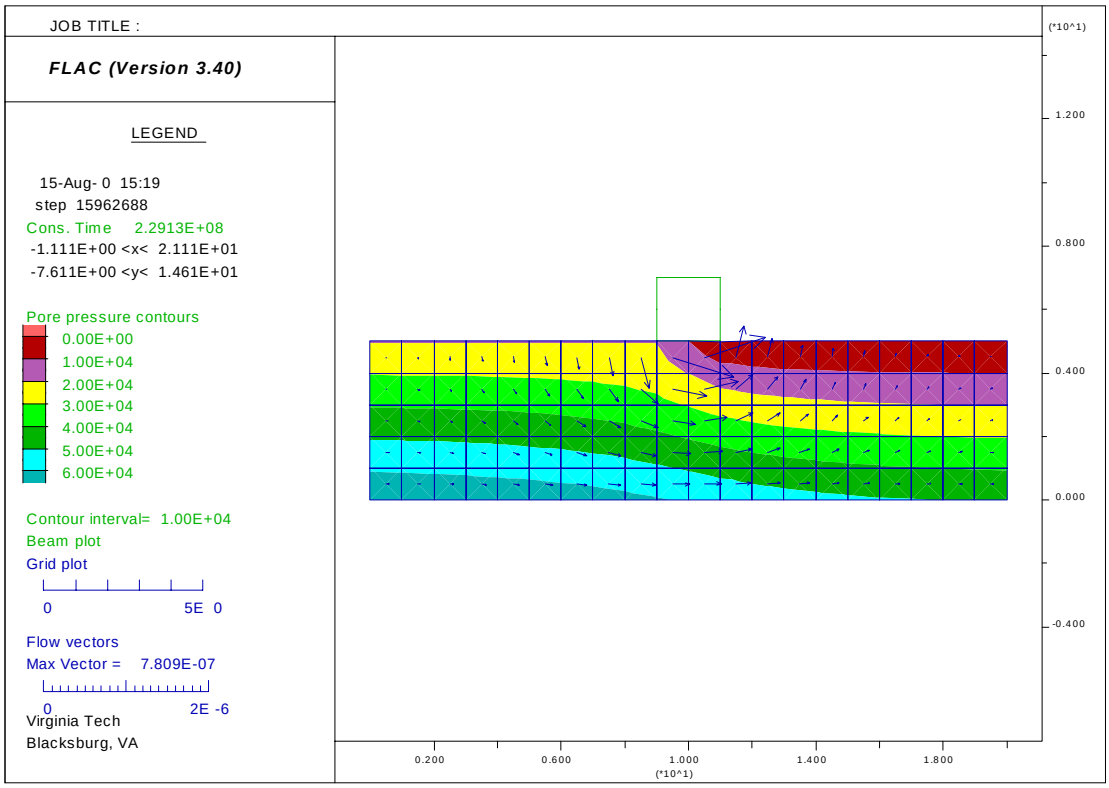

Figure B.5: Pore pressure distribution

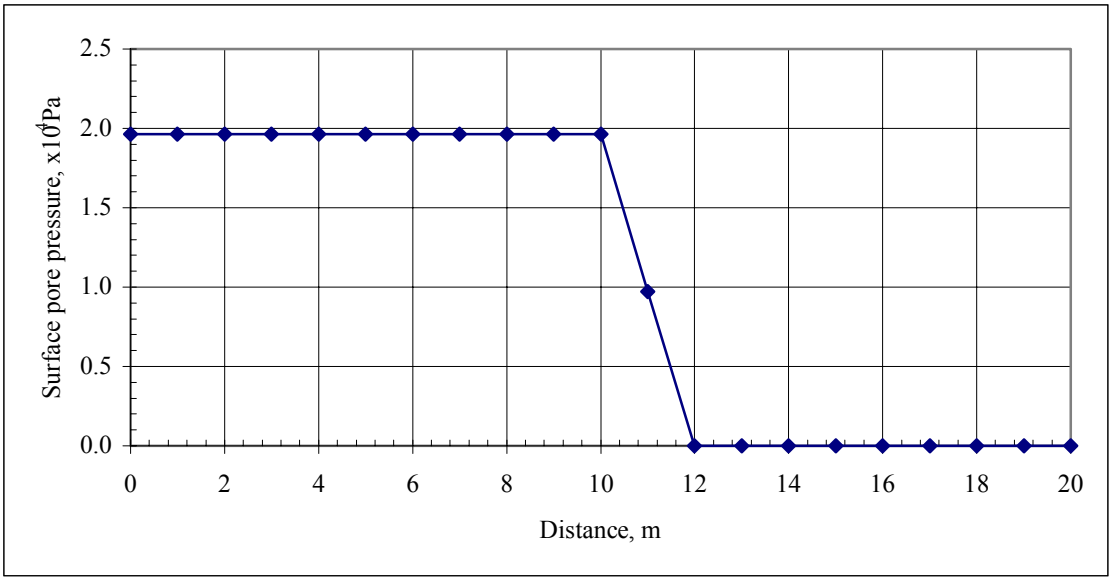

Figure B.6: Surface pore pressure versus distance from the left edge

B2.3 Normal stresses at the interface with pore pressure effect

FLAC does not fully model the interaction between the interface and the soil with pore water pressure. The effects of pore pressure on normal pressure and normal displacement at the interface are not calculated (Itasca, 1998). To better understand the limitation of FLAC, a test is carried out.

Now, a point load of 72000N is applied on the center of the bottom side of the mass, and the mechanical calculation mode is turned on. After the system is in equilibrium, the normal stress and the associated contact length for each node at the interface are retrieved from FLAC. These results are manipulated and shown in Table B.7.

The results show that the total normal reaction is about the same as the applied load (72,000N). By using equation B2.3, the effective normal reaction at the interface is 52,380N. Therefore, FLAC reports the total normal stress instead of the effective normal stress at the interface.

Table B.7: FLAC's normal reaction at interface

	Node	Normal Stress (N)	Contact length (m)	Normal Reaction (N)
Side A	7	-30990	0.25	-7748
	8	-26210	0.50	-13105
	1	-30980	0.25	-7745
Side B	i j			
	10 6	-30300	0.50	-15150
	11 6	-26210	0.50	-13105
	12 6	0	0	0
		Total Normal Reaction		-72008

B2.4 Sliding resistances at the interface

The same soil mesh as shown in Figure B.1 is used, but the soil is assumed to be very stiff to reduce the settlement of the mass. If no settlement occurs for the mass, the passive force at the front of the mass will not exist. Then, an assumption can be made that only sliding resistance resists the applied horizontal load. The soil properties used are:

Shear stiffness = 10^{10}Pa

Bulk modulus = $2x10^{10}$Pa

Internal angle of friction = 36°

Interface friction angle between soil and mass = 28°

The load magnitude and configuration are the same as in the previous section, and will remain the same throughout the remaining tests in this Appendix.

B2.4.1 Sliding resistance without pore pressure effect

A gradually increased point load is applied on the left of the mass towards the right. To check whether FLAC computes the correct sliding resistance without the effect of pore pressure, no surface pore pressure is applied at this time. The horizontal stresses and contact lengths at the interface are retrieved from FLAC. The horizontal reactions are computed by multiplying the horizontal stresses with the contact lengths, and are shown in Table B.8. The mass slides at 38,285N and is unable to resist the 38,500N applied horizontal load.

Table B.8: Horizontal reaction at the interface corresponds to the applied horizontal load

Applied horizontal load (N)	Horizontal reaction (N)
25000	25000
37000	37000
38000	38010
38283	38285
38500	38285 (sliding)

The maximum manually calculated horizontal reaction is 38,283N, which is the total vertical load (72,000N) multiplied by the interface friction coefficient (tan28°). The critical horizontal resistance computed by FLAC is the same as in the manual results.

B2.4.2 Sliding resistance with pore pressure effect

For the sliding resistance with the effect of pore pressure, the pore pressure is applied as was described in section 2.2. After the groundwater pressure is distributed, the groundwater flow is switched off. Then, the mechanical calculation mode is used to include the pore pressure effect in the system. The mechanical calculation and flow modes are not turned on at the same time to avoid slowing down the convergence to a solution. Finally, a horizontal point load is applied on the mass and increased until the mass slides.

The results are shown in Table B.9. Once again, the vertical reaction at the interface is almost equal to the applied load of 72,000N. The critical sliding resistance is 27,853N, and the mass

was unable to resist the 27,900N applied load. This critical resistance is almost the same as the manually calculated maximum resistance, which is 27,851N and is computed as follows:

Maximum horizontal resistance = (vertical load – pore water resistance)tan28°

= (72000N – 19620N)tan28°

= 27851N

Table B.9: Horizontal resistance at the interface with pore pressure effect

Applied horizontal load (N)	Horizontal resistance at interface (N)	Vertical reaction (N)
25000	24990	72000
26000	25995	72000
27000	26997	72005
27851	27848	71995
27900	27853 (Sliding)	72000
29000	27583 (Sliding)	72005

B2.4.3 Comparison between sliding resistances with and without pore pressure effect

The critical sliding resistance with pore pressure effect is smaller than the critical sliding resistance without pore pressure effect. As shown in Figure B.7, the slopes for both cases are about the same when the mass is in static equilibrium. This slope is approximately equal to one, which means the reaction is equal to the applied load. Depending on the magnitude of the pore pressure, the larger the pore pressure, the smaller the sliding resistance will be at the interface, if the applied horizontal and vertical loads remain the same. These tests show that FLAC does consider the effect of pore pressure on sliding.

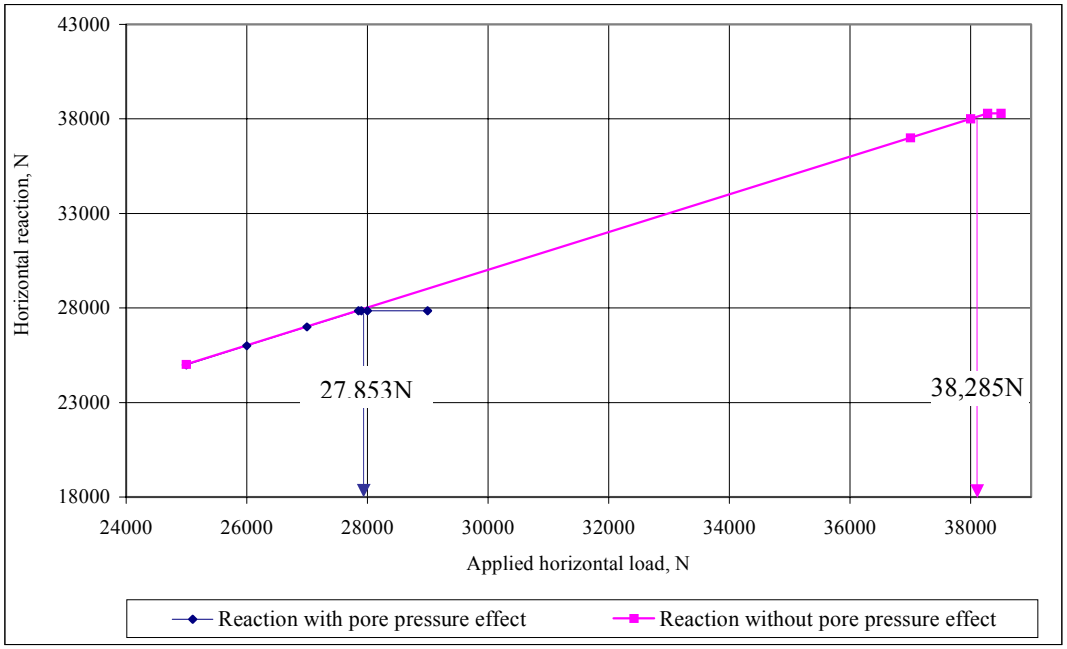

Figure B.7: Horizontal reaction versus applied horizontal load

Vita

Tung Chun Huong was born on February 14, 1968 in Marudi, Malaysia. He graduated Magma Cum Laude from the University of Texas at San Antonio in May 1999 with a Bachelor of Science degree in Civil Engineering. In August 1999 he came to Virginia Polytechnic Institute and State University to pursue his Master of Science degree in Civil Engineering. After graduation, he will pursue his career as a civil engineer.